Landau Energy Loss in Liquid Scintillator and the Search for WIFs with the LVD Experiment

by

Jie Tang

B.S., Applied Physics
Shanghai Jiao Tong University
(1984)

Submitted to the Department of
Physics in Partial Fulfillment of
the Requirements for the
Degree of

Doctor of Philosophy
in Physics

at the

MASSACHUSETTS INSTITUTE OF TECHNOLOGY

June 1994

Signature of Author ....
Department of Physics
May 2, 1994

Certified by ....
Irwin A. Pless
Professor of Physics
Thesis Supervisor

Accepted by ....
George F. Koster
Chairman, Physics Graduate Committee

Landau Energy Loss in Liquid Scintillator and the Search for WIFs with the LVD Experiment

by

Jie Tang

Submitted to the Department of Physics
on May 2, 1994, in partial fulfillment of the
requirements for the degree of
Doctor of Philosophy
in Physics

Abstract

The LVD experiment at Gran Sasso, Italy, is described, and data since the completion of the first tower (one fifth of the whole LVD) are analyzed. The dE/dx distribution of reconstructed high-energy muons in the scintillator counters is obtained. This distribution is compared with predictions by a GEANT3 Monte Carlo simulation of cosmic muons going through the LVD detector. Its shape is similar to the Landau approximation. In the data from a total running time of 245 days, 159286 clearly separable charged tracks going through the detector were reconstructed. No WIF (Weakly-Interacting Fractionally-charged particle) is observed.

Since the early 1930's to the 1980's, theories on the dE/dx distribution of charged particles in matter have evolved from the fundamental work done by Bethe, Bloch, Landau, Symon, Vavilov and others with the inclusion of more precise corrections of the *density effect* and the *shell effect.* At the LVD experiment, through a procedure of gain-factor calibration at every period of 20 days, to compensate for instability and nonuniformity of the scintillator counters and their readout, the muon dE/dx distribution is measured; it conforms to the Landau approximation. The precision of the dE/dx measurement is 7.6% (one σ).

WIF particles are speculated by modern theories. Because dE/dx is proportional to the square of the charge carried by the incident particle, any WIF going through the LVD liquid scintillator will reveal itself by its dE/dx being on the low side of the carefully calibrated muon dE/dx distribution. Calculation has shown that when the charge of a WIF is as low as $\frac{2}{3}e$, it still generates enough ionization in the LVD limited streamer tubes and thus its track is as visible as a muon track in the detector. Such events are not found. Assuming a uniform flux distribution of WIF particles coming from the atmosphere, the upper limit of their flux at the LVD site is $4.4 \times 10^{-14}\,\mathrm{cm}^{-2}\mathrm{sterad}^{-1}\mathrm{sec}^{-1}$.

Thesis Supervisor: Irwin A. Pless
Title: Professor of Physics

Acknowledgments

I wish to express my deepest gratitude to my thesis advisor Professor Irwin A. Pless for his excellent guidance in the whole work and in many details (particularly in how to exclude background events and in finding a new method to search for WIFs systematically), and for his generous support. I am glad to have learned much from him in how to do physics.

I thank Dr. Elizabeth S. Hafen for the help in all aspects of the LVD data analysis. The raw data processing, track reconstruction, and GEANT3 Monte Carlo simulation of LVD were based on her programs.

I want to thank Dr. Padmanabhan Haridas for many discussions and constructive advice on this work and on other subjects and for the help he provided in finding many related writings. The help from him and from Dr. Jorge Moromisato of Northeastern University throughout the three years while I worked at Gran Sasso is greatly appreciated.

Professor E. D. Alyea from Indiana University, Bloomington and Professor P. Giusti from University of Bologna have offered very essential support to all aspects of the detector construction. M. Pu, W. Tian, X. Lin, and Professor J. Ma from the Chinese Academy of Sciences and the I.C.S.C. World Laboratory have given indispensable help in the construction and testing of detector components. A. De Silva from Brown University has provided most remarkable expertise on the data acquisition software. It has been a great pleasure to work with them.

I wish to thank all members of the LVD collaboration, whose names are gratefully acknowledged in Appendix A. Their collective effort makes the LVD experiment and this thesis possible. I also thank Prof. E. Bellotti, who as director of the INFN Gran Sasso Laboratory has given the LVD experiment enthusiastic support.

Contents

Chapter 1

Introduction

Experimental evidence manifests that all particles observable carry integral charge in units of e, although since the concept of *quarks* [GM64, Zwe64] was invented in physics, theories to some extent confirmed by observation [Dal83, HK83, DM83, FK83] suggest the existence of fractionally charged particles. The LVD (Large Volume Detector) [A$^+$86] experiment, with its distinctive features of large sensitive volume, high precision tracking, and low background, furthers the search [Lyo85, K$^+$83, K$^+$84, B$^+$91a, A$^+$94a] for free fractionally charged particles. This search at LVD is based on how charged particles lose energy in matter. In this work the energy loss of charged particles in thick scintillator ($\sim$ 1 meter) counters is measured. The Landau dE/dx distribution describes the measurements quite well. Fractionally charged particles are not found. A good upper limit on their flux is established.

1.1 The Energy Loss of Charged Particles in Matter

The energy loss of charged particles in matter has been studied both experimentally and theoretically in increasing detail and precision over the last 90 years [Fan63, Ahl80, LKV85]. Charged particles going through matter lose energy via four different processes: (1) elastic and inelastic atomic collisions, (2) incident-particle bremsstrahlung, (3) pair productions, and (4) nuclear interactions.

The first process, also called ionization loss, which is the dominant process when the energy of the incident particle is not ultrahigh (not beyond a few TeV in the LVD scintillator), was summarized [Leo87] in the well known Bethe-Bloch formula [Bet32, Blo33] plus two correction terms: the *density effect* [SBS84] correction δ, and the *shell effect* [BB64] correction C

$$-\,dE/dx = 2\pi N_{\mathrm{a}} {r_{\mathrm{e}}}^2 m_{\mathrm{e}} c^2 \rho \frac{Z_0}{A_0} \frac{z^2}{\beta^2} \left[\ln\left(\frac{2 m_{\mathrm{e}} \gamma^2 v^2 W_{\max}}{I^2}\right) - 2\beta^2 - \delta - 2\frac{C}{Z}\right] \qquad (1.1)$$

with $2\pi N_{\mathrm{a}} {r_{\mathrm{e}}}^2 m_{\mathrm{e}} c^2 = 0.1535\,\mathrm{MeVcm^2mol^{-1}}$, and

r_{e}: classical electron radius $= 2.817 \times 10^{-13}$cm
m_{e}: electron mass
N_{a}: Avogadro's number $= 6.022 \times 10^{23}\mathrm{mol}^{-1}$
I: mean excitation potential
Z_0: atomic number of absorbing material
A_0: atomic weight of absorbing material
ρ: density of absorbing material
z: charge of incident particle in units of e
$\beta =$ v/c of the incident particle
$\gamma =$ $1/\sqrt{1-\beta^2}$
δ: density correction
C: shell correction
$W_{\max}$: maximum energy transfer in a single collision.

The maximum energy transfer is that produced by a head-on collision,

$$W_{\max} = \frac{2 m_{\mathrm{e}} c^2 \eta^2}{1 + 2s\sqrt{1+\eta^2} + s^2},$$

where $s = m_{\mathrm{e}}/M$, M is the mass of the incident particle, and $\eta = \beta\gamma$.

Formula 1.1 was found quantum mechanically and relativistically. It gives the average ionization loss. Both the *density effect* correction (significant when $\gamma > 1$) and the *shell* *effect* correction (a very small term, only significant when $\gamma \ll 1$) have been parametrized in empirical formulas.

The fluctuation of ionization loss and the distribution of this fluctuation was explained by theories, notably that of Landau [Lan44]. The most probable ionization loss over a small thickness (so that the energy of the incident particle is large compared to the energy loss) of material is also given very accurately by Landau's theory. Other authors [BL50, MFO80, Vav57, SGK$^+$67] have treated this subject taking into account more detailed aspects. The differences between their results and Landau's are mainly in the lower end of the dE/dx distribution when the energy of the incident particle is small ($<$ 3 GeV in the LVD scintillator). The muons reaching LVD have an average energy of 280 GeV; less than 1.6% of them are below 3 GeV. So the Landau prediction for the most probable dE/dx (the peak) in the distribution, which changes very little ($< 1\%$) over the muon energy and track length ranges in the LVD scintillator counters, can be used for the calibration of the LVD scintillator counters, as explained in chapter 4.

This peak coincides with the Monte Carlo prediction taking into account also bremsstrahlung, pair production, and nuclear interactions, besides ionization, as shown in Fig. 1-1. Those three discrete processes, prominent when the muon energy is above 100 GeV, widen the dE/dx distribution, especially its right side, but do not noticeably affect the location of the peak in the LVD scintillator counters in the muon energy range at LVD.

The muon dE/dx [1] distribution at LVD, summed over all muons, regardless of their energy, is conspicuously a Landau distribution. This is indicated in Fig. 1-1. It displays the dE/dx distribution when all these processes are included (pair production has only e^+e^-, but no $\mu^+\mu^-$, which has a much smaller cross section, by a factor 10^{-3}). It is from an LVD Monte Carlo program based on the GEANT3 package [BBM$^+$87], using simulated

---

[1] In this thesis dE/dx is E/L, where E is the measured energy deposited in a counter, L is the length of a reconstructed, straight-line track in the counter.

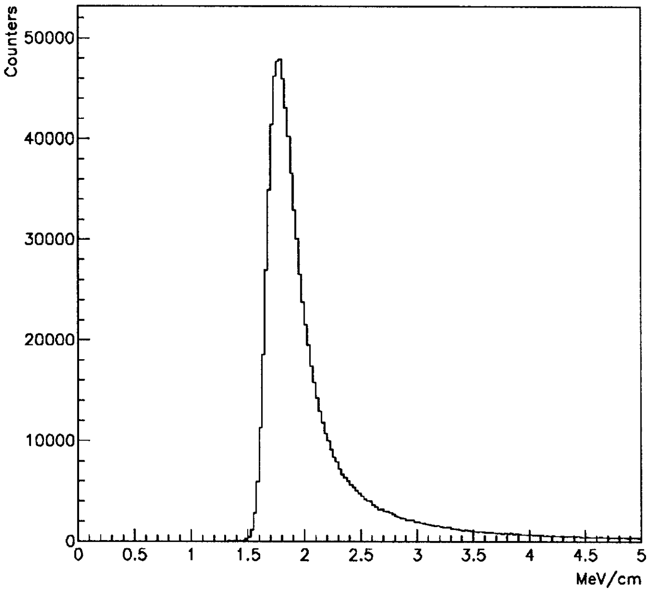

Figure 1-1: Monte Carlo E/L of cosmic muons in the LVD scintillator counters, where E is energy loss in a counter, not including instrumental errors; $L(\geq 50\,\text{cm})$ is length of reconstructed track in the counter.

incident muon angular and energy distributions underground. No errors due to instrumental imprecision are incorporated into it.

Reference [LKV85] contains a more recent account of how the contributions to dE/dx of all the four different processes can be calculated. Bremsstrahlung of the incident particle has been calculated by Bethe and Heitler [BH34] and improved by Petrukhin and Shestakov [PS68]. Electron pair production is calculated by Kelner and Kotov [KK68] and more conveniently parametrized by Kokoulin and Petrukhin [KP71]. The same formula can be used for muon pair production replacing the electron mass by muon mass. Reference [BB81] gives the formulas for nuclear interactions.

1.2 Predicted dE/dx Distribution in LVD Scintillator

The base material of the LVD liquid scintillator has the molecular composition C_nH_{2n+2}, with $\langle n \rangle = 9.6$[2]. Its density is $0.8\,g/cm^3$. Knowing these parameters, and the energy of the incident particle, the Landau dE/dx distribution and its peak can be analytically calculated using eq. 1.1 and eq. 5.4 (see chapter 5). The *density effect* δ is calculated by the formulas in ref. [SBS84]. It cancels out about 60% of the relativistic rise in the first term of eq. 1.1, and almost 100% of the relativistic rise in eq. 5.4. The *shell effect* calculated in ref. [BB64] is insignificant. The calculation is accurate to 2–3% when $E_\mu > 3$ GeV. Table 1.1 shows the energy loss over 100 cm of LVD scintillator by muons of various energies. The second column is the average energy loss due to ionization. The third column is the most probable ionization energy loss by Landau's theory [Lan44, SP71].

Using the differential cross sections for the bremsstrahlung, pair production, and nuclear interaction processes, given in the references [PS68], [KK68], and [BB81] respectively, the average energy loss caused by these processes are also calculated and are listed in columns 4–6 of Table 1.1. The last column in that table is the sum of the average losses by all processes.

The Landau peak of ionization dE/dx , as can be seen in Table 1.1 is almost independent of the energy (3 GeV–10 TeV) of muons when they reach LVD, although the average energy loss increases rather significantly as the muon energy rises. This peak is also almost independent (constant within 3%) of the track length variation in the relevant range (0.5 m–1.5 m) in the LVD scintillator counters.

The location of the dE/dx peak in Fig. 1-1 from the GEANT3 Monte Carlo when all processes are taken into account is slightly higher than the peak of ionization which can be calculated by the explicit formula (eq. 5.4 in chapter 5).

---

[2] During the earlier period of LVD, it was claimed $\langle n \rangle = 10$. The calculation in this thesis uses $\langle n \rangle = 10$, which gives a slightly higher dE/dx in the scintillator.

Table 1.1: Average energy loss (in MeV) through ionization, bremsstrahlung, pair production, and nuclear interaction as a function of muon energy in 100 cm of LVD scintillator.

E_μ (GeV)	Ioni.	Ioni. Peak	Brem.	e^+e^-	Nucl.	Total
1.	177.	168.	0.0262	0.00238	0.00263	177.
3.	192.	169.	0.112	0.0416	0.00865	192.
5.	199.	169.	0.213	0.110	0.0149	199.
7.	203.	169.	0.321	0.188	0.0212	203.
10	207.	169.	0.494	0.337	0.0309	207.
20.	214.	169.	1.12	0.944	0.0635	216.
50.	222.	169.	3.24	3.17	0.163	228.
100.	227.	169.	7.12	7.60	0.330	242.
200.	233.	169.	15.4	17.5	0.666	266.
500.	239.	169.	42.0	49.6	1.67	332.
1000.	244.	169.	88.3	106.	3.34	442.
2000.	249.	169.	184.	221.	6.66	661.
5000.	255.	169.	478.	572.	16.5	1323.
10000.	261.	169.	976.	1160.	32.8	2429.

This singular feature of a relatively constant peak dE/dx is utilized in the calibration of the LVD scintillator counters. This is done by scaling horizontally the Monte Carlo E/L distribution to best fit the observed part (at low statistics) of the whole distribution in a counter. The best scale found is the *gain* of the counter. The energy loss E calculated in the Monte Carlo is randomly smeared by a Gaussian to account for instrumental errors. The only other assumption is that almost all charged tracks through LVD are muons. After calibration the lower side of the dE/dx distribution is investigated for possible WIFs. The linearity of the counters will be tested using a method discussed at the end of chapter 4.

1.3 Experimental Searches for WIFs

Many experiments on cosmic rays have been done to look for new particles or new phenomena. They have discovered e^+, μ, π, and strange particles. Different types of experiments have been performed on accelerators, cosmic rays (above and below the ground), and stable matter, searching for free quarks or other free fractionally charged particles [Lyo85].

In particular, experiments have been done underground looking for fractionally charged particles in primary cosmic rays or their secondaries produced in the atmosphere [K^+84, B^+91a, A^+94a]. Such particles are assumed to be Weakly Interacting besides being Fractionally charged, to be observable by their electromagnetic interaction with matter, and so can be called WIFs. There have been theories postulating their existence. One example is unconfined, color singlet particles of fractional charge in superstring models in which a grand unified O(10) or E_6 gauge group is broken [WW85].

1.4 The Search for WIFs Using dE/dx

The most typical method of looking for fractionally charged particles is to use the low dE/dx feature of their energy loss in material. This is because dE/dx is proportional to the square of the charge carried by the incident particle. Such experiments were performed with proportional chambers, water Cherenkov detectors, and scintillator counters.

Scintillator provides an unambiguous method for detecting WIFs. The distinction of the LVD experiment is its large volume of sensitive material—liquid scintillator, plus the fine tracking capability of limited streamer tube layers sandwiched horizontally and vertically among the scintillator counters forming a three-dimensional grid.

This experiment reconstructs charged particle tracks through the detector from the tracking signals (hits) they create while traversing the streamer tubes in the tracking system of LVD. Programs developed for this thesis find the energy (E) deposited in the scintillator counters along a track and calculate the track length (L) inside each scintillator counter. The search for WIFs in this thesis uses the dE/dx method, namely examining E/L. The technique will be described in detail.

1.5 Thesis Objective

The precision of the measurement of energy loss in the LVD scintillator depends on the stability of the system, and uniformity among the counters. The different amplification or *gain* factors of the individual counters are calibrated within time periods in which these factors are considered constant and there is in addition sufficient statistics in a dE/dx distribution for each counter to measure the *gain*.

In the LVD experiment, the *gain* factors of liquid scintillator counters are determined directly by experimental data of reconstructed cosmic muons, not by any additional data from other calibration techniques. Because of the low rate of cosmic muons at LVD, data from more than a few days are needed to obtain sufficient statistics in each calibration period. In each such period the *gain* of a counter is assumed to be unchanging, within the precision of this calibration.

A further step in gain factor correction takes into account the peculiar geometry of the LVD scintillator counter—a bulk volume ($1\,\mathrm{m}\times 1\,\mathrm{m}\times 1.5\,\mathrm{m}$) with three photomultipliers of 15 cm in diameter, all on one side. To account for this geometrical nonuniformity, tracks going through the counter in different ways are grouped into different units, the dE/dx distribution in each unit is then calibrated against a template distribution. Because of low statistics, the geometry (including the liquid scintillator, the counter inner surface properties, and the relative gains of the 3 photomultipliers) of all counters is assumed identical. Data from all counters, after being corrected by the counter-by-counter gain factors, are used in the unit by unit correction. This is described in detail in this thesis.

In the search for WIF particles at LVD, tracks clearly separable from noise and from other tracks[3] in the same event are selected from all events first processed by the LVD track reconstruction program. A track is selected on the basis of the tracking data and

---

[3] The percentage of multi-muon events in all reconstructed ones is less than 5%, so for simplification in the final analysis only single-muon events are used.

geometrical features of the event with no reference to the dE/dx of the scintillator counters along the track. This is a crucial point for preventing biases in the search for WIFs. The dE/dx of these tracks in any scintillator counter is then calculated using the track and detector geometry and the results of scintillator *gain* calibration.

Specifically, the following are the objectives of this thesis:

1. Calibrate the scintillator counters, obtaining the gain factor of every counter as a function of time.

2. Find the geometrical corrections to the gain of the counter for tracks entering the counter in different locations and directions.

3. Compare the dE/dx distribution of muons in the LVD scintillator with the Monte Carlo predictions, and determine the precision of the dE/dx measurement.

4. Based on the summed single-counter dE/dx distributions used as single-counter dE/dx probability density functions, and the assumption that the different counters along a track are independent of each other in dE/dx , a function is found[4] (details in chapter 6) that can be used to systematically search for WIFs.

5. If the result of the search is negative, calculate the acceptance of the detector for a uniform distribution of WIFs and establish an upper limit on their flux.

The thesis contains seven chapters. Chapter 2 describes the LVD detector. Chapter 3 describes the track reconstruction technique at LVD, based on work by E. Hafen. Chapter 4 explains the calibration procedures. Chapter 5 illustrates the dE/dx distribution of muons in LVD scintillator and compares it with Monte Carlo simulation. The search for WIFs is described in Chapter 6. The WIFs search results from this thesis and comparison with those from some other underground experiments are given in Chapter 7.

---

[4] Also see ref. [PP93].

Chapter 2

The LVD Detector

LVD is a large volume underground experiment composed of liquid scintillator counters and a tracking system of limited streamer tubes. When the whole detector is completed, it will contain 5 identical towers arranged next to each other along the axis of the experimental hall. Since July 17, 1992 the complete first tower at the northwest end of the hall has been operating.

Besides the search for WIFs, the physics capabilities of the detector also include the detection of stellar collapse in our galaxy [A^+92a] by neutrino signals (which is the foremost purpose of the experiment), neutrino oscillations, supersymmetric proton decay, boron neutrinos from the sun, astrophysical neutrino-emitting point sources, dark matter and massive monopoles, muon distributions [A^+94b], muon bundles and hence some determination of the primary cosmic ray composition, etc. A general description of the whole detector and its physics objectives is given in references [A^+86, B^+89]. This chapter describes in detail the first tower of the detector, concentrating more on the aspects related to the measurement of muon dE/dx and the search for WIFs.

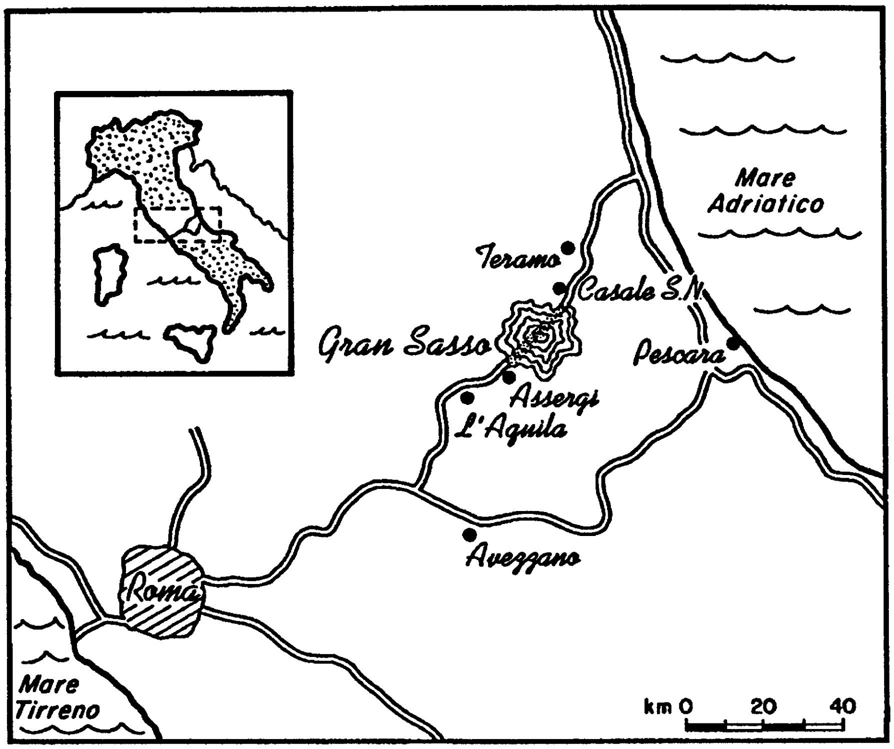

Figure 2-1: Location of LVD, in the tunnel under the Gran Sasso Mountain, central Italy.

2.1 Overview of the LVD Detector

The LVD detector is located in one of the three large underground halls (Hall A) of the Gran Sasso National Laboratory [Zic81, Zic] of Italy, one branch of INFN—National Institute for Nuclear Physics. The laboratory is 137 km northeast of Rome, near the village of Assergi in the Abruzzo region of central Italy (Fig. 2-1). It is under the Gran Sasso Mountain (Fig. 2-2). The underground halls for experimental equipment are beside one of the two tunnels along the Rome–Teramo highway (Fig. 2-3). Its geographical coordinates are 13°34′28″E (from the Greenwich meridian) and 42°27′09″N. The altitude is 963 m above the sea level. The rock overburden is about $3200\,\mathrm{hg/cm^2}$ at minimum. This rock overburden attenuates the cosmic ray flux by about a factor of 10^6, significantly reducing the background for the detection of cosmic neutrinos or other rare events. At this depth only muons and neutrinos are able to reach the LVD experiment from the atmosphere. Fig. 2-4 shows the average

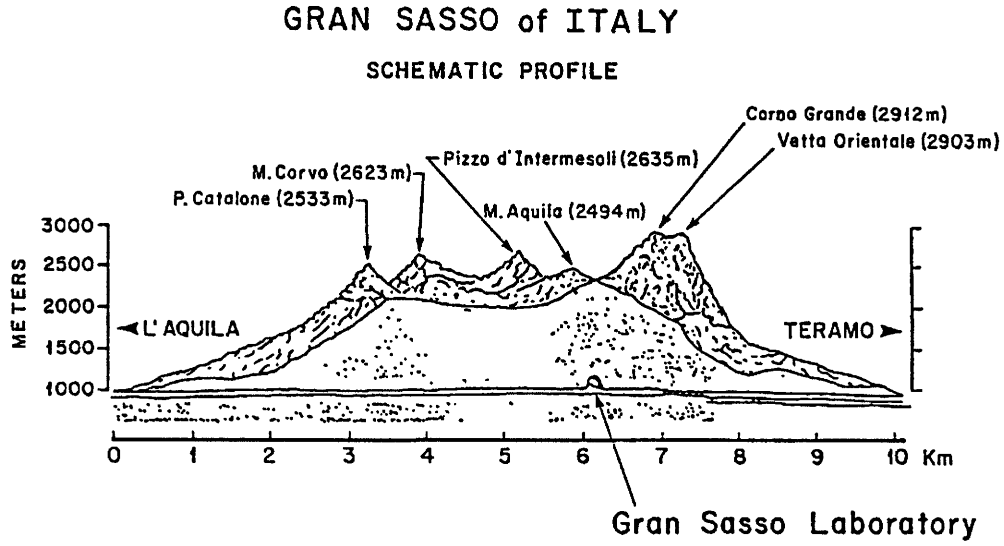

Figure 2-2: The Gran Sasso Mountain above the laboratory.

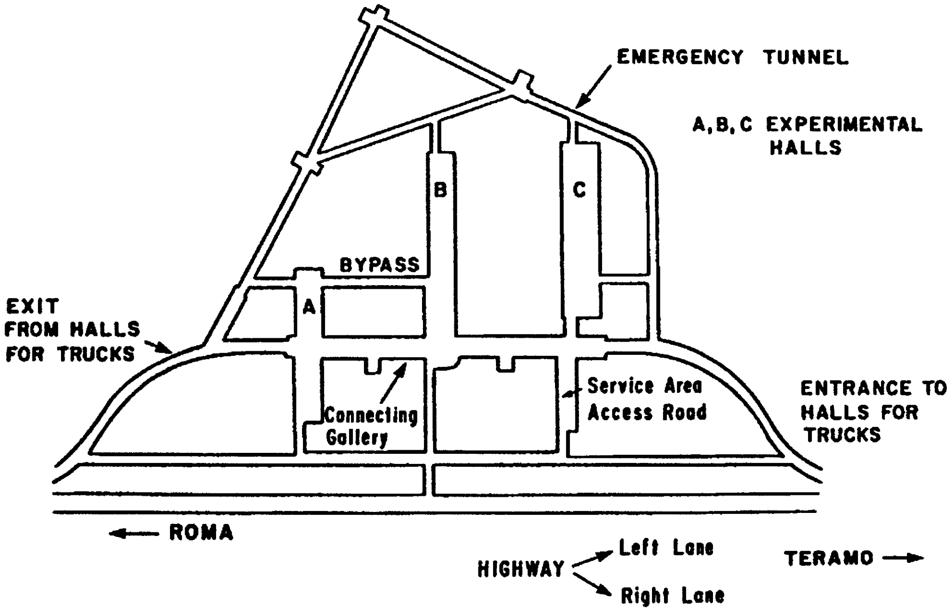

Figure 2-3: The Gran Sasso National Laboratory of INFN, LVD is in the upper half of Hall A.

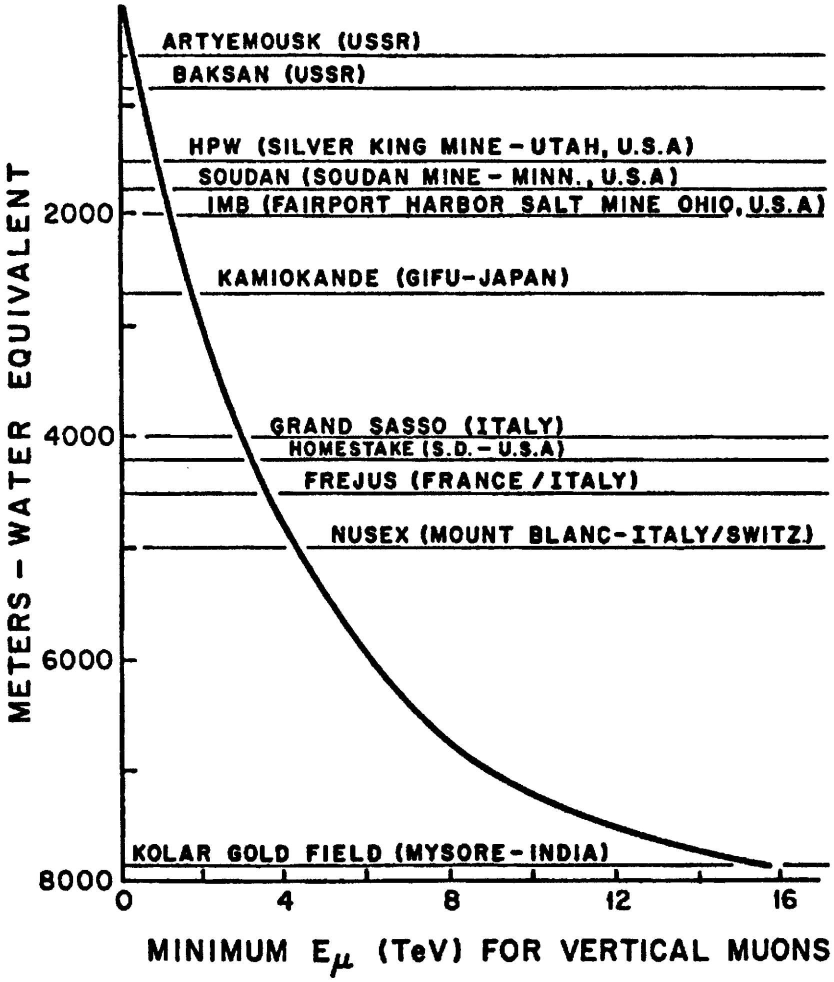

Figure 2-4: Vertical depths of underground laboratories.

depths of some underground laboratories. LVD is about twice as deep as Kamiokande.

The detector has a modular support structure. The whole detector is divided into 5 towers along the y-axis of the LVD coordinate system, as shown in Fig. 2-5. Each tower, composed of 38 modules, is divided along the x-axis into 5 columns, and in the vertical (z-axis) direction into 8 levels. The top level is only in the 3 center columns because it has reached the arched ceiling of the experimental hall.

Each module (Fig. 2-6), of dimensions 2.2 m×6.2 m×1.2 m, consists of a steel tank carrier (named portatank) which contains 8 liquid scintillator counters (each enclosed in a 4 mm

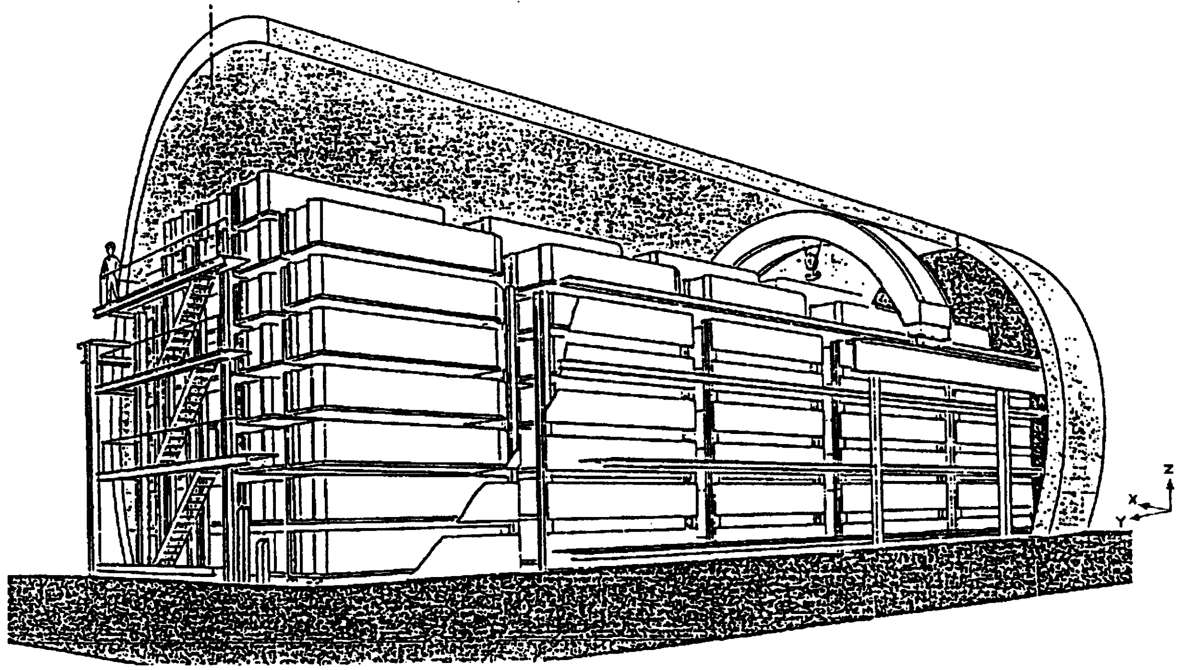

Figure 2-5: General view of LVD.

thick stainless steel tank), and provides mechanical support to two layers of limited streamer tubes and their readout strips on its southwest side vertically and beneath its bottom horizontally. The streamer tubes are first mounted on an L-shaped structure [A^+93] (named hood) of horizontal and vertical panels before being attached to the portatank. The support module rests at its four couners on small plates welded to vertical I-beams in the steel support structure of the detector. The module contains 9.6 tons of scintillator and 6.7 tons of steel.

The separation between towers is 2.0 m, between columns is 0.55 m, and between levels is 0.30 m. Starting from the ground level, the horizontal double-layer of streamer tubes under every second module is wider than the intervening double-layers by 0.51 m (6 more streamer tubes), thus filling the gap between two columns of modules while allowing human access to the detector components (Figs. 2-7 and 2-8).

The dimensions of the complete detector will be 13.2 m×39.4 m×11.8 m

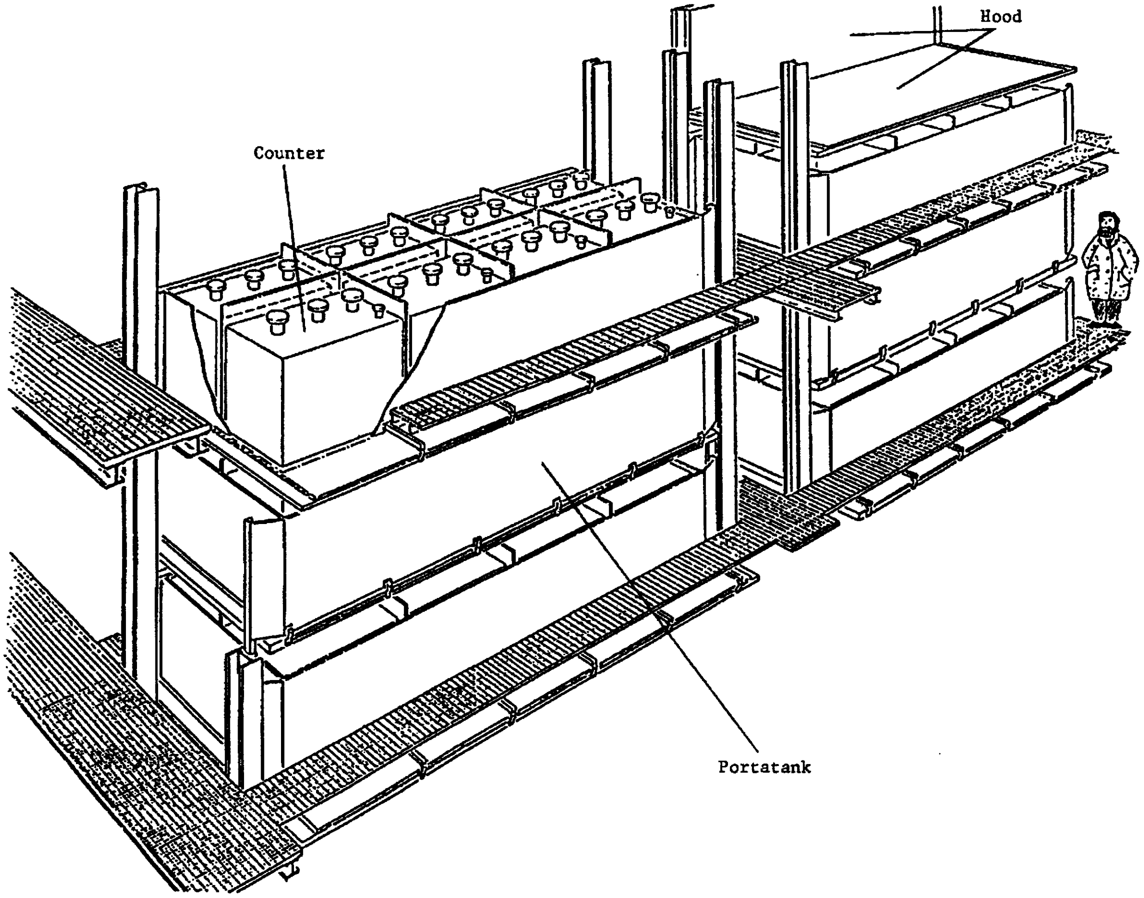

Figure 2-6: Modular structure of LVD.

(width×length×height). Its geometrical acceptance for isotropic particles will be $\approx 7000\text{m}^2\cdot$sterad.

Since February 9, 1992, while the installation was continuing, the first tower gradually became active and a growing fraction of it was producing data. On June 17, 1992, installation of the whole first tower was completed. Full tower data acqisition continued from that time till this day, except for the period between November 20, 1992 and January 11, 1993 during which the tracking system was not functioning while a nonflammable new gas mixture was introduced and some of the corroded high voltage connectors were replaced. The scintillator system underwent overall changes and adjustments in the photomultiplier readout impedence, high voltages, and readout thresholds, starting from May 31, 1993.

Table 2.1: Characteristics of Tower 1.

Characteristic	Value
Area	$660\,\mathrm{m}^2$
Geometric Acceptance	$\simeq 1700\,\mathrm{m}^2$·sterad
Length × Width × Height	6.8 m × 13.2 m × 12 m
Scintillator Volume	$456\,\mathrm{m}^3$
Scintillator Mass	360 tons
Steel Mass	360 tons
Tracking Channels	17,408
Streamer Tubes	2,928
Tracking Spacial Resolution	$\simeq$1 cm
Angular Resolution	$\leq$4 mrad [Haf89a]
Energy Resolution	15% at 10 MeV [A^+92a]

Data from the first tower in the two periods July 1, 1992–November 19, 1992 and January 11, 1993–May 30, 1993 are used in the analysis of this thesis.

The characteristics of the 1st tower are listed in Table 2.1.

Fig. 2-9 shows the active elements of one tower.

2.2 Limited Streamer Tubes and Readout System

A single LVD limited streamer tube [Iar83] (LST) is 6.3 m long, 8.15 cm wide, and 1.1 cm thick (Fig. 2-10). It has 8 parallel cells, within the 8 consecutive U's of the extruded PVC profile coated with a resistive graphite paint (0.08–2 MΩ/cm). The profile structure is enclosed in a PVC tube and two small end caps (with connections for high voltage and gas flow). Each cell has a $9 \times 9\,\mathrm{mm}^2$ active cross section, and a silver-plated $\phi\,100\,\mu$m Be-Cu anode wire stretched along the center of the cell. The 6.3 m long anode wires are attached to a plastic bridge (Fig. 2-11) every 0.5 m along its length and soldered at the two ends to printed circuit boards.

Because not all the tubes have the same plateau, the high voltage is applied to the anode wires through manifolds, each of which feeds 12 tubes. The high voltage (4.7 kV) applied to the wire is close to the knee of the limited streamer mode plateau (Fig. 2-12) to ensure that no tube is operating beyond the plateau and discharging.

Before November 20, 1992, the gas mixture in the tubes was argon and isobutane (1:3 by volume). After that time, a nonflammable mixture of carbon dioxide, isobutane, and argon (88:10:2 by volume) has been employed.

The critical ingredient of the limited streamer tube is the thin, diluted carbon coating painted on the surface within the $1\,\mathrm{cm}\times 1\,\mathrm{cm}$ U's of the plastic profile in the tube. This carbon coating is connected to the ground of the high voltage supply. The property of this carbon coating to a large extent determines the characteristics of a tube. It is not only the amount of carbon per unit area and the surface conductivity that affect the performance; the type of the carbon particles used in the paint also determines whether a tube may function or not [Pyr91].

The aluminum readout strips (Figs. 2-13 and 2-14) placed outside the plastic casing of the tube are 4 cm wide. The X-strips (measuring the x-coordinate) are as long as the tube, 6.19 m, parallel to the wires. They are placed under the streamer tubes in the horizontal layers, 2 strips covering each tube of 8 streamer cells. The Z-strips (measuring the z-coordinate) are the same as the X-strips. They are placed beside the streamer tubes in the vertical layers. The Y-strips (measuring the y-coordinate) are perpendicular to the wires and are L-shaped (Fig. 2-15), each strip covering both the vertical and the horizontal layers of streamer tubes around a module[1]. They are 1.02m long on the vertical side, and either 2.05 m or 2.56 m (when they are in a wide horizontal layer) long on the horizontal side. The X-strips parallel to the anode wires have a higher probability to pick up a signal, so they are placed below the U's of the carbon-coated profile inside the streamer tube. The Y-strips are on the other side of the tube where the signal amplitude is higher.

The tubes of the 2 layers (and hence also the X-strips) in a double-layer (called a plane)

---

[1] This feature reduces the total number of readout channels in the tracking system, and hence their cost, by 43%.

are staggered by 1.5 cell widths (Fig. 2-8), approximately half the strip width. The Y-strips of the 2 layers are staggered by half the strip width, 2 cm. This increases the spacial resolution and overall efficiency of the tracking system, yielding an effective strip width of about 2 cm and an angular resolution less than 4 milliradians [Haf89a], with no dead gaps. The two tracking layers in a plane are shielded from each other and from the portatank by aluminum-coated (in wide stripes) PVC boards connected to ground.

The dimension of the tracking system of the whole tower is 13.2 m ×6.2 m×11.8 m (x-y-z). It has 8 horizontal double-layers (a sandwich of 4 wide modules and 4 narrow modules) and 5 vertical double-layers of streamer tubes. Its geometrical acceptance for isotropic particles is[2] 1700m^2·sterad.

The numbers of readout strips are listed in the following (note there are 2 horizontal and 2 vertical layers in a module; in one tower there are 22 modules with a narrow horizontal panel, and 16 modules with a wide horizontal panel; the vertical panels are identical):

X-strips:

narrow module	*wide module*	*whole tower*
48/layer	60/layer	4032

Z-strips:

module	*whole tower*
24/layer	1824

Y-strips:

module	*whole tower*
152/layer	11552

---

[2] Throughout this thesis, tracks with less than 3 points of tracking readout signals on them are rejected. The reduced acceptance is calculated in section 6.4.

module by module, the total numbers of X-, Y- and Z-strips are

448 when horizontal layers are narrow,
472 when horizontal layers are wide.

The electronic readout from the strips are module by module. The strips are connected individually to the amplifier and shift register elements on a board called SGS card (from the Italian firm Thomson-SGS). All the strips (448 in narrow hood, 472 in wide hood) in a module are connected to one shift register (parallel-in, serial-out) formed by 16 SGS cards (32 channels per card).

The logical signal indicating a pulse from a strip over the threshold is held by a one-shot for $2.5\,\mu$s. When a trigger signal comes within this period, these one-shot signals will be latched into the shift register and then the content of the whole shift register is in series read out by a CAMAC module called STROC (Streamer Tube Readout Card, designed at Padua University) [C$^+$92]. Eight such shift register chains are connected in parallel to a line driver, which is connected to a STROC module. These 8 shift registers are read out in parallel.

At the far end of each shift register chain there is a pattern generator card which is used to test and ensure the integrity of the data. In any one event, when the pattern bits read out from a module are different from their preset contents, the data from that module are not used.

The X-strip signals, before they are latched into the shift register by a trigger signal, are first OR-ed on the SGS card and a trigger fan-in card on each hood to form 4 logical-OR signals (from 2 horizontal layers and 2 vertical layers). These 4 signals from every module are used by the tracking trigger system.

Fig. 2-16 is a block diagram of the tracking data acquisition electronics.

2.3 Liquid Scintillator and Readout Electronics

The base material of the liquid scintillator used at LVD is C_nH_{2n+2} ($\langle n \rangle = 9.6$). It is extracted from an oil well in Russia. The activator PPO (1 g/l) is added for scintillation, and POPOP (0.03 g/l) used as wave length shifter is added in a laboratory in Ukraine. This liquid scintillator [VDR70] is similar to that used at Artyomovsk [B^+79], Baksan [A^+79], and Mont Blanc [B^+84] underground experiments. The properties of this scintillator are: $\rho = 0.8\,\mathrm{g/cm^3}$, attentuation length $> 15\,\mathrm{m}$ ($\lambda = 420$ nm), decay time = 5ns, light output equivalent to that from standard plastic scintillator.

The Russian members of the LVD collaboration developed a modular counter (Fig. 2-17) for the liquid scintillator. It is a 4 mm thick stainless steel container of inner dimensions 149 cm×99 cm×98 cm. The internal surface of the steel walls is covered with aluminum-plated mylar film for the reflection of scintillation light. Three photomultipliers of 15 cm in diameter (FEU-49B, built in Russia) are mounted on top of a counter at the 7 cm thick plexiglass windows. The quantum efficiency of the photocathode is 10–15%. For an energy loss of 1 MeV in a counter, the effective number of photoelectrons at each phototube is 5.7±0.5 [Rya92].

Eight such counters are placed inside one support module in LVD. In the whole LVD experiment there will be 1820 tons of liquid scintillator. In one tower the amount is 364 tons.

The coincidence sum of the output from the three phototubes on a counter, when each of the three signals passes threshold, is read out by CAMAC electronics. This technique effectively eliminates phototube noise. The signals are first sent to a discriminator module C175 before the fast ADC/TDC module C176. Both C175 and C176 have 8 independent channels, convenient for 8 counters in a portatank. They are made by the Italian firm CAEN.

Each of the 8 independent channels (Fig. 2-18) of the discriminator module C175 has 3 inputs for the 3 photomultipliers on a scintillator counter. There is a wide-band amplifier

(46 dB) at each input. The 2 different thresholds at each input: the high threshold at about 7 MeV, the low threshold at 0.8 MeV (1.5 MeV up to June 1993), are set through a 6-bit DAC via CAMAC. The 3 inputs for a counter are set separately. Any of the 6 logic signals indicating an input above the threshold (Ha, Hb, Hc, La, Lb, Lc) can be disabled by online software when the channel is found malfunctioning before a run of data taking.

The 3-fold coincidence signals HIGH and LOW (high-threshold coincidence and low-threshold coincidence respectively) go to the gate logic of C175 (Fig. 2-19). The logic generates a "general OR" from the 8 HIGH signals of 8 counters connected to that module. This "general OR" opens for 1 ms a window for a LOW signal of any channel in the module to generate a gate signal. The HIGH signal generates the gate signal for a counter by itself. The gate starts the fast ADC/TDC of C176 in that channel, which uses the linear sum of the 3 inputs, also provided by C175, as the input to ADC.

The level of high threshold is determined by the natural radioactivity background in the laboratory. The 1 ms window opened by a high threshold signal to low threshold signals is to capture the neutrino event

$$\begin{array}{rcl} \tilde{\nu}_{\mathrm{e}}\, p & \rightarrow & n\, e^{+} \\ & & \downarrow \\ & & n\, p \rightarrow D\, \gamma \end{array}$$

which has a prompt high-threshold signal followed by a delayed (mean life time $\tau \approx 185\,\mu\mathrm{s}$) 2.23 MeV low threshold signal from the γ.

Because an event which generates a high-threshold signal in one counter very often deposits energy in other counters, the 1 ms window opened to low-threshold signals is also sent to neighboring C175 modules by back-panel connections. The arrangement of these connections is by dividing the whole tower into 4 "quarter"s, lower-right, lower-left, upper-right, upper-left, each containing 10, 10, 9, 9 modules respectively (80 or 72 counters), the "general OR" of one module is sent to all the other modules in the same quarter. Therefore any counter that has a high threshold hit will allow the low threshold hits in all the other counters in the same quarter to be recorded. This happens by the front-end electronics itself, before any trigger signal arrives. The trigger signal starts the readout of the C176 memory. The C176 has a FIFO memory for the ADC and TDC data of 512 hits, shared by the 8 independent channels in the module.

The electronics block diagram for a single counter is shown in Fig. 2-20. Note that the dynode signal "pm D" and its readout ADC, for very high energy deposit, is not currently implemented.

The "general OR" from any C175 module is also the scintillator trigger signal, which goes to form the Master Trigger with the tracking trigger.

Every signal going into the C176 fast ADC/TDC is flagged by its HIGH status (indicating whether there is a high-threshold coincidence among the 3 inputs of a channel; if not, it is from a LOW gate) regardless of its being the initial HIGH signal which opens the window and generates the scintillator trigger or being a subsequent one in the same event, or a previous one left over[3].

Only signals above the high threshold (about 7 MeV) are used in this analysis. This is done by checking the High/Low flag bit in the 48-bit ADC and TDC data of each scintillator hit. The low threshold hits are mostly from the radiation background.

2.4 Data Acquisition System

The front-end electronics of the LVD data acquisition system for the first tower is based on CAMAC modules. For speed of CAMAC access a STARBURST module (containing a PDP J-11 cpu) inserted in the CAMAC system crate is used for the first stage readout and

---

[3] Because there is a preset maximum of 50 hits to be read out from each C176 module after a trigger, to save the readout time, there is a very small possibility of leaving some hits to the next readout. It is found in a small sample of data that this happens less than once in 500,000 events. A label is being designed to indicate where it happens in the raw data from the data acquisition system.

data assembling.

The trigger is formed by a logical OR of the scintillator trigger and the tracking trigger.

The scintillator trigger is generated at the back of the C175 discriminator modules whenever there is a high-threshold coincidence signal HIGH from any counter.

To form the tracking trigger, the 4 logical OR signals from each hood, provided by the SGS cards and the fan-in card, are used by CAMAC logical modules to generate *Layer* signals and *Plane* signals. A *Layer* is a single layer of streamer tubes through the whole tower. Vertical and horizontal layers are distinguishable at this early stage because only X-strip logical OR's are used for the trigger. A double-layer is a *Plane*. A programmable tracking trigger is formed from these *Layer* and *Plane* logical OR's. The logic adopted most of the time is a *Layer* majority 4. When the number of *Layer*s containing hits on the X-strips are ≥ 4, there will be a tracking trigger.

A master trigger is the OR of the scintillator trigger and the tracking trigger. This trigger is sent through the tracking line driver cards to the SGS cards to latch the one-shots of all aluminum strip channels into the shift registers. It also starts the CAMAC data readout by the STARBURST module, which is also located in CAMAC crate, from all CAMAC modules in the tower. The scintillator data stored in the FIFO memory of the C176 module are read out module by module in series. The contents of the shift registers containing the hit tracking strip addresses and the preset pattern words are read out by the STROC module. 5 STROC modules, each connected to 8 hoods in parallel, provide the tracking data of the whole tower.

The data are then stored in one of the two memory buffers in STARBURST, which signals to the *tower* μVAX sitting next to it in the electronics rack when any one of its two buffers has data. The *tower* μVAX, using the facilities of the MODEL package from CERN [B^{+}91b], transfers the data in a STARBUST buffer into its own memory buffer. It then assembles the data adding geometrical and universal clock time information. This *tower*

μVAX is connected to CAMAC through Q-bus. It also initiates all the CAMAC modules, especially the programmable logic modules, before a run is started.

In the present design of the LVD data acquisition system [F^{+}89], the *tower* μVAX sends data via Ethernet to the *boot node* μVAX, which assembles data of an *event* from the *tower* data, adding more information, such as VAX time, program and format version numbers, and special blocks of data such as calibration parameters of the scintillator ADC's. The data are assembled in EPIO [GM 2] format at the boot node and written to a disk file.

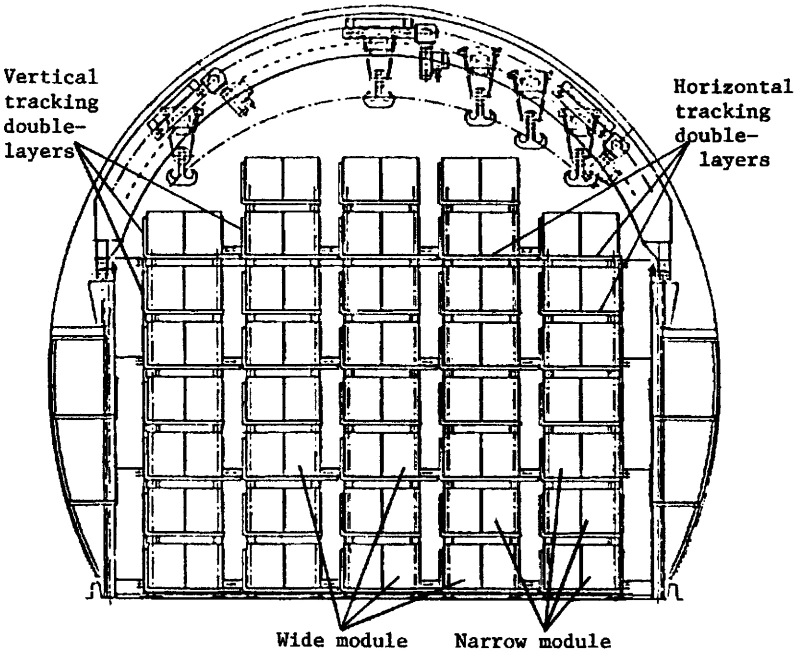

Figure 2-7: LVD viewed along the axis of Hall A.

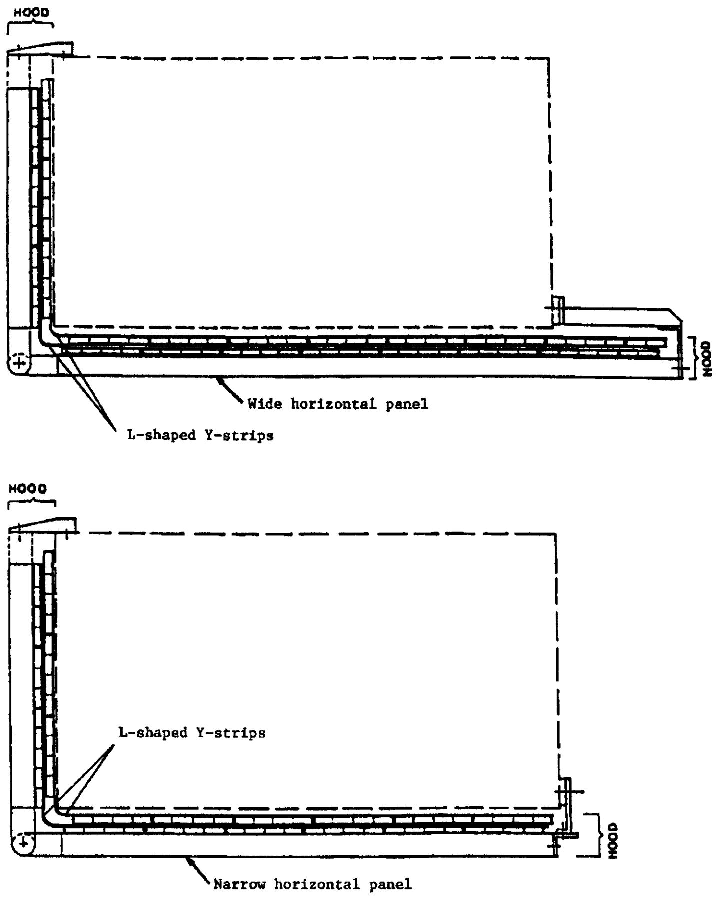

Figure 2-8: Narrow and wide modules.

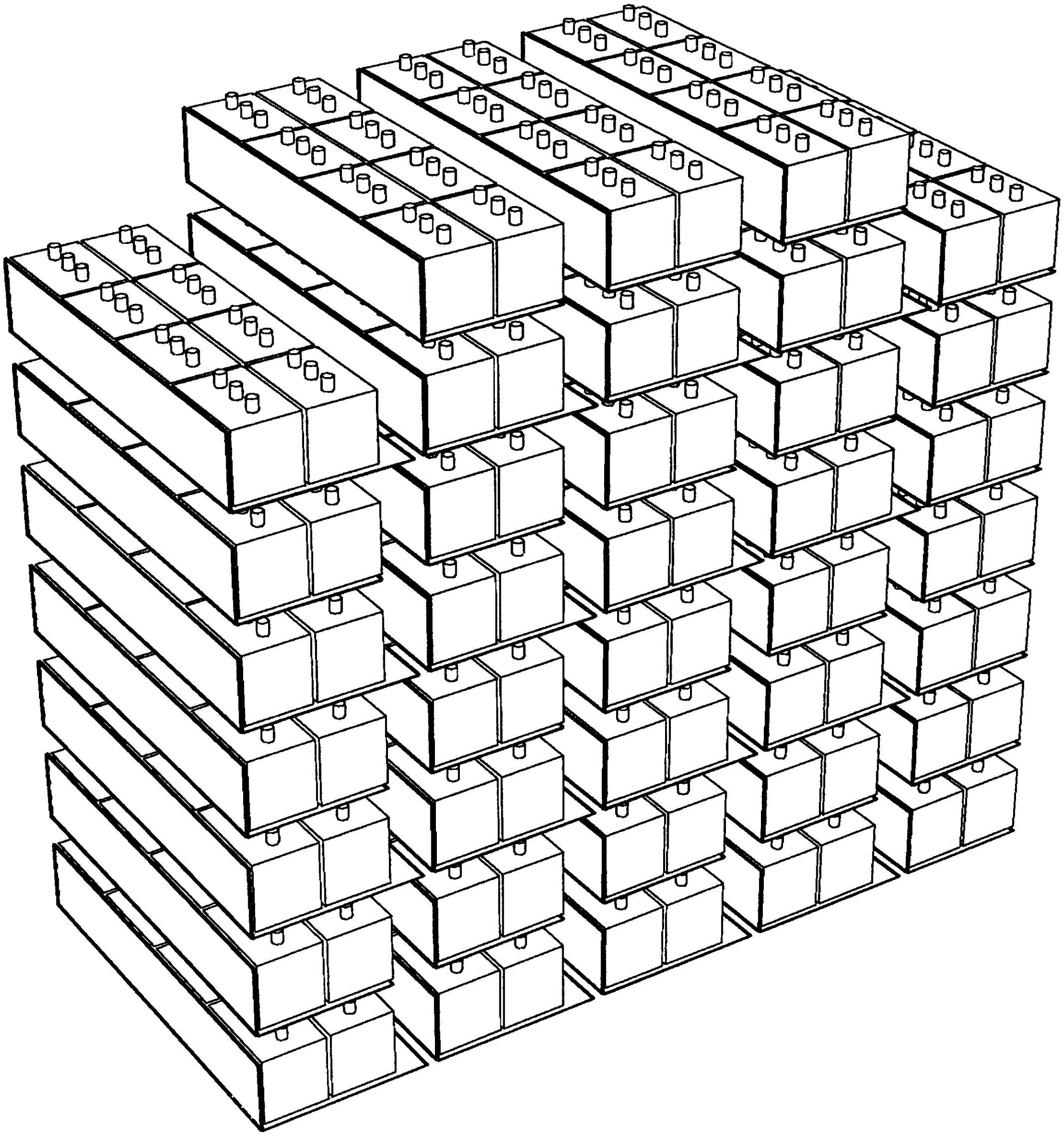

Figure 2-9: The L-shaped tracking panels (each containing two independent layers of streamer tubes and their readout strips), scintillator counters, and the photomultipliers, in one tower.

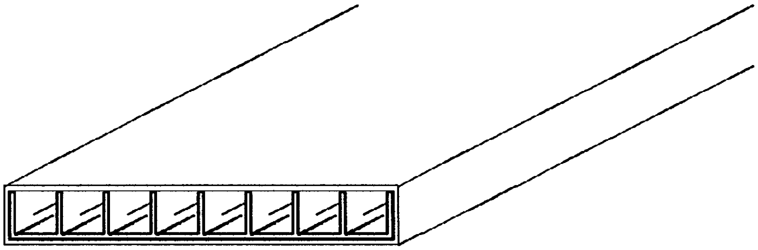

Figure 2-10: Limited Streamer Tube used in LVD.

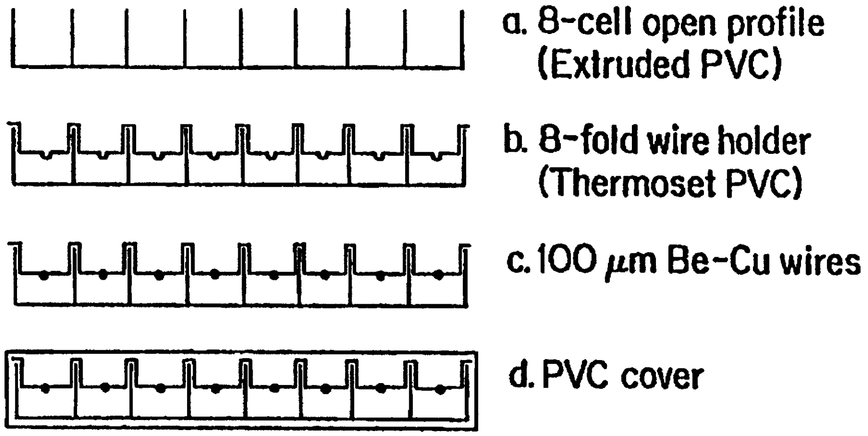

Figure 2-11: Inside a streamer tube.

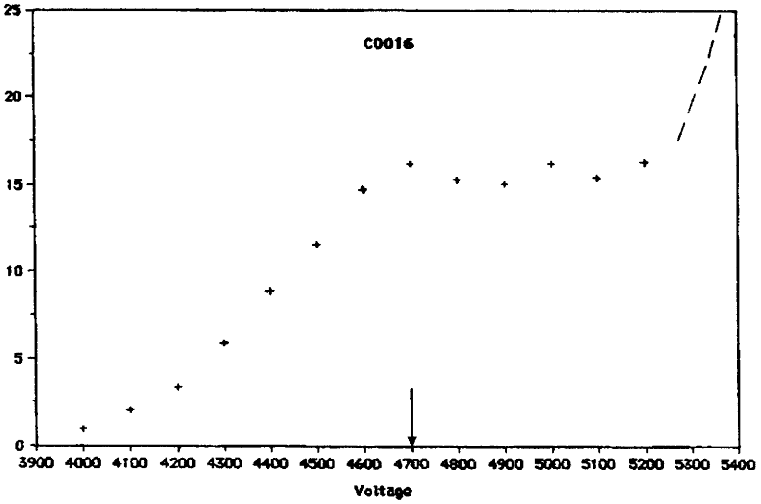

Figure 2-12: The plateau (with gas mixture Ar : isobutane = 1 : 3) of one tube in a horizontal layer inside a hood in Hall A.

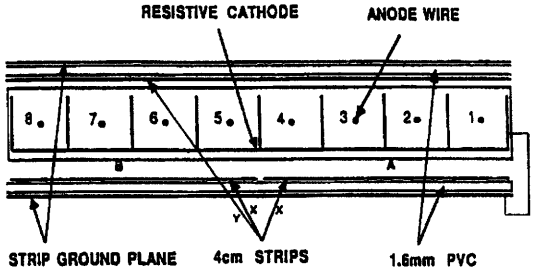

Figure 2-13: The pickup strips outside a tube.

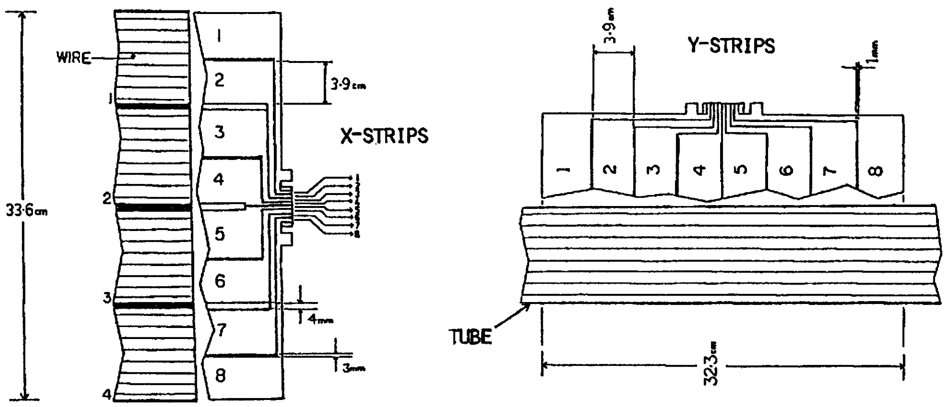

Figure 2-14: The pickup strips.

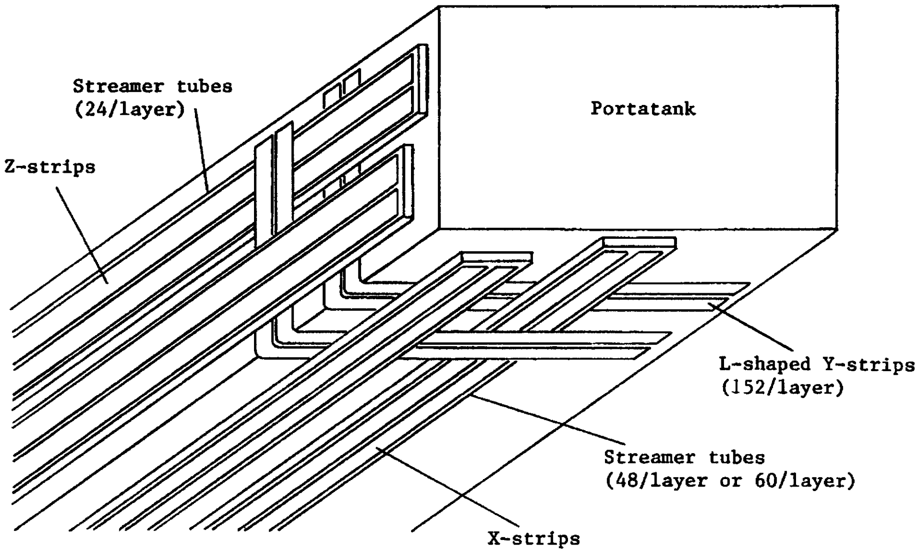

Figure 2-15: The streamer tubes and their pickup strips around a module (the widths of the tubes and strips are not in proportion in this figure, they are magnified by about 10 times). Note that between the X- or Z-strips on the inner layer of streamer tubes and the Y-strips on the outer layer, there is in total about 1 cm of mostly plastic material and shielding.

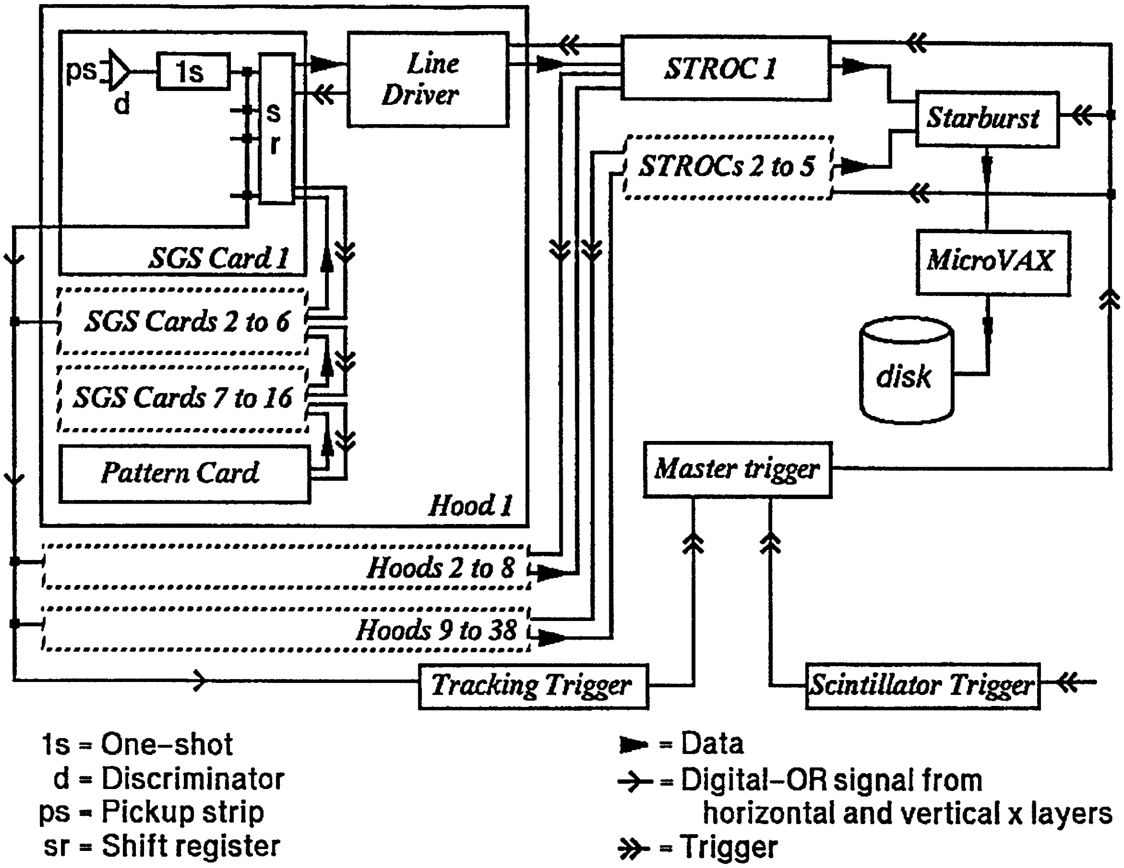

Figure 2-16: LVD tower 1 tracking electronics.

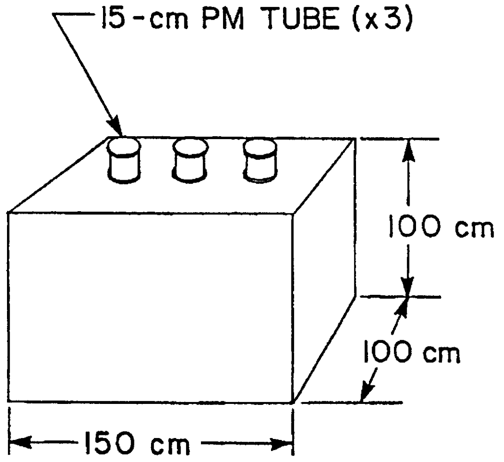

Figure 2-17: A scintillator counter.

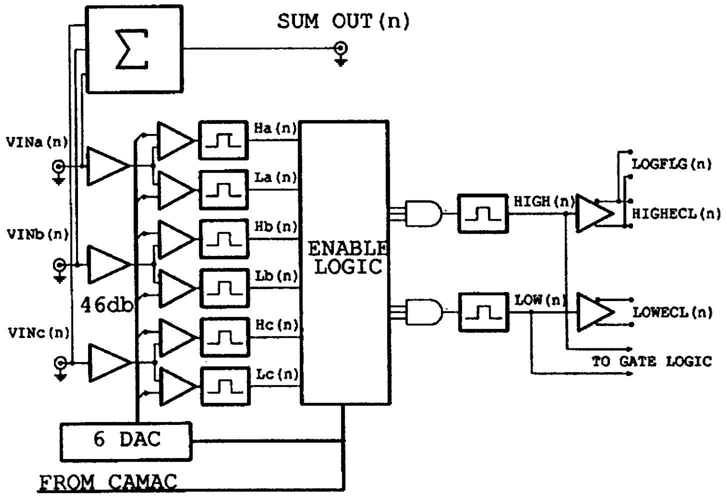

Figure 2-18: The discriminator C175.

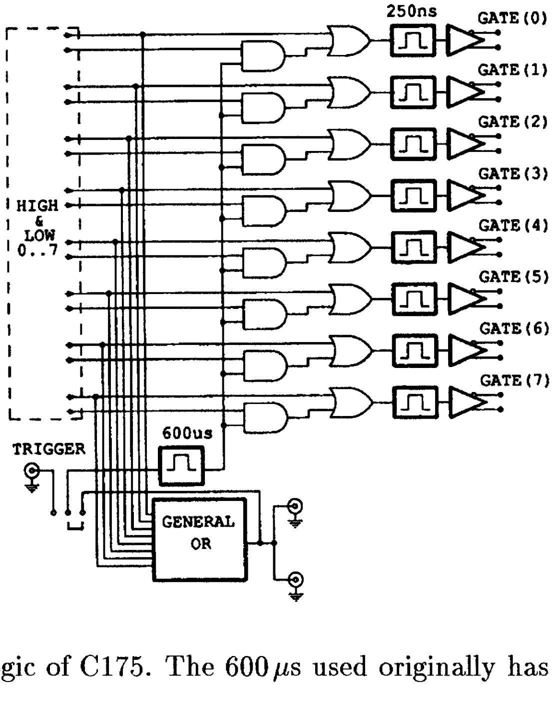

Figure 2-19: Gate logic of C175. The 600μs used originally has been changed to 1 ms.

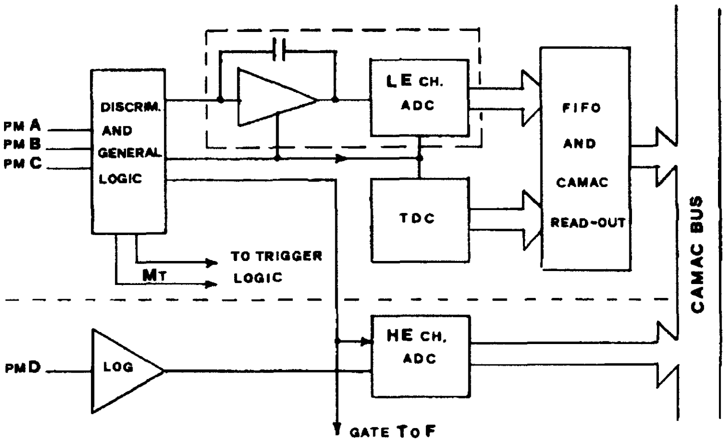

Figure 2-20: Readout electronics of a counter.

Chapter 3

Track Reconstruction at LVD

The LVD is a volume detector without a vertex. The LVD reconstruction algorithm therefore operates on the list of tracking strip hits, selecting from it strings of hits located on a straight line. When there are multiple possibilities, the subset with the smallest number of shared or missed hits is identified as the found tracks.

3.1 Main Features

The program [Haf89a] finds a "master point" (a clean pair of X- and Y-strips, or Z- and Y-strips hit in one plane[1]), then finds another "master" point from a nearby module or from the other, perpendicular panel of the same module (or from a most remote plane in another, complementary search mode), fits a line to the strips in these 2 master points, adds all hits along the line, and fits a track from all selected hits. The procedure iterates, discarding hits that are too far away from the line or are singlets (without a perpendicular hit strip in the same plane and also on the line), until there is no more change in the list of

---

[1] There are 4 strip layers in a plane (which is a double-layer of streamer tubes): X-, Y-, X-, Y- in a horizontal plane, or Z-, Y-, Z-, Y- in a vertical plane. Any 2 hits in 2 crossed strip layers out of 4 are sufficient to form a point; when there are overlapping strips in 3 or 4 strip layers in a plane, they are also a point. A hit in any strip layer is usually a cluster of consecutive strips. The definition of X-, Y-, Z-strips can be found in Fig. 2-15.

hits on the line. The fit is 3-dimensional (see ref. [Haf89b]).

The same procedure continues, with the first "master point" coming from the remaining hits, until the list of hits is exhausted. From all these fitted lines the subset with least missed hits and least conflicts between lines (in a multi-track event) is selected as the reconstructed tracks.

When the detector is operating without inactive or discharging elements, single track reconstruction reaches an efficiency above 99.9% [A^+94b] for high energy muons having at least two tracking points in the detector, provided the muon does not cause a wide shower.

Over 95% of the events reconstructed are single muons [A^+94b]. Multi-muon events are processed up to a time limit of 200 seconds per event on a 25 MIPS cpu. A first pass shows that when multiplicity exceeds 8, about 50% of the events are not completetly processed in 200 seconds. Preliminary tests demonstrate that when large shower events are excluded, further passes allow reconstruction of events of multiplicity above 35 in the first tower of the detector; although the tolerances in the program would be modified in a new pass when the tracking layers are very cluttered.

A short track having only two points on it from the same module is ambiguous, due to the L-shaped Y-strips covering both horizontal and vertical streamer tube layers. This ambiguity cannot be resolved without using additional information from the scintillator counters if any can be used conclusively.

Because only straight-line tracks are searched for, bent tracks of low energy muons are not accurately reconstructed. These are relatively rare, but they introduce some inaccuracy to the measured dE/dx distribution and some background to the search for WIFs.

3.2 Algorithm

The core of the algorithm is the PIPR (arbitrarily named) program for track finding in the LVD. The peripheral routines convert data format from one to another; establish the current status of the detector elements and cross-reference arrays for fast access to related data; check the quality of the data in each event; and do a quick geometrical simulation of any reconstructed track passing the detector taking into account the current status of the detector elements. The result of a quick simulation is compared with actual data in the event in order to accept or reject a track candidate.

The LVD geometry is known to better than 2 cm. Raw data from the tracking system are in the format of hit strip IDs. The IDs are transformed into the spatial coordinates according to the detector geometry. The 3-dimensional fitting routines are based on a set of equations to minimize the deviations between the detector elements and a line [Haf89b]. The fast simulation of a track going through the detector is based on the geometrical relation between a box and a line. The procedure that uses these functional blocks in the track reconstruction follows logical considerations and incorporates the various criteria found out from the testing of the program and from closely examining typical events of different geometries and multiplicities.

3.3 Flow Chart of the Program

Because the track reconstruction program and other offline analysis programs, including Monte Carlo simulations, were developed parallel to the detector construction and the data acquisition system, has a different from the one provided by the online data acquisition system. Before track reconstruction (by the program LVDPIPR), the first step in the analysis of the raw data from online programs is data reformatting. This is combined with detector (element by element) status analysis (Fig.3-1). The detector status variables, found out by comparing hit rates with the average, are used in the fast simulation of muon tracks going through the detector. This is required because the LVD is composed of a large number of elements, some of which were being turned on while others were already operating normally, and because some are not functioning 100% of the time.

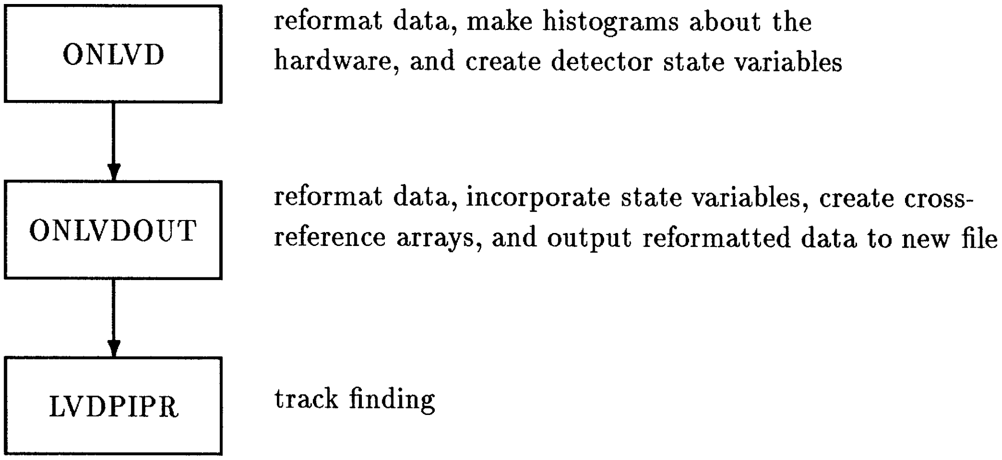

Figure 3-1: Three phases in the LVD track finding.

In the dE/dx measurement and in the search for WIFs, the status of the scintillator counters is tested more stringently. Data from abnormal counters are not used in the calibrated dE/dx distribution. Errors and imprecision are also taken into account in the calculation of probability for the occurrence of a muon track with a set of dE/dx values in the counters it traverses.

The reformatting and status finding programs are named ONLVD and ONLVDOUT. Their flow charts are shown in Figs. 3-2 and 3-3. Their outputs are described in ref. [Haf92].

The flow charts of the LVD track reconstruction program LVDPIPR and its main subroutine block PIPR are shown in Figs. 3-4 and 3-5. Only the main steps more directly connected to the logical flow of data are shown. Most of the auxiliary functional units, for example, those (re)ordering hits and clusters, those finding a "next" "clean" cluster of hits, and those used in the 3-dimensional track parameter fit (based on a set of equations of second-order regression calculation), are not shown. In Fig. 3-5 the vertical lines on the left side indicate do-loops.

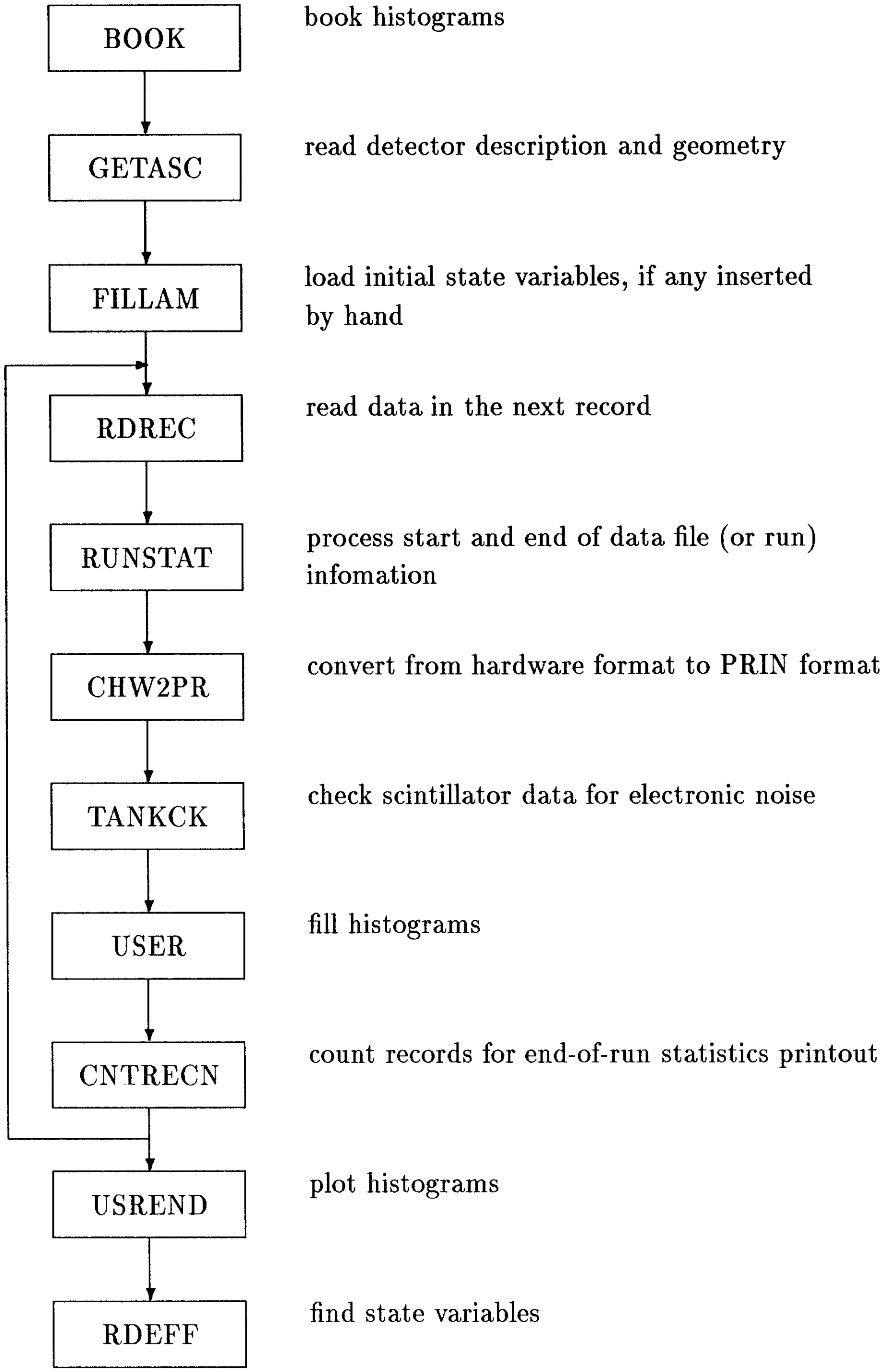

Figure 3-2: Flow chart of program ONLVD.

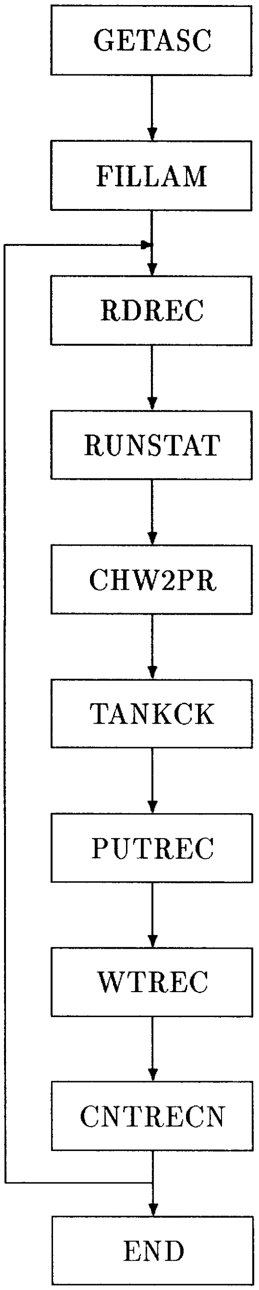

read detector description and geometry

load initial state variables from ONLVD

read data in the next record

process start and end of data file (or run) infomation

convert from hardware format to PRIN format

check scintillator data for electronic noise

assemble a record of reformatted data

write record to new file

count records for end-of-run statistics printout

Figure 3-3: Flow chart of program ONLVDOUT.

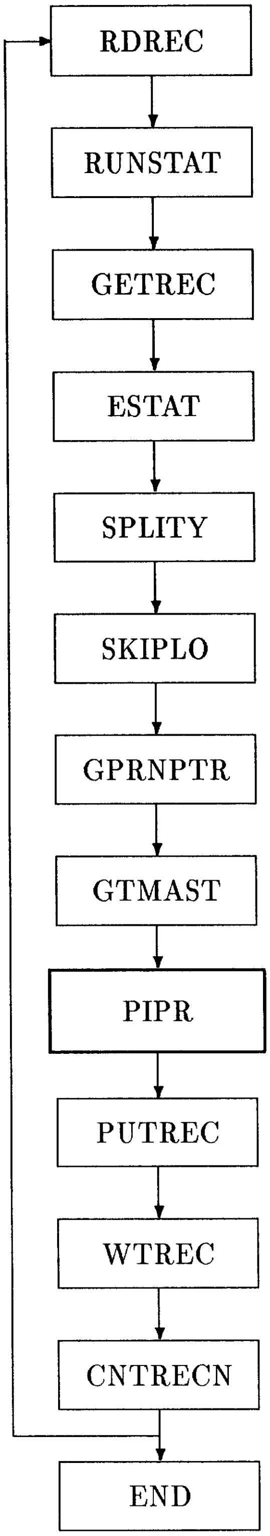

read next event

process start and end of data file (or run) information

separate the block of data for one event into named variables and arrays in common blocks

find tracking modules with static discharge in this event

temporarily split wide Y-strip clusters

delete low threshold scintillator hits

set up pointers to arrays about clusters, and about the layers and modules they are in

find "master points" for tracks to start with

track finding

assemble a record of data for this event, including results from PIPR

write record to new file

count records for end-of-run statistics printout

Figure 3-4: Flow chart of program LVDPIPR.

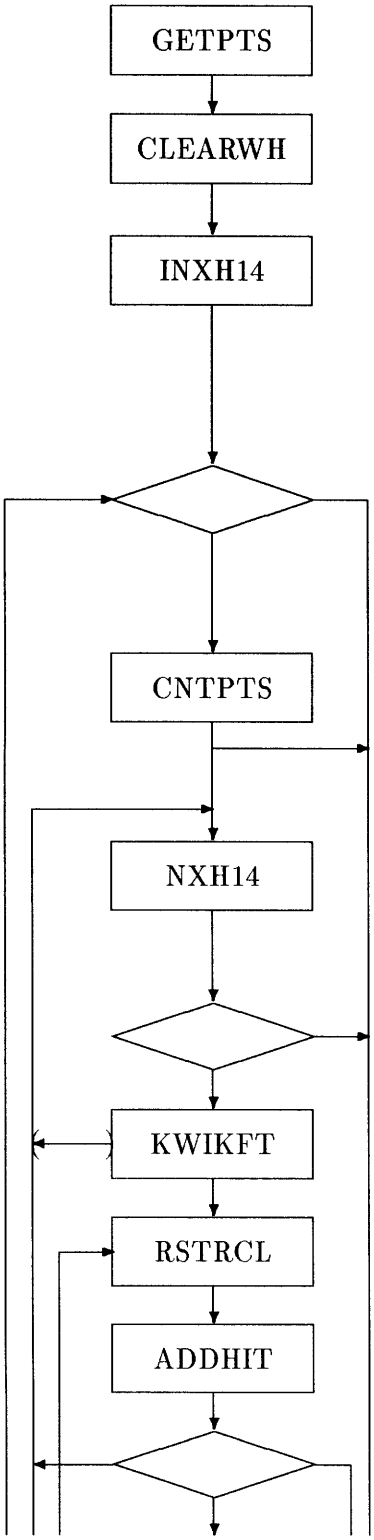

find spatial coordinates of hit tracking strip clusters from their channel numbers

clear “used” flag of clusters

initialization of the procedures to fetch 2 master points for any track candidate to start with, in modes of: nearby-points, remote-points, and remaining-points

if only ≤ 5 master points exist in > 2 modules remaining-points mode only; otherwise nearby-points, remote-points, remaining-points modes one after another on unused master points (any of the first two modes may be rejected by INXH14). if master points < 2, skip this event

count remaining master points, if unused master points < 2 exit PIPR

find 2 master points, the first must be unused come here to look for a new track candidate; also come to this point to look for a different second master point, from all failures in this loop (the 2 master points must not be on the same L-shaped Y-strip cluster)

if too much time used, clean up, exit PIPR

initial best 2-point fit (may fail)

in last cycle of this loop, restore full width of the 2 initial master points

add hits along the line

if total points < 2 reject this track; if no new hits added, exit this loop and go to final quality check

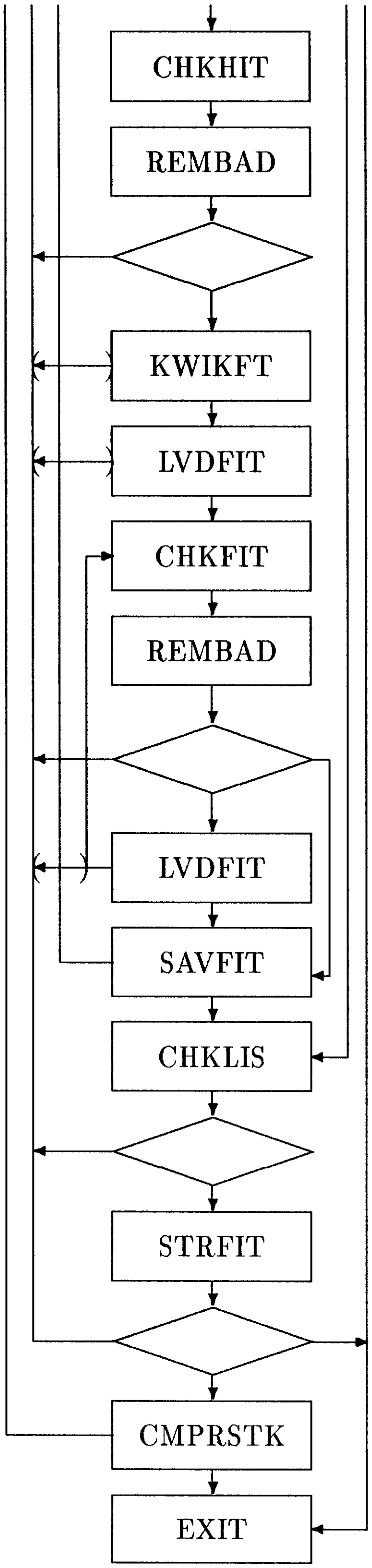

check singlets (hits not accompanied by a perpendicular hit in the same double layer)

remove flagged hits

reject this candidate if the first two master points are affected or total clusters < 2

acquire new best 2-point fit, if in the 1st cycle of this loop or if some hits are removed (may fail)

3-dimensional line fit (may fail)

eliminate bad χ^2 by narrowing wide clusters or skipping clusters too far from fitted line

remove flagged hits

reject this candidate if the first two master points are affected or total clusters < 2, if no change in list of hits exit this loop

3-dimensional line fit (may fail)

save the temporary parameters of this track

compare expected list of hits with actual list of hits

reject this candidate if discrepancy too big e.g., event starts or stops in detector

store good candidate

if array is full after compressing exit PIPR, otherwise find next candidate

clean up debris and find the “best” subset of tracks

Figure 3-5: The PIPR algorithm.

Chapter 4

Gain Factor Calibration of Scintillator Counters

To convert the ADC readout from a scintillator counter into measured energy deposited in the counter, both the ADC channel, and the *gain* of the scintillator counter and photomulipliers as a whole have to be calibrated.

The ADC channel is calibrated in two stages [A$^+$92b]: (1) outside the experimental setup using a DAC to determine the slopes and intercepts of the linear relations between output and input of the ADC; (2) in the experimental setup before each run to measure the shifting pedestals[1].

The *gain* of a scintillator counter and its three photomultipliers is calibrated using reconstructed cosmic muon tracks going through the counter, in two steps: (1) find the gains counter by counter in every 20-day period, which are typically 22% (1σ) away from the average of all normal counters, and show in average a 6% (1σ) fluctuation as a function of time; (2) find the geometrical corrections to the gain of all counters for tracks traversing

---

[1] Once the first is done the shape of the response curve is determined. It is stable because the parameters are only those of the stable and passive elements, the resistors. The overall shift of the curve is caused by the *drift* at the differential input of the amplifier, due mainly to temperature changes. This is corrected by the measured pedestal shift.

the counter in different paths.

4.1 Linearization of the ADC Readout

The ADC used at LVD is in the C176 (CAMAC Model 176, made by CAEN, an Italian firm manufacturing electronics modules) fast ADC/TDC module [BFP$^+$90]. One module has 8 independent channels for 8 counters. The full dynamic range of an ADC is divided into 6 linear regions each of half the slope of the previous. This arrangement allows both precision and a large 12-bit dynamic range in a compact data format of ADC output number 0–383 (divided into 6 equally wide regions). In the first region (0–63) the resolution is $\frac{1}{4}$ pC/count, in the second (64–127) $\frac{1}{2}$ pC/count, and so on, until in the last (320–383) 8 pC/count (Fig. 4-1).

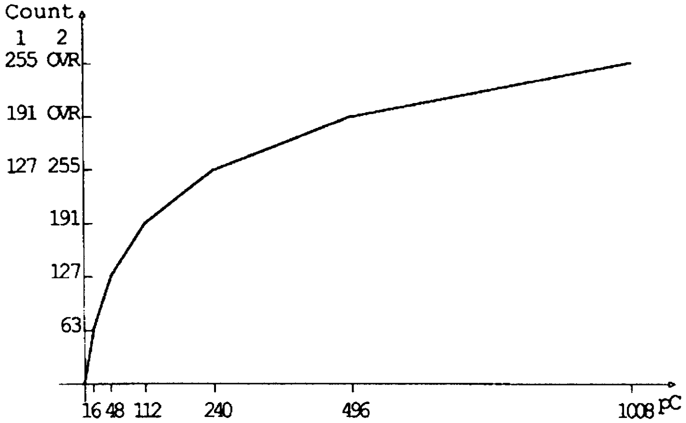

Figure 4-1: Conversion curve of the C176 ADC. When the OVR bit is on, output count number is ADC1 + 127. Two 8-bit flash ADCs are used in each channel. Input × 4 is internally applied to ADC2. Not shown is the pedestal. A pedestal P (in count number, found always in the first region) would move the whole curve to the left, to a location where the curve intercepts the y-axis at P.

The ADC modules were calibrated once with a DAC before they were connected to the C175 linear sum output (A+B+C, from the 3 phototubes of a counter). The slopes A_r and intercepts B_r of the 6 linear regions of a channel were determined by fitting the measurement (through a DAC) points in each region to a straight line

$$I_{\mathrm{r}} = A_{\mathrm{r}} \times Q + B_{\mathrm{r}}, \tag{4.1}$$

where r (1–6) is the region number, I_{r} is the ADC readout count number, Q is the charge input to ADC in $\frac{1}{4}$ pC from the DAC[2]. Or,

$$Q = (I_{\mathrm{r}} - B_{\mathrm{r}})/A_{\mathrm{r}}, \tag{4.2}$$

B_1 is accurately the pedestal at the time of that measurement.

The slopes and in fact the shape of the whole connected curve of these 6 regions do not change because they are determined by the stable resister elements in the electronics module. However, the pedestal is not constant, because of the *drift* at the differential input of the amplifier due to mainly temperature changes. As a result, the conversion curve shifts as a rigid whole to the left when the pedestal increases, or to the right when it decreases.

After the ADC's have been installed in the experiment, only their pedestals are measured before each run. The method is to read out from every ADC channel 1000 times without threshold (while the whole circuitry, linked to the the photomultipliers, is intact, for signal pulses from them are rare, due to the low rate of events underground) and calculate the average of these 1000 ADC readouts per channel, P. This is the new pedestal [Ful91]. The new relation between input charge Q and output count number I_{r} becomes (because P is in the first region)

$$Q = (I_{\mathrm{r}} - B_{\mathrm{r}})/A_{\mathrm{r}} - (P - B_1)/A_1 \tag{4.3}$$

---

[2] Because the DAC used in this calibration has a different unit of output reading, Q is not in $\frac{1}{4}$ pC, but rather in a larger unit about $1.4 \times \frac{1}{4}$ pC. This will not affect the calibration; what's required here is only linearity. After the output of the ADC is linearized, the gain factors linearly convert the measured Q/L distributions into an arbitrary unit of charge over length (approximately $1.4\times\frac{1}{4}$ pC/cm) into E/L (or dE/dx) distributions in the units MeV/cm. The factors are found by matching the Q/L distributions to a Monte Carlo E/L distribution scaled horizontally for a best fit. The actual procedure, described in the following sections of this chapter, is in several more steps in order to reach a precision of about 2–3%.

This Q, linearized in the full dynamic range, is the amount of charge in $\frac{1}{4}$ pC (see footnote 2) at the output of the photomultipliers. For any one counter, Q is considered proportional to the amount of energy E deposited within the counter, except for secondary geometrical errors inside a counter to be corrected later. However, this proportion (called *gain*) is different from counter to counter because of nonuniformity among the counters, and different from time to time due to instabilities and deliberate modifications.

The following sections in this chapter describe the method of finding the individual *gain*s counter by counter in periods of time, and one method of correcting the differences in gain as a function of location within a counter (in this correction all counters are assumed identical, after the gain factors for individual whole counters have been taken into account).

4.2 Selecting Reconstructed Muons and Scintillator Hits

Reconstructed cosmic muons through the scintillator counters are used to calibrate the *gain* (conversion factor from Q to E) of a counter. From chapter 1, it is known that the peak of the dE/dx distribution in the LVD scintillator is very constant. The Monte Carlo simulation, as will be discussed in the next chapter, shows that the dE/dx distributions of muons in all counters are the same and that the peak is close to 1.8 MeV/cm. These characteristics are utilized for the calibration of the counters.

Although the inner surface of the counter container is covered with a diffusively reflective film (aluminum plated behind mylar), the light collection is not 100%, and not geometrically uniform. Besides, the location of the counter is known to a precision of 1–2 cm, and for most muon tracks which are nearly vertical the spatial resolution of the detector is about 2 cm. For these reasons only muon tracks sufficiently long inside the counter and sufficiently away from the walls of the container are used for the calibration.

For this purpose one variable D is defined as the average distance of all the points along the track to their nearest inner walls of the counter. Note that by this definition the maximum possible value of D is only 25 cm for most tracks which are sufficiently vertical, only infrequent tracks close to horizontal would approach a larger value up to about 32 cm. The criteria used to select the muon tracks for the calibration are

$$D \geq 5\text{cm}, L \geq 50\text{cm}$$

where L is the length of the track inside a counter.

To reduce errors caused by short tracks (more likely to be inaccurately or wrongly reconstructed) crossing only 2 points in the detector, or scintillator counters hit by more than one track at the same time, or low energy muons whose actual bent trajectory is found very approximately or which stops in the middle of the detector, only tracks which have the following 4 characteristics are selected for the analysis:

1. have at least 3 tracking points at different "legs"[3];
2. are at least 2.5 m away from other tracks in the same event;
3. have no more than 1 tracking point at a distance less than 20 cm from the track and at least 2.5 cm off the track (to exclude bent tracks of low energy muons);
4. pass no normal counter with $L \geq 50$ cm and $D \geq 5$ cm while there is no readout from that counter at the time (due to either a stopped muon or an incorrectly reconstructed track).

Each of these problems occured a few times within a scanned sample of about 300 events. Condition 3 may also exclude very high energy muons with hard bremsstrahlung in the detector. Condition 4 also excludes occasional events not completely read out in one cycle.

---

[3] A "leg" is either the horizonal or the vertical double-layer of any hood, with at least 2 crossed hits in any of the 4 strip layers. This requirement ensures a spatial point, while not causing a large loss of acceptance due to gaps and sometimes malfunctioning elements in any single layer of streamer tubes or readout strips.

In addition, to avoid spurious tracks reconstructed from coincidental or correlated noise in the tracking system, events without any scintillator data are excluded. Events containing showers are removed by requiring $[(N_{tk} < 3)$ AND $(N_{sc} < 4)]$ OR $[(N_{tk} < 6)$ AND $(N_{sc} < 2)]$[4]

where N_{tk} is the number of X-strip tracking hits at a distance between 4 cm and 60 cm from the track; N_{sc} is the number of high-threshold hits at scintillator counters not crossed by the track, yet no more than 750 ns different in time from the average time of those scintillator hits on the track.

The counters traversed by these tracks, that pass the above mentioned cuts on D and L, and satisfy the requirement on TDC readout discussed in the next paragraph, are accepted and used in the calculation of the *gains*.

Among all the scintillator counter hits in an event, a list of hits in the counters passed by an accepted track is found by using the geometry of the detector and the location of the reconstructed track. The scintillator data consist of both ADC and TDC readout hit by hit. The time from TDC is in units of 12.5 ns, with a fluctuation of the clocking circuitry of up to 50 ns. The time spent by a relativistic muon passing the detector is 20–60 ns. To ensure that the hits used in the calculation of dE/dx are those caused by the muon track, a time window of 650 ns is applied to all the hits along the track. The largest subgroup of these hits[5] within any window of 650 ns[6] is chosen for the dE/dx calculation.

The only other type of very infrequent scintillator hits not used are those having a

---

[4] This set of cuts is applied during the gain factor calibration of the counters and the various geometrical "units" within the counter. During the search for WIFs a more stringent set is used: $[(N_{tk} < 2)$ AND $(N_{sc} < 2)]$ OR $[(N_{tk} < 3)$ AND $(N_{sc} < 1)]$. The calibration is based on the whole dE/dx distributions, the higher the statistics the more precise it is. The search for WIFs needs a cleaner sample because it is based on the several dE/dx values in the counters along one track. An erroneous dE/dx value at a counter due to any of the reasons cited above will lead to a wrong calculated probability for the track. See chapter 6.

[5] As mentioned earlier, throughout this analysis, only high-threshold hits are examined. See section 2.3.

[6] This limit is found by a close look at the time distribution as a whole and by individual counters. Two C176 modules, covering 16 counters, frequently give TDC time regularly wrong by 250–450 ns; they also, and another module, very infrequently give a very wrong TDC time, by more than 1000 ns. The distribution goes down to zero at 650 ns, starts at 750 ns to rise to a low and flat distribution above 1000 ns, indicating noise.

high-threshold label but a zero ADC readout number. They are obviously erroneous data because the high threshold is at about 7 MeV, corresponding to an ADC readout number of at least 20 (depending on the gain of a counter) above the pedestal (in the range 0–63). Only this exclusion is hit by hit based on the ADC readout; the criteria listed in the previous paragraphs and some more in the following sections are applied on the geometrical features of an event, or of a whole track, or on the way a track passes a counter, regardless of the particular ADC readout. Hence they do not introduce any bias against any track that passes some counters with low dE/dx readout. This point is important as it means that tracks are selected without reference to the energy deposited in the counters they pass.

The distribution of the linearized charge Q from a counter is histogrammed into 50 bins plus an overflow bin. Abnormal or inoperative counters are excluded from the analysis by setting the following requirements for every 20-day period:

1. $\sum_{i=8}^{50} N_i > 0$;
2. $\sum_{i=3}^{50} N_i \geq \langle\sum_{i=3}^{50} N_i\rangle - 5\sigma$;
3. $\sum_{i=3}^{50} N_i \leq \langle\sum_{i=3}^{50} N_i\rangle + 5\sigma$;
4. $N_{over} \leq 0.075 \times \sum_{i=3}^{50} N_i$.

The first 2 bins of the histogram are unused because they contain all the radioactivity background. $\sum_{i=8}^{50} N_i$ is the sum from the 8th bin up; the lower limit of bin 8 is approximately 100 MeV. If this sum is zero the counter was found to be dead or very abnormal, and no typical muon track was detected in it. $\sum_{i=3}^{50} N_i$ is the sum of all bins except for the first two. $\langle\sum_{i=3}^{50} N_i\rangle$ is the average of this sum among counters, σ is the standard deviation. Condition 2 rejects dead or occasionally dead counters. Condition 3 rejects noisy ones. N_{over} is the number of times when the ADC readout from a counter in the same period is its highest and overflow number $I = 383$, which causes distortion to the Q/L distribution.

Only 2–3 counters in any calibration period are rejected by condition 4. These conditions were found after a counter by counter examination of all the numbers.

4.3 *Nominal* dE/dx Distribution at Every Counter

Q/L, where Q is the charge at the output of the photomultipliers and L is the track length inside the corresponding scintillator counter, is for every counter proportional to E/L, where E is the energy deposited in that counter. The distribution of Q/L can be called the *nominal* dE/dx distribution. This distribution, counter by counter (see Fig. 4-2), is used to find the gain of a whole counter.

Data from a 20-day period provide sufficient statistics to display a locatable peak in the Q/L distribution of every counter. This differential (Fig. 4-2) distribution still has considerable statistical fluctuation and so a rather wide bin is chosen for the distribution. The peak location of this Q/L distribution, in the unit of approximately $1.4 \times \frac{1}{4}\,\mathrm{pC/cm}$ (see footnote 2), divided by the Monte Carlo value of 1.8 MeV/cm for the peak of the E/L distribution, gives the gain factor of a counter during a 20-day period.

There is visible shift of the peak ($\frac{\sigma}{average} > 6\%$) between 20-day periods. To find this shift of gain accurately from a relatively small amount of data in each counter, an iterative procedure is used to fit the whole distribution to a Monte Carlo template, after the initial step that finds the approximate location of the peak.

4.4 Locating the Peak of the *Nominal* dE/dx Distribution

Before fitting the 20-day period Q/L distribution of every counter to a Monte Carlo template, a less rigorous method finds an initial gain factor of any counter to convert Q/L to E/L. This is done by first integrating the Q/L distribution into a much smoother integral distribution (Fig. 4-3), finding the fastest rising section along the integral curve, and taking

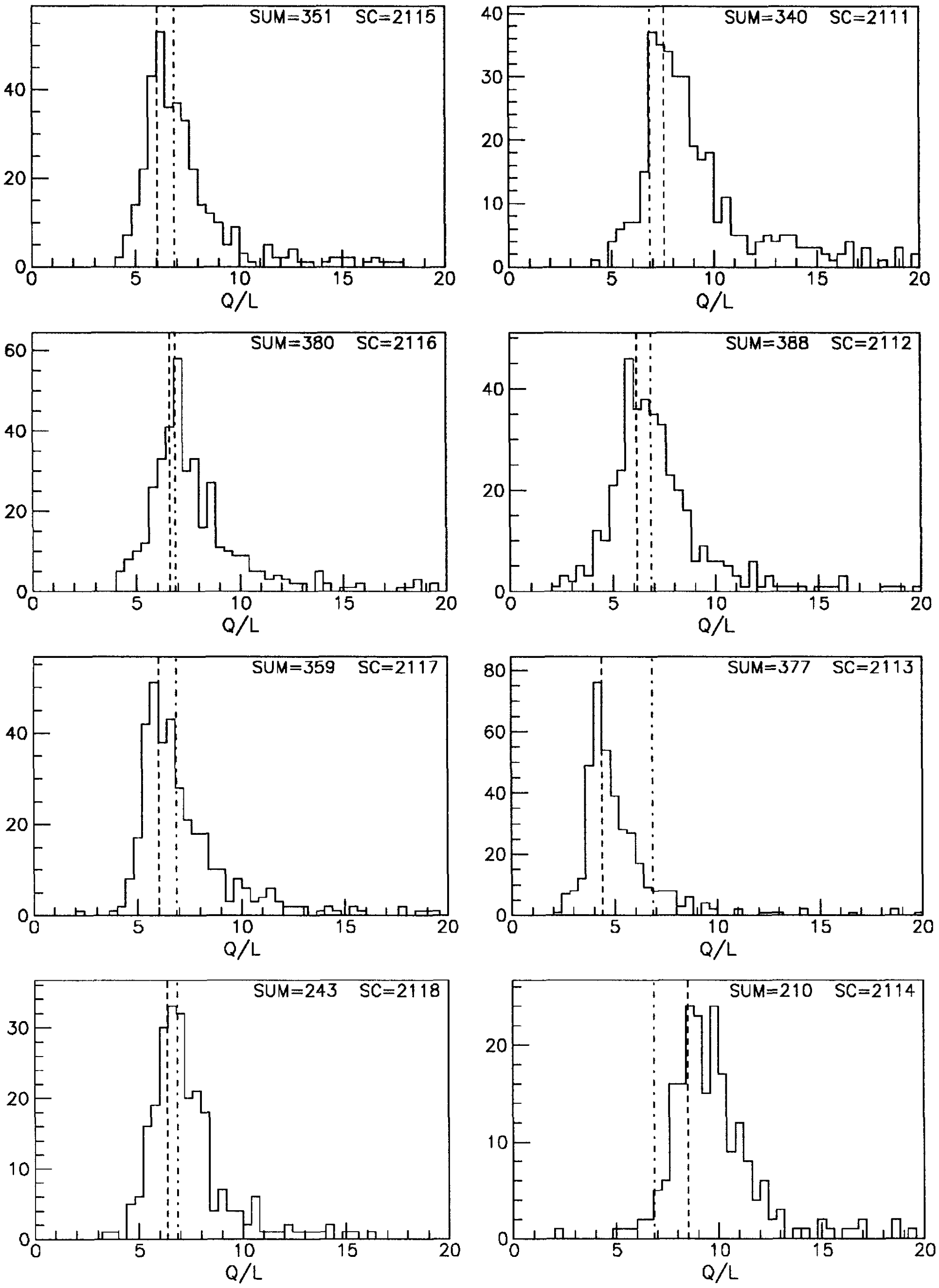

Figure 4-2: The Q/L distributions of 8 counters in a typical support module, in one 20-day period. The horizontal unit of charge over length (in centimeters) is explained in footnote 2, the vertical is the number of accepted tracks that traverse the counter. "SUM" is the total number of times these tracks pass it (required minimum set at 60), "SC" is the software ID number of the counter. The vertical dashed line indicates the location of the peak found by the way explained in Fig. 4-3, the dash-and-dot line is at the average peak of all counters in this period. One standard deviation from the average is 17% in this period among all counters; it ranges between 16% and 27% (depending on in which period) and its average is 21%, for all periods.

the center of gravity of that section in the differential distribution, then multiplying it by $\frac{15}{16}$ to move it toward the peak[7] and dividing the result by 1.8 MeV/cm. These initial gain factors (g_0) are used to generate the initial E/L distributions both counter by counter and over all counters. After this step, the distributions are all E/L, no longer Q/L. In getting the E/L distributions, for any specific value of L, regardless of what the ADC readout is from the counter, one condition should be satisfied for any E/L to be included:

$$E_{max}/L \geq 5.0\,\mathrm{MeV/cm} \tag{4.4}$$

where $E_{max} = Q_{(I_{max}-1)}/g$, g is the found gain factor in any step for that counter, $Q_{(I_{max}-1)}$ is the linearized charge when the ADC readout $I = 382$. The readout $I_{max} = 383$ is never used because it contains all the overflow data and will cause distortion of the E/L distribution.

When this condition is not satisfied, the readout (whatever it is) is not included in the E/L distributions. This is because all E/L distributions are limited in the range 0.0–5.0 MeV/cm (5.0 is found to be a suitable limit, as no considerable amount of data is lost). This criterion will ensure that all contributions to the E/L distributions span the whole range 0.0–5.0 MeV/cm, and that after all gain corrections all counters can be considered equivalent. It is an important criterion in the search for WIFs in this analysis as after all the corrections the summed dE/dx distribution of all counters will be used as the dE/dx probability density functions (two of them, in two ranges of L) of any counter.

4.5 The Fitting Procedure to Find the *Gain* of a Counter

After the initial *gains* g_0 and E/L distributions of the individual counters are found, they are next each fitted to a Monte Carlo template distribution common to all counters. The

---

[7] The distribution is asymmetrical. This factor is found, on average, to move the center of gravity, near the peak, to the peak.

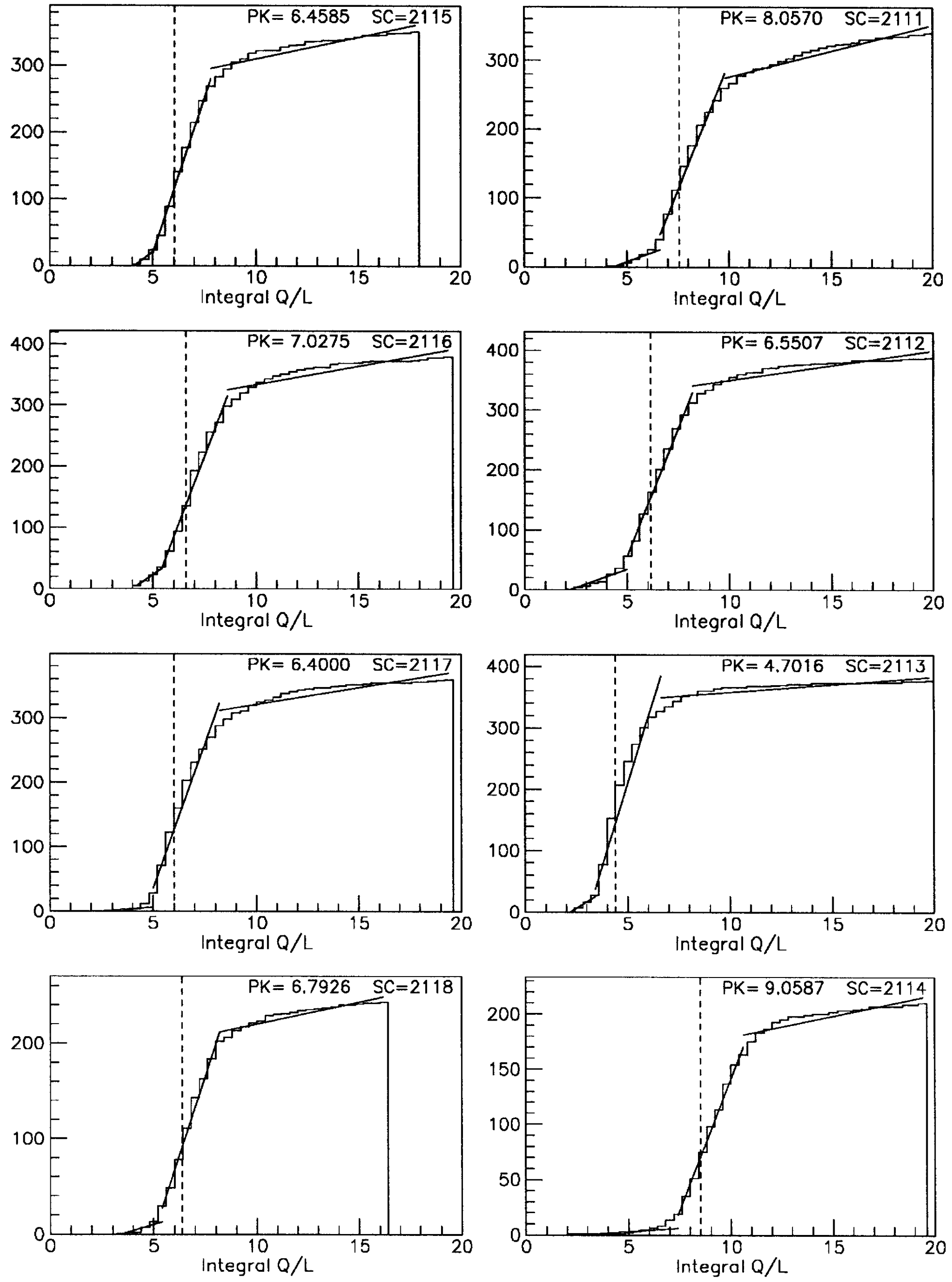

Figure 4-3: The integral of Q/L distributions of Fig. 4-2. The fastest rising section is slightly wider than 20% of the width between the first and the last nonzero bins in Fig. 4-2 and increases as square root of the overall width. The vertical dashed line indicates the position of the peak of the distribution.

template is linearly scaled to the left and right to best fit (smallest χ^2) the E/L distribution of a counter. The best scale factor found (s_1) modifies the initial gain factor g_0 to get a new factor g_1.

The first fit (see Figs. 4-4 and 4-5) uses a Monte Carlo E/L distribution as the template. This template is obtained by a complete simulation (described more fully in the next chapter) including muon energy and angular distributions, detector responses to a passing muon, reconstructed track, and E/L calculated from energy deposit and reconstructed track length in a counter. An additional Gaussian fluctuation[8] is added onto E to take into account the energy resolution of the LVD counter and to make the E/L distribution match the measured distribution from the experiment.

The new *gains* g_1 are applied and a summed E/L distribution of all counters is obtained. The summed distribution is fitted to the MC template, giving an overall scale factor c_1. Then the result is used as the template for the individual counters. The *gains* to be modified in the next step are g_1 as given in eq. 4.5 below.

The procedure iterates; for step n, using the summed E/L distribution of all counters and its horizontal scale factor c_{n-1} from the previous step as the template, one determines a new set of counter by counter scale factors s_n and gain factors g_n. The summed E/L distribution of all counters must be used as the template for the next fit because it is not exactly the same as the Monte Carlo template and it fits better. Convergence to the MC is assured by fitting the template each time to the same Monte Carlo E/L distribution to find its own needed scale factor c_n. This iterative procedure to determine the gain of any counter in any 20-day period can be expressed in

$$g_n = g_{n-1}/(s_n \times c_{n-1}), \qquad n = 1, 2, \ldots \tag{4.5}$$

---

[8] $\sigma = 12\%$ in this Gaussian fluctuation.

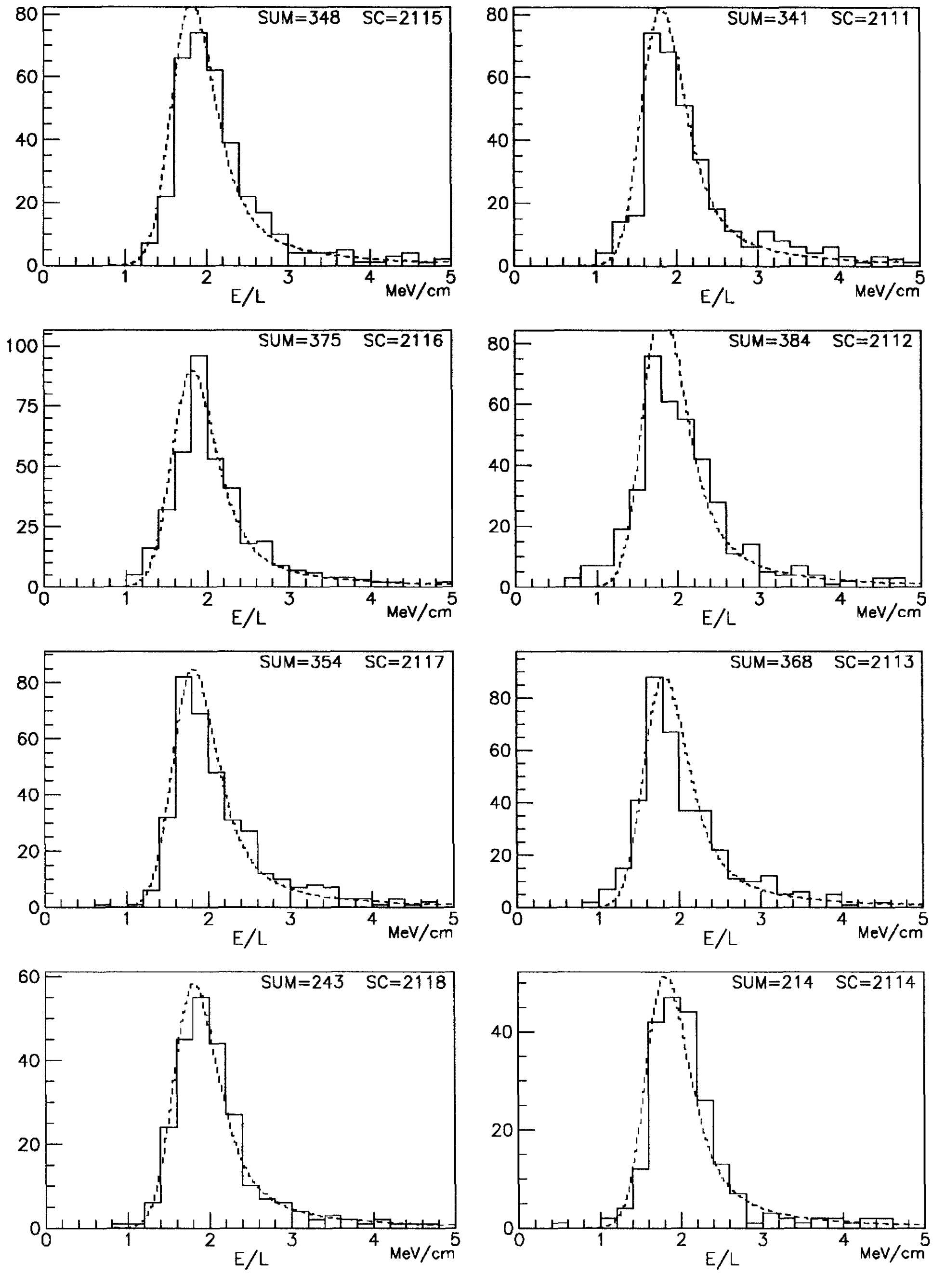

Figure 4-4: These are the same counters in the same 20-day period as those in Figs. 4-2 and 4-3. The solid line is E/L from data, the dashed line from Monte Carlo (with very high statistics, but normalized to the data in solid line). No horizontal scaling takes place in this figure. $L \geq 50\,\text{cm}$. When the total amount of data, "SUM" is less than 60, that counter is excluded for that period.

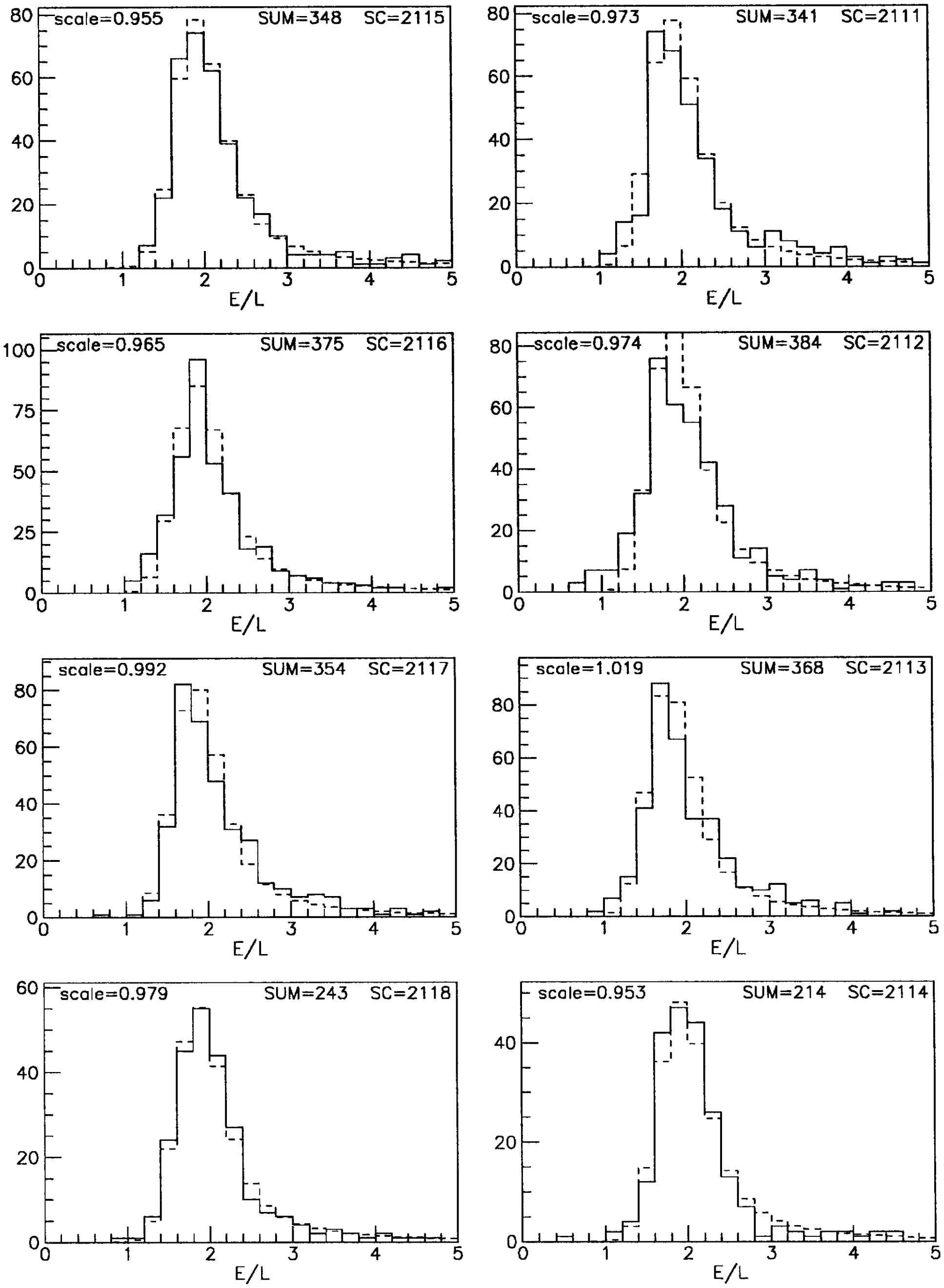

Figure 4-5: The scale factor that scales the E/L distribution from data horizontally actually is not applied on the data, because of low statistics and more inaccuracy that would be introduced; rather, the Monte Carlo E/L distribution, in high statistics and 4-times thinner bins, is scaled by a factor $\frac{1}{scale}$ in the horizontal, then normalized to the same total. The scale factor that causes the smallest difference (χ^2) between the two distributions is shown in the figure. Note the wide bins used to calculate χ^2, because of low statistics.

where g_0 is found by the method of finding the fastest rising fraction in the integral Q/L curve. The peak near the center of gravity of that fraction in the differential Q/L distribution (as described in the previous section) is scaled to 1.8 MeV/cm. s_n is the best scale factor found to fit the E/L distribution of that counter to the template distribution. At the step $n = 1$ the template is from Monte Carlo, $c_0 = 1$. In the next cycles the template is the summed E/L distribution of all counters after the corrections of the previous steps, c_{n-1} is the scale factor needed to best fit the top part (above half maximum) of this template distribution to the Monte Carlo distribution. Fig. 4-6 shows such a fit at the step $n = 5$. The Q/L peak to E/L peak ratio, improved by the scale factors found by fitting individual counter E/L distribution to template E/L distributions in successive steps, gives the gain of a counter. The Q/L peak in average is about 6.7 $\times(1.4 \times \frac{1}{4}\,\mathrm{pC/cm})$ [9], and the Monte Carlo E/L peak is close to 1.8 MeV/cm). Note that at each step those counters in any period whose scale factors differ too much from the average close to 1.0 are rejected during that period[10]. Figs. 4-7 and 4-8 are the distributions of the scale factors s_0 and s_5 of the normal counters during the same 20-day period.

Fig. 4-9 shows the *gain*s of the same eight typical scintillator counters in one support module as a function of time since the completion of the first tower. For any particular counter, the gain fluctuates as a function of time. One standard deviation of this fluctuation is 1–16% of the average over fifteen 20-day periods. In average it is 6% over all counters. The one σ precision of the iterative fitting procedure at the last step (n=6) is 0.53–0.91%, depending on in which period. This can be considered the precision of the gain, assuming constancy in each period[11].

Fig. 4-10 shows the distribution of the *gain*s of all counters in all 20-day periods.

---

[9] The unit of charge is not exactly known, and does not need to be exactly known. See footnote 2.

[10] The cuts used in the successive steps $n = 1, 2, 3, \ldots, 6$ to get to the selected g_6 are, $\pm 7\sigma$, $\pm 7\sigma$, $\pm 6\sigma$, $\pm 6\sigma$, $\pm 5\sigma$, $\pm 4\sigma$ away from the average of the respective $s_1, s_2, \ldots, s_6$. Additional steps are not taken because the dispersion of s_n reaches its asymptotic value at step $n = 6$. See Fig. 4-8.

[11] The actual lengths of the periods range from 18.0 to 21.2 days, the boundaries were chosen between some more apparent shifts of gain.

Knowing these gain factors, the energy loss E in the counters can be directly calculated from the linearized charge Q at the output of the photomultipliers. The nonuniformity of efficiency inside a counter determined in the next section varies by about the same magnitude as the difference in gain among counters in different periods of time.

This procedure of measuring the energy loss assumes that the output from the counter and its photomultipliers as a whole is sufficiently linear with respect to the actual energy deposited in the scintillator. The photomultipliers operate at 10% of their saturation level, so they can be safely assumed linear. The light yield and collection efficiency in the liquid scintillator is more complicated due to the geometry of the counter and the location of the photomultipliers. These problems are discussed in the next section.

4.6 Geometrical Corrections to the *Gain*

The nonlinear geometry of the LVD scintillator counter with only three medium-sized photomultipliers all on one side of the bulk volume makes it difficult to do an accurate geometrical gain correction based on a few parameters. The low rate of cosmic muons at LVD makes it impossible to do counter-by-counter geometrical corrections if the small amount of dE/dx data at each counter are to be further divided into many groups according to geometrical features.

Under the assumption that all counters are identical after the whole-counter gain factor correction described in sections 4.4 and 4.5, the dE/dx data from the entire 245 running days analyzed and from all normal counters are grouped into one sample, as if they were from one counter. After symmetry of the counter is taken into consideration, the data are divided into 7273 "units" according to the two points where a track enters and exits a counter. For each "unit", the dE/dx distribution is fitted to a template distribution horizontally scaled to get the best fit. This scale factor of a "unit" is used as the geometrical gain correction factor for the dE/dx data in that "unit".

Fig. 4-11 shows how such a "unit" is defined. The surface of a counter is divided into 6×6×8 sections along its 1 m×1 m×1.5 m height, width, and length. Because of 2×2-fold reflection symmetry (along the x-axis and y-axis) the total number of end-to-end "units" is reduced by a factor of 4 and the data are all reflected so that the upper end of a track is in one quarter of the counter. After this grouping there are in total 7273 "units"[12]. The two surface areas of a "unit" are either 16.67 cm×16.67 cm or 16.67 cm×18.75 cm. Some have a large amount of data and can be fitted well enough to horizontally scaled template distributions. Some are passed by too few muons and so their gains cannot be corrected accurately. The requirements $D \geq 5\,\text{cm}$ and $L \geq 50\,\text{cm}$ (see section 4.2) reject tracks and "units" too close to the surface, or of short end-to-end distance.

In this analysis only those "units" passed by at least 50 muon tracks (some geometrically reflected into them) are corrected. When the energy deposited by a track in a counter is not geometrically correctable, the data from that counter are disregarded in the search for WIFs, and not included in the corrected dE/dx distribution.

The other error in E/L is caused by the error in L. The reconstruction precision of a track is expressed in standard deviations $(\delta x, \delta y, \delta z)$ of a point on it in the middle between its ends in the detector and the standard deviations $(\delta\theta_x, \delta\theta_y, \delta\theta_z)$ of its direction cosines. Based on these parameters the deviation δL of the track length L inside a counter can be calculated by varying the middle point and direction cosines (in 16 combinations) perpendicular to the track by one standard deviation, calculating L in each variation, and using the difference between the maximum and the minimum L after these variations as δL.

When the value of $\delta L/L$ exceeds 0.12 (14.6% of all scintillator hits which have passed the requirements $L \geq 50\,\text{cm}$, $D \geq 5\,\text{cm}$, and others described in section 4.2 are in this category),

---

[12] Many "units" are empty because of the conditions $L \geq 50\,\text{cm}$, $D \geq 5\,\text{cm}$. The total number of ultimately corrected and accepted "units" is only 2053. The other conditions described later include: a minimum of 50 tracks in each "unit", scale factor does not diverge out of a set of limits in the iterative calibration precedure, width of E/L distribution in a "unit" not exceedingly large.

the widening of the E/L distribution in the $50\,\mathrm{cm} \leq L < 98\,\mathrm{cm}$ region relative to that in the $L \geq 98\,\mathrm{cm}$ region (the maximum possible L is 204 cm) becomes very conspicuous[13] even after the geometrical "unit" corrections. Apparently $\delta L/L$ is large when L is small. "Units" at the corners of the counter have small L. Theoretically the E/L distributions in these two regions of L should be about the same except for a very small shift ($< 1\%$, as shown by Monte Carlo), but because of errors, the measured E/L distributions in the two regions differ. The scintillator data with $\delta L/L > 0.12$ are not used during the procedure to find the "unit" geometrical correction factors and in the calculations after this point. This was not required on the data during the whole-counter calibration. At that point statistics were more important and the E/L distribution was not split into two regions of L.

The location of a scintillator counter is determined to a precision of about 2 cm in the horizontal plane, and about 1 cm in the vertical direction. This much misalignment will cause an error of 4.2 cm in L for a $\theta = 45^\circ$ muon track crossing one horizontal side and one vertical side of a counter. When $L = 50\,\mathrm{cm}$, this error in L is 8.5%, and will be passed on to E/L. For longer L, the track is more likely to be through two parallel sides (mostly the top and the bottom because horizontal muons are rare) of a counter and so the misalignment will not introduce error into the calculated L. This is another reason, besides the δL due to track reconstruction errors, why data with short L are not used.

The iterative procedure of "unit" by "unit" calibration is similar to the counter by counter calibration explained in the previous section. The differences are: (1) the Monte Carlo template E/L distribution used in the initial step is smeared by a smaller amount, instead of the Gaussian with $\sigma = 12\%$ applied in the previous section to account for all errors, now it is $\sigma = 7.6\%$; (2) whenever the E/L distribution in a "unit" is very wide[14], the data that belong to it are not used in the analysis. This excludes those very nonuni-

---

[13] Especially on the left side which is sensitive in the search for WIFs.

[14] The cuts applied at the steps n = 0,1,2,...,5 are, $\frac{FWHM}{Peak E/L} \leq 0.45, 0.47, 0.45, 0.46, 0.47, 0.44$, which are found by examining both the distribution of the width (weighted by amount of data in a "unit") and the actual E/L distributions of the "units". Less than 4% of data is lost by these cuts.

form "units" which contain too large efficiency fluctuations or too much difference among counters.

The relation

$$u_n = u_{n-1} \times (s_n \times c_{n-1}), \qquad n = 1, 2, \cdots \tag{4.6}$$

holds in the calibration of "units". The new parameters u_n, s_n are "unit" by "unit", u_n is the geometrical gain correction to be *multiplied* to the energy E found by the whole-counter calibration in the previous section, s_n is the best horizontal scale factor to fit the E/L distribution of a "unit" to the template; c_{n-1} is the scale factor to fit the template (a summed E/L distribution of all "units" after the geometrical gain corrections in the previous steps) to a less smeared ($\sigma = 7.6\%$) Monte Carlo distribution. In the initial step $n = 1$ the template for all "units" is the Monte Carlo E/L distribution itself, and $c_0 = 1.0, u_0 = 1.0$.

Fig. 4-12 shows the distribution of u_0. The "units" are weighted by the amount of E/L data in them. Fig. 4-13 are the distributions of amount of data, and the width of the E/L distribution in each "unit", both weighted by amount of data. Fig. 4-14 shows the distribution of s_4. Again, the "units" are weighted by the amount of E/L data in them. The cuts applied on the two sides of the average of s_n in the steps $n = 1, 2, 3, 4, 5$ are $\pm 6\sigma$ from the average (or about ± 0.15 times the average near 1.00) when $n = 1$, and then $\pm 0.08, \pm 0.06, \pm 0.06, \pm 0.06$ times the average. After the step $n = 1$ the cuts are all a little over 5σ. Those units with any s_n outside the cuts are dropped from the analysis. This is because after the step $n = 1$ all the $s_n (n > 1)$ should be close to 1.00 unless a unit cannot be very accurately fitted to a template.

Fig. 4-15 shows the summed E/L distribution of all units after the geometrical corrections till step $n = 4$, and the best horizontal scale factor to match it to the Monte Carlo distribution. Note the considerable difference between this figure and Fig. 4-6.

After these steps the adopted set of geometrical correction factors u_5 are as shown in Fig. 4-16. When these factors are applied to the energy E found after the whole-counter gain corrections described in the previous section, the peaks of E/L distributions of all "units", with different average length of track L in the counter, will be moved to the same place. However, this is not exactly right. Eq. 5.4 (in which t the material thickness is used instead of L) in the next chapter indicates that the most probable E/L due to ionization loss shifts as a function of $\ln(L)$, although the average ionization dE/dx is independent of length, so the E/L distribution as a whole shifts accordingly. This shift can be numerically calculated (for how to calculate the *density effect* and the negligible *shell effect* see ref. [SBS84] and ref. [BB64] respectively), the result is that a factor

$$(1. + 0.07077/1.79 \times \log(\frac{L}{100\,\mathrm{cm}})), \tag{4.7}$$

in addition to the geometrical correction factors, is applied each time an E/L is calculated.

After these corrections, the ultimate measured E/L distributions in the two regions $50\,\mathrm{cm} \leq L < 98\,\mathrm{cm}$, and $L \geq 98\,\mathrm{cm}$ are as shown in Fig. 5-4 in the next chapter.

4.7 Test on Linearity of the Counter

One method of testing the linearity of a counter is to calculate the average E/L at different intervals of L; this average should be almost constant if there is perfect linearity and when all errors are identical at different points of L. Fig. 4-17 shows the test after the whole-counter calibration, and both before and after the geometrical unit-by-unit corrections. Clearly, before the geometrical corrections the regions of the highest light collection efficiency are around $L \approx 100\,\mathrm{cm}$ and $L > 150\,\mathrm{cm}$, corresponding to vertical and horizonal muons going well through the middle of the scintillator counter. After the geometrical corrections the average E/L shows a systematical drop when L increases. This is due to larger measurement errors at smaller L that move the average E/L upward although the peak E/L stays the same. Since the photomultipliers function at about 10% of their saturation level when a typical vertical muon deposits about 180 MeV in the counter, linearity is much less a concern than the gain calibration of the counters and the geometrical corrections.

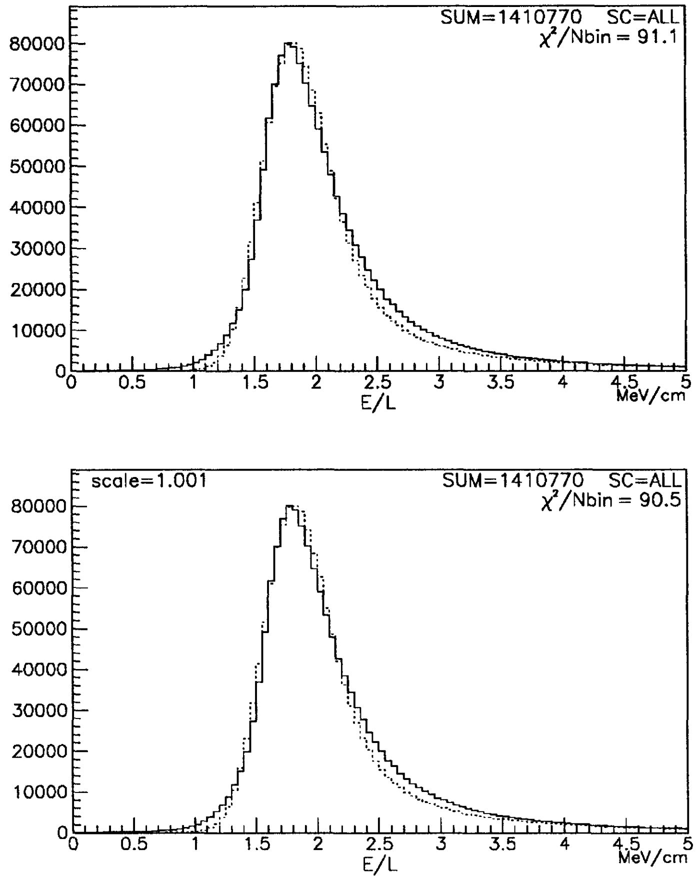

Figure 4-6: The summed E/L distribution of all counters using the gain factors g_4 is in solid line, the Monte Carlo E/L is in dashed line. The upper histogram is before scaling, the lower is after the Monte Carlo distribution has been scaled by a factor $\frac{1.}{1.001}$ to get the smallest χ^2. Note, because it is impossible to fully match the data to the Monte Carlo E/L smeared by some Gaussian fluctuation to account for all instrumental errors, the best Monte Carlo distribution found this way is still slightly higher than the data, only the part above half maximum height is used in the fit after the MC is normalized to data and is further vertically scaled by a factor 0.95.

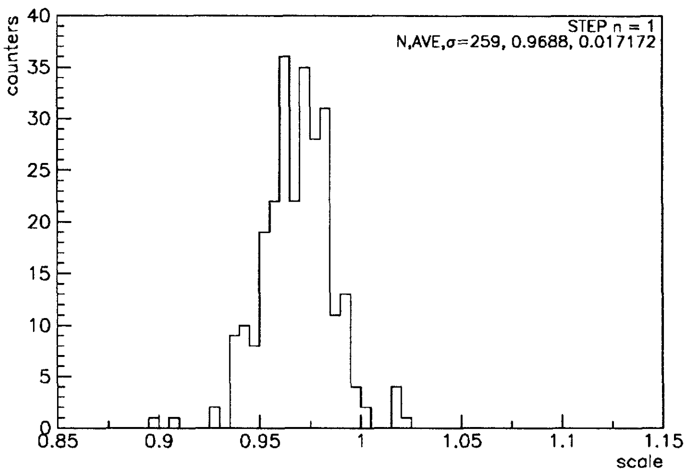

Figure 4-7: s_0, the scale factors found at the step n = 0 (when the template is the Monte Carlo distribution), and within 7 standard deviations from the average.

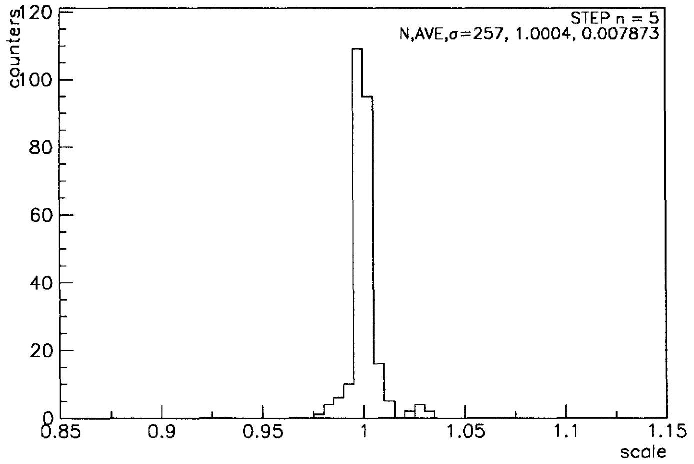

Figure 4-8: s_5, the scale factors found at the step n = 5, and within 5 standard deviations from the average. The template distribution is from the data of all counters using the previous set of scale factors s_4.

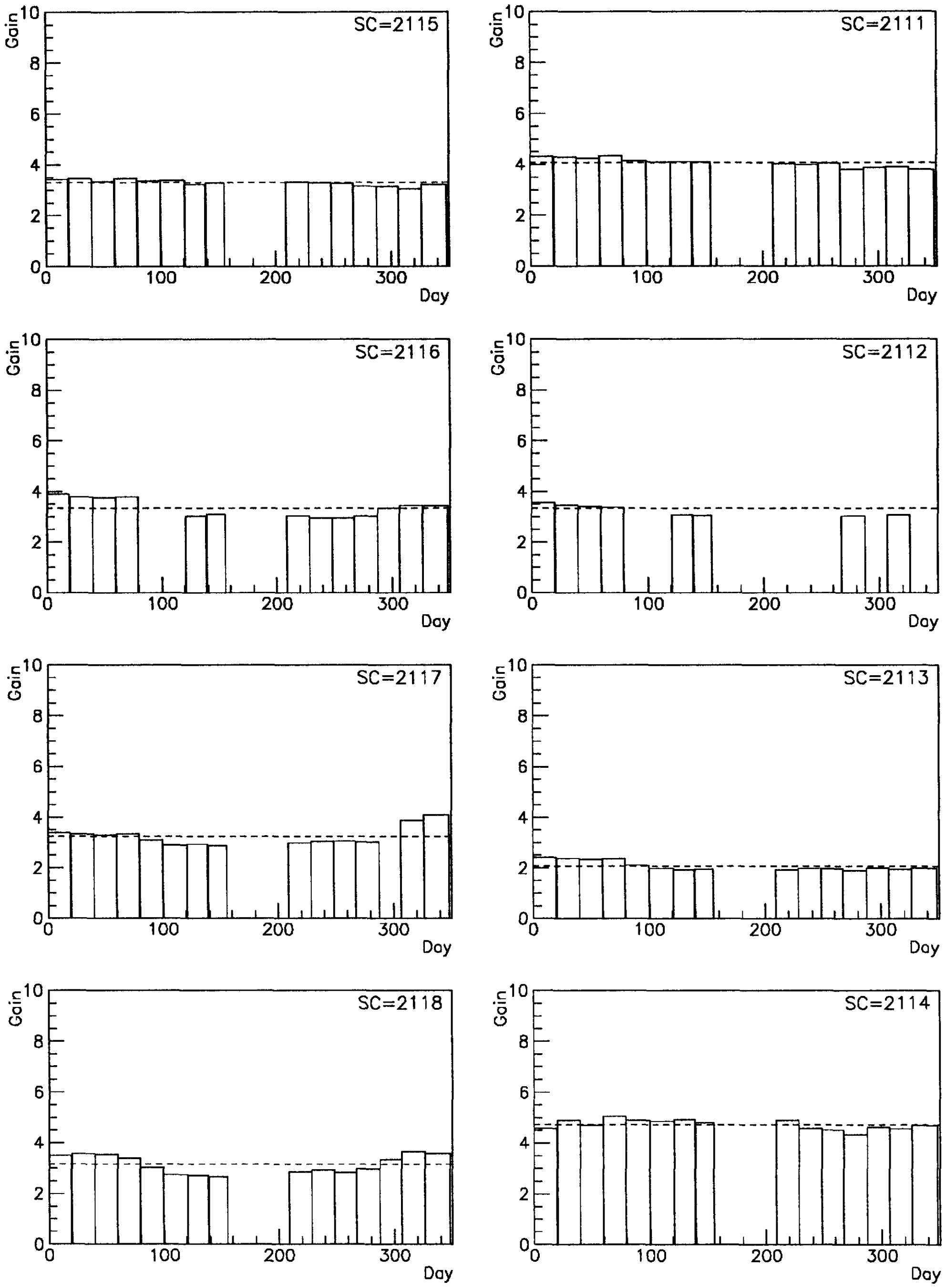

Figure 4-9: The gain factors of the same 8 counters as a function of time, in approximate 20-day periods. The dashed lines are the average over time.

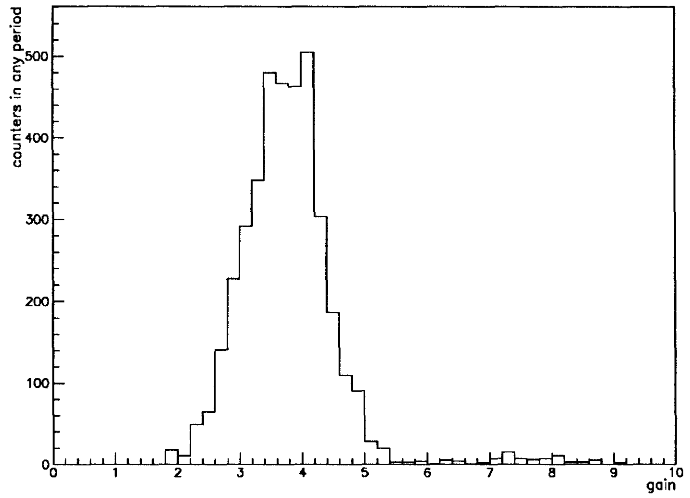

Figure 4-10: The gain factors of all counters in all periods. The linearized Q divided by the gain is the energy E in a counter, before secondary corrections inside a counter.

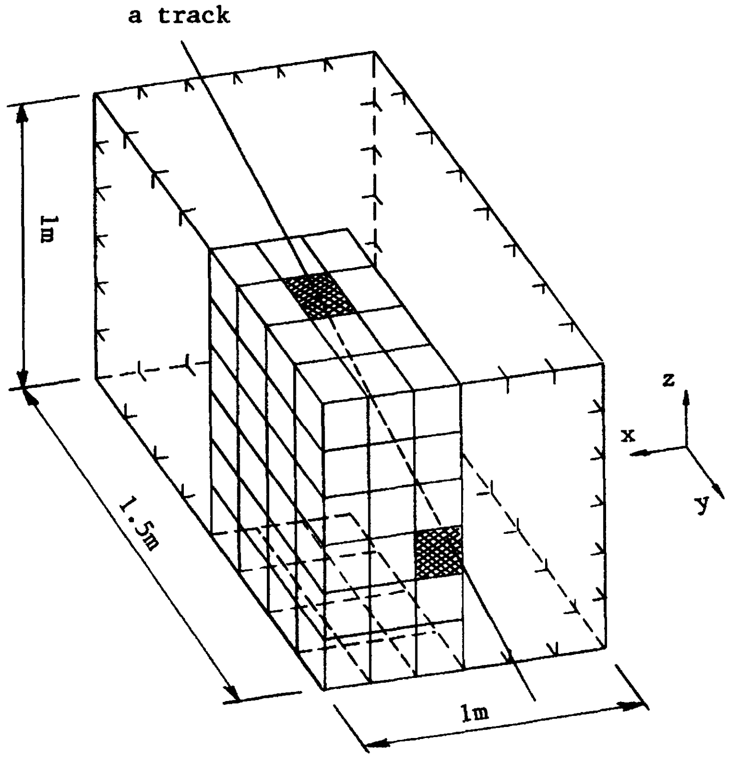

Figure 4-11: After the gain factor correction on whole counters, the dE/dx data from a bundle of tracks going through a "unit" defined by its two end areas are used to calibrate the gain factor of that "unit".

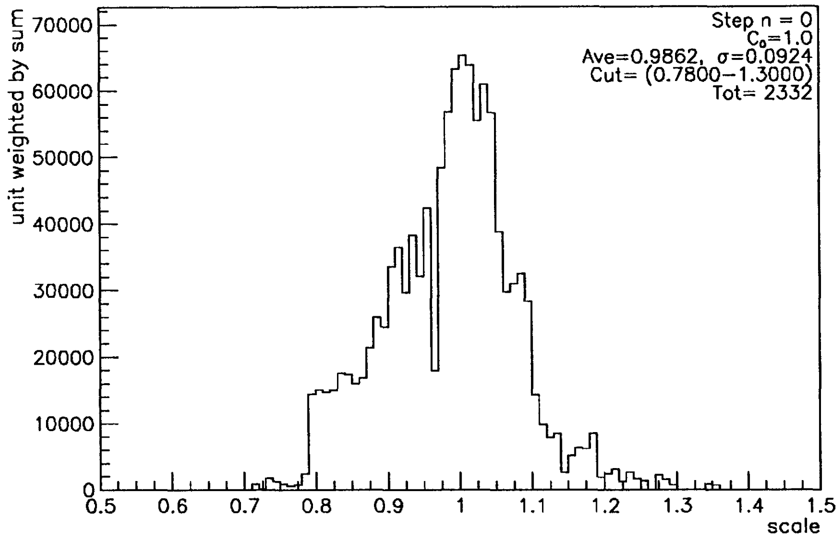

Figure 4-12: The geometrical correction factors found in the initial step, the "units" are weighted by the amount of data in them in this distribution. "Tot" is the total number of "units" that contain sufficient data (sum $\geq$ 50).

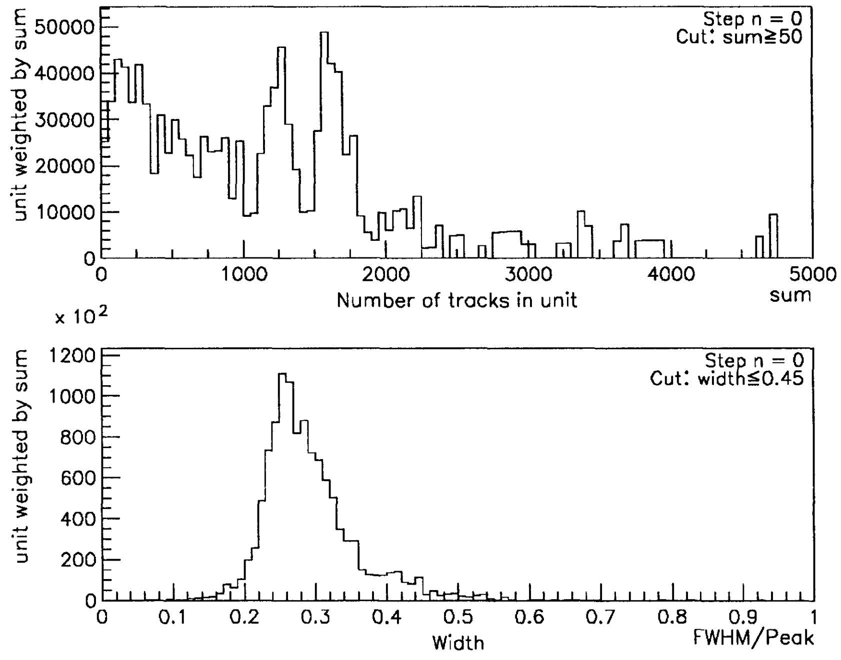

Figure 4-13: The total amount of data in a "unit", and the width of the E/L distribution in it. The distributions are weighted by the amount of data in each unit. The width is defined as FWHM divided by the location of the peak in a distribution. When it is too large the "unit" is likely to be shared by diverse counters. The cuts employed are indicated.

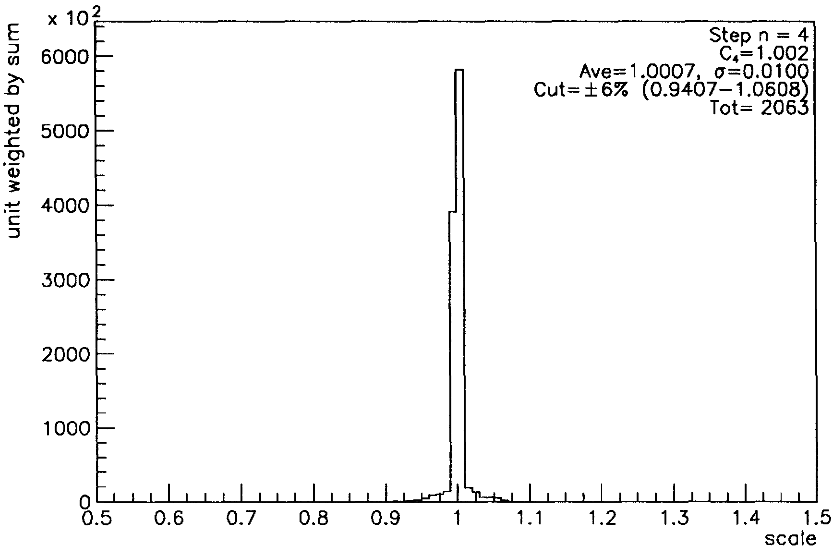

Figure 4-14: The best scale factors of the "units" found at step $n = 4$, weighted by the amount of data in a unit. "Tot" is the total number of "units" that contain sufficient data (sum ≥ 50).

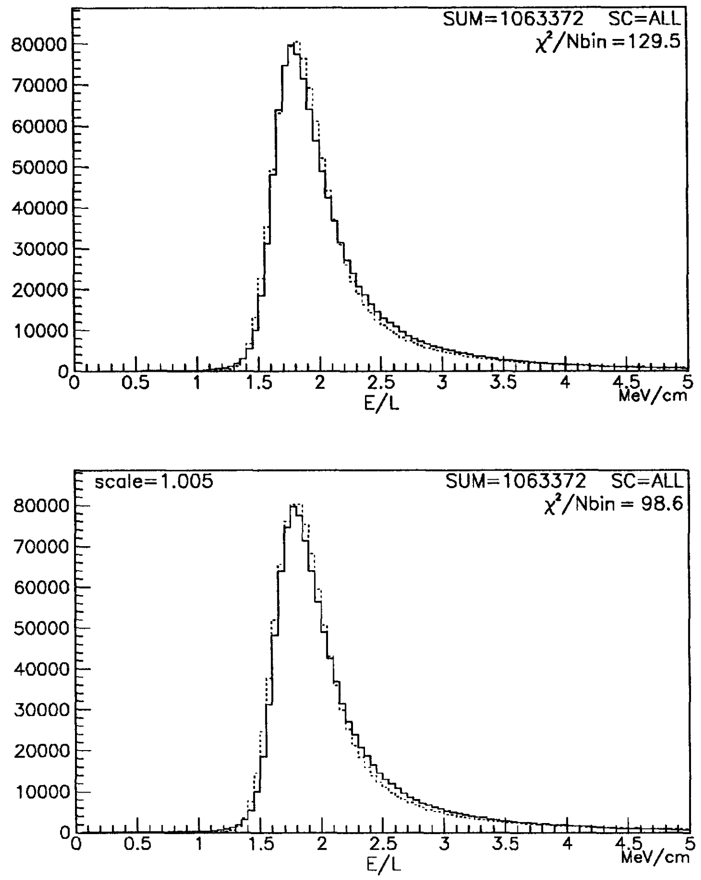

Figure 4-15: The summed E/L distribution of all counters after the corrections of u_4 is shown as solid line, the Monte Carlo E/L is shown as dashed line. The upper histogram is before scaling, the lower is after the Monte Carlo distribution has been scaled by a factor $\frac{1.}{1.002}$ to get the smallest χ^2. Only the part above half maximum height is used to calculate the χ^2.

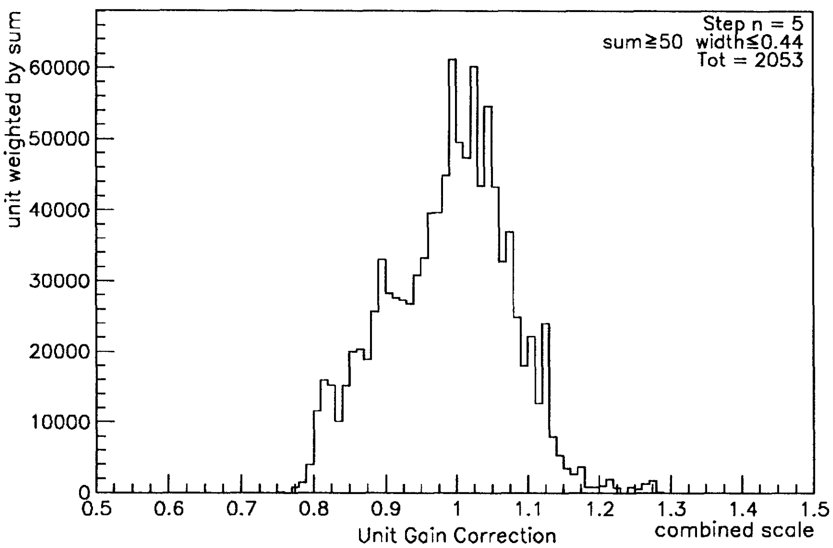

Figure 4-16: The geometrical correction factors finally used in the analysis. Only 2053 units are found correctable, they are weighted by the amount of data in them in this distribution.

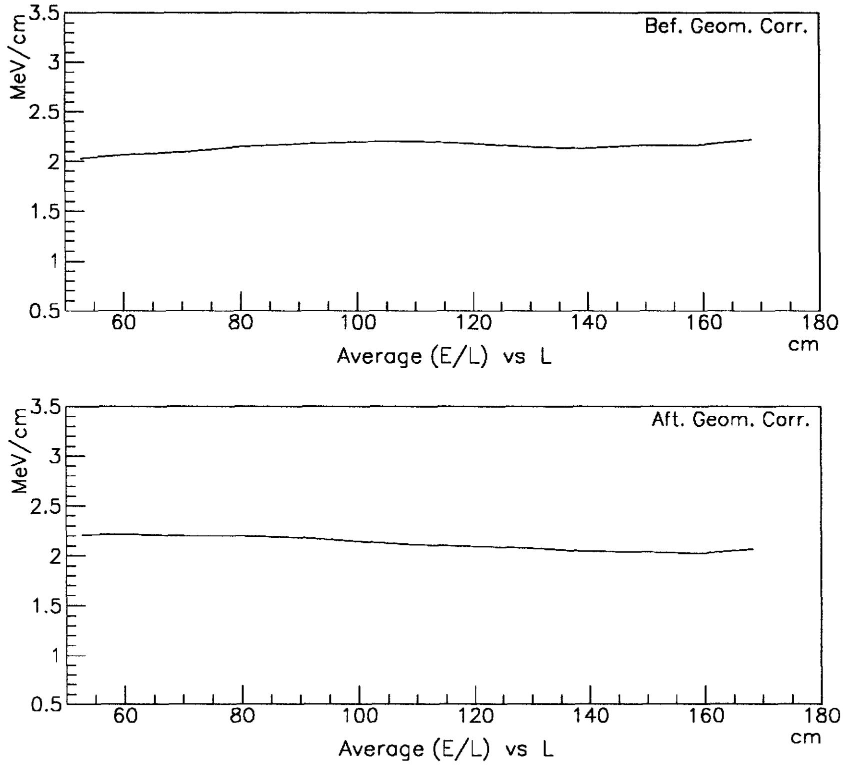

Figure 4-17: Linearity test, before and after the geometrical unit-by-unit corrections, but after the whole-counter gain calibration.

Chapter 5

dE/dx Distribution of Muons in LVD Scintillator Counters

This chapter describes how the Monte Carlo dE/dx distribution of cosmic muons in the LVD scintillator is calculated. It is compared to the measurement by this experiment.

Because the total energy of the incident muon cannot[1] be measured by LVD, the measured dE/dx distribution is integral over all incident muon energy. By an approximate model on pages 75–77 of ref. [Gai90] for the passage through rock by muons and using a power function muon energy spectrum at sea level with an index $(\gamma + 1) = 2.7$, the energy of the muons that reach LVD is mostly (96–97%) below 1 TeV, at an average of 280 GeV. Although the energy spectrum underground is model-dependent, and the average muon energy according to another more complete model [GZM76, VZK79, EZK$^+$88] is higher with a less steep energy spectrum, the inclusive E/L distribution of muons of all energy is almost model-independent[2]. The angular distribution used was taken from ref. [SB$^+$78][3].

---

[1] When energy is above 2 TeV, it may be roughly determined because in that region the energy loss in the scintillator is mainly through bremsstrahlung and pair production, which increase more rapidly as a function of the incident muon energy. However, some of such extremely high energy muons would have been discarded by the cut on $N_t k$ as described in section 4.2.

[2] This has been tested in a simpler method by changing the index γ of the power-function energy spectrum

5.1 Angular and Energy Distribution of the Cosmic Muons at LVD

The angular distribution is both measured and calculated[3] by empirical formulas based on the rock slant depth in any direction along a line from the surface of the ground to the experimental site [SB⁺78, B⁺83]. Fig. 5-1 shows the measured angular distribution of single-muon tracks that satisfy the criteria stated in chapter 4 (mainly: clean event, no shower, straight track) and are accepted in the analysis of this thesis. Fig. 5-2 shows the angular distribution of Monte Carlo single-muon tracks that satisfy the same criteria. Note that the coordinate system in these figures is based on the $x-, y-, z-$ axes of the LVD detector. The relationship between the azimuthal angle clockwise from the geometrical north and the LVD azimuth is $\varphi(\text{geo.}) = 218.4° - \varphi(\text{LVD})$. The distributions are not corrected by the uneven geometrical acceptance of the detector and the rules of acceptance applied in this thesis. However, they are closely similar to each other. The Monte Carlo angular distribution is

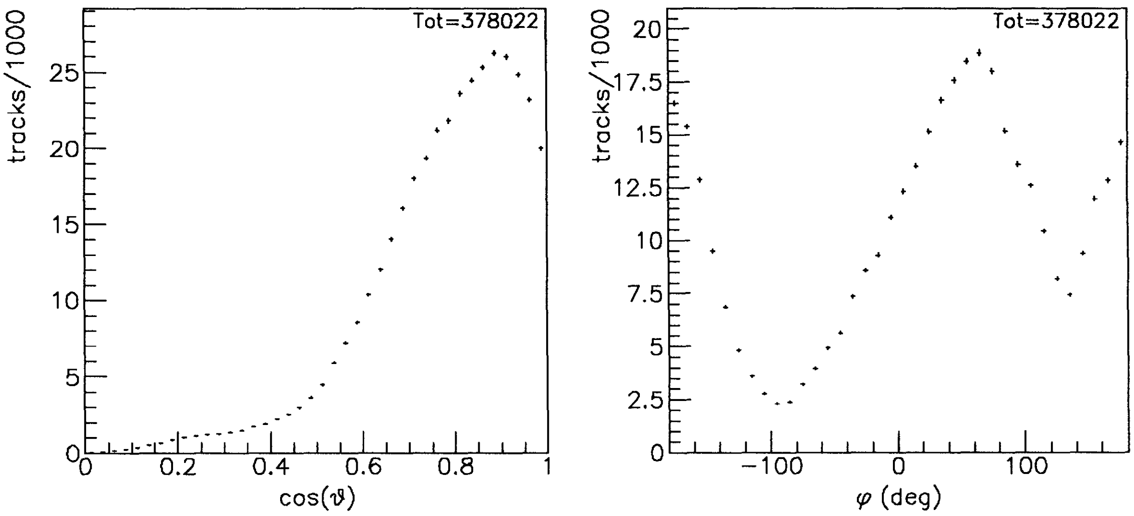

Figure 5-1: The measured angular distribution of clean, high-energy, single muons.

---

in the range from 1.5 to 1.8, around the generally accepted value 1.6–1.7.

[3] The formula in ref. [SB⁺78] is used because it goes beyond $\theta = 60°$, while the formula given by ref. [B⁺83] does not.

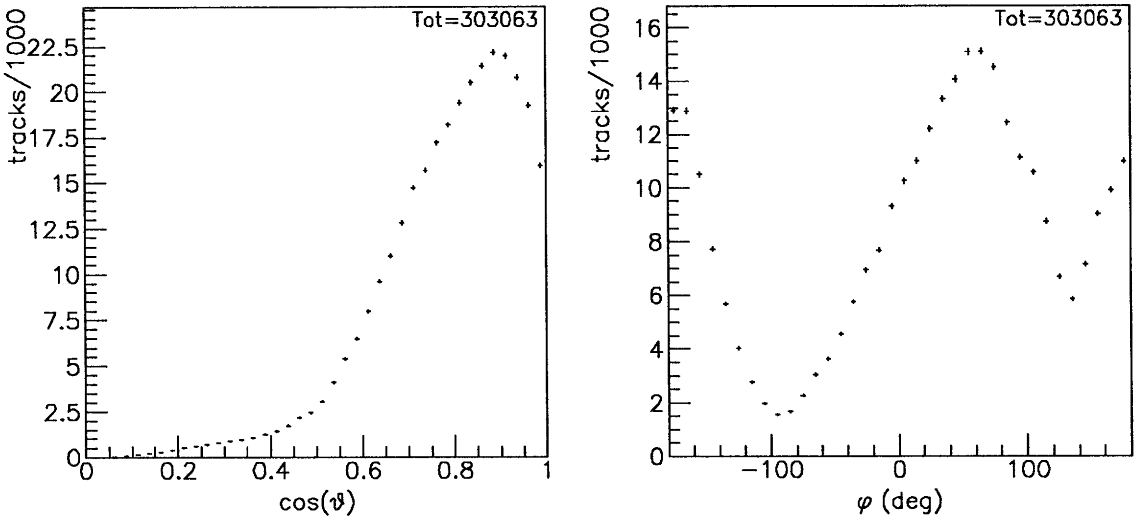

Figure 5-2: The Monte Carlo angular distribution of single muons that satisfy the same criteria.

lower than the measured distribution when $\cos(\theta)$ is below 0.5. This is because the angular distribution taken from ref. [SB+78] is inaccurate in that region. The measured angular distribution is almost identical to the one found in ref. [A+94b], except that here the total amont of data is smaller by 18% mainly because of the additional requirement in this thesis that a track has to be in a very clean event accompanied by few readout signals near it, to indicate that it is a high-energy, straight muon track. The proportion of reconstructed Monte Carlo muon tracks rejected by this requirement is much smaller for three reasons: (1) noise, either from the background in the electronic readout system, or induced by genuine signals or by background radiation, is not simulated; (2) the width of a readout strip cluster in the tracking system is only simulated in an ideal geometrical way, no coupling and not all delta-rays are taken into account; (3) About 10% of the total amount of steel in the support structure is not entered into the detector simulation program, mainly concentrated in the vertical, horizontal, diagonal I-beams, the attachment pieces (even less regularly shaped) at the corners of the steel support modules, and a fraction of the vertical steel panels inside a support module.

The valleys in the azimuthal distribution correspond to the directions of major groups of mountain peaks in the vicinity of the laboratory. The fall in the cosine-of-zenith distribution near $\cos(\theta) = 1.0$ is due to the peak vertically above the underground experimental halls.

The shape of the rock overburden over the Gran Sasso underground laboratory is known in the zenith angle range beyond[4] $\cos(\theta) = 0.5$. The rock thickness from the surface of the ground to the LVD site as a function of direction is calculated from the mountain survey data [Jec88]. The sea level muon distribution (uniform in φ, and according to the secant law in θ), attenuated by the known rock overburden using the empirical formulas of ref. [SB$^+$78] (regardless of the energy spectrum, which is dealt with in the next paragraphs), becomes the muon angular distribution underground. This distribution, weighted by the detector acceptance at various directions (applied to each simulated track during the Monte Carlo calculation), gives the Monte Carlo angular distribution in Fig. 5-2. The energy spectrum is also taken into account because the Monte Carlo muons are generated with an energy spectrum. But since the energy spectrum of the muons that reach LVD does not vary much as a function of direction and most muons are above a few GeV, the detector angular acceptance is almost geometrical.

There are small differences between the measured and the Monte Carlo distributions. This is because the calculation is accurate to a few percent, and the detector acceptances in these two distributions are not exactly the same. In the Monte Carlo a perfect detector is assumed, while the measurement data are not from a perfect detector. The reason for the difference in the distribution of $\cos(\theta)$ when $\cos(\theta) < 0.5$ (the Monte Carlo distribution is lower than the measured distribution in that region) is that there are inaccuracies in that region in the formulation of angular distribution taken from ref. [SB$^+$78].

The muon energy distribution underground at any given direction can be calculated

---

[4] Note that the altitude of the experimental site, though underground, is 963 m above the sea level, and that it is possible to reach very close to 90° at that location.

using the following two approximate relations [Gai90]:

$$I(> E_0) \sim E_0^{-(\gamma+1)} \mathrm{cm}^{-2}\mathrm{s}^{-1}\mathrm{sr}^{-1}, \tag{5.1}$$

$$E_0 = (\epsilon + E_\mu)\mathrm{e}^{X/\xi} - \epsilon. \tag{5.2}$$

Where $I(> E_0)$ is the flux of all muons (in the energy and slant depth range relevant to LVD and to this analysis, *prompt* muons, which become important when muon energy is above 10–100 TeV, need not be considered) of energy above E_0 at sea level in the zenith direction θ (for $\theta < 60°$). E_μ is the muon energy underground after transversing a slant depth X in $\mathrm{g/cm}^2$, $\xi \approx 2.5 \times 10^5\,\mathrm{g/cm}^2$, $\epsilon \approx 500\mathrm{GeV}$. Eqs. 5.1 and 5.2 give

$$dI/dE_\mu \sim \mathrm{e}^{X/\xi}((\epsilon + E_\mu)\mathrm{e}^{X/\xi} - \epsilon)^{-(\gamma+2)}. \tag{5.3}$$

This energy spectrum, after the total flux angular distribution is determined by the rock overburden data and empirical formula, is generated in the Monte Carlo simulation. A value 1.7 is used for γ.

5.2 Muon Track Length in Scintillator

The other relevant element in the calculation of an inclusive dE/dx distribution is the track length L inside a counter. This is not a constant. Its distribution is shown in Fig. 5-3. The height of the liquid scintillator in a counter is 98 cm. 21% of all E/L data that pass the various cuts described in the previous chapter are in the region $50\,\mathrm{cm} \leq L < 98\,\mathrm{cm}$ (data in the region $L < 50\,\mathrm{cm}$ are not used). This is where measurement errors in both E and L are larger, so the E/L distribution is presented in two regions of L.

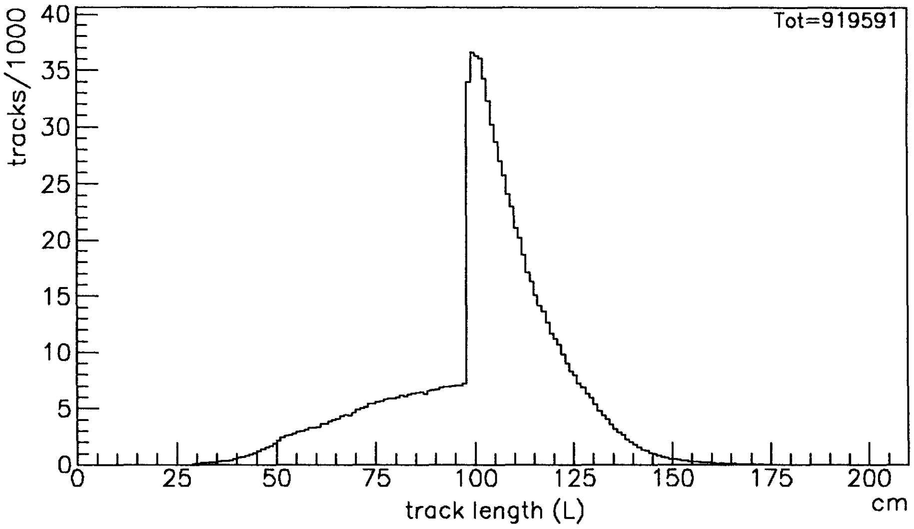

Figure 5-3: The distribution of track length L of measured muons in any counter. The effect of the requirement $D \geq 5\,\mathrm{cm}$ is that L is at least $20\sqrt{2} \simeq 28\,\mathrm{cm}$. The peak near 98 cm is from the majority of tracks almost vertically going through the counters.

The most probable energy loss in the Landau distribution is [Lan44, MP69] given by

$$\epsilon_{\mathrm{prob}} = (At/\beta^2)[B + 0.891 + 2\ln(\beta\gamma) + \ln(At/\beta^2) - \beta^2 - \delta - 2C/Z], \tag{5.4}$$

where $A = 2\pi N_{\mathrm{a}} r_{\mathrm{e}}^2 m_{\mathrm{e}} c^2 Z_0/A_0 = 0.1535(Z_0/A_0)\,\mathrm{MeV}/(\mathrm{g\,cm^{-2}})$, $B = \ln[m_{\mathrm{e}}c^2 \times (10^6\,\mathrm{eV})/I^2]$, $t = \rho x$, x is the thickness of material in cm. The other symbols are the same as those of eq. 1.1 in chapter 1.

$\epsilon_{\mathrm{prob}}/x$—the most probable dE/dx , or the peak of the dE/dx distribution, is a logarithmic function of x (or L). The logarithmic term of incident energy is almost completely canceled by the density correction term δ. The shape of the Landau dE/dx distribution by relativistic muons is little affected by incident energy or track length. The location of the dE/dx peak moves as a logarithmic function of L. At LVD the muon energy range is a few GeV to $\sim$ 1 TeV. The track length range in the LVD scintillator is 0.5 to $\sim$ 1.5 m, but more populated near 100 cm. In these ranges the peak location of the dE/dx distribution is little affected (by only 1–1.5%) by the variation of track length L in two separate regions of L, one below and the other above 98 cm. For this reason, in the "unit" by "unit" geometrical corrections of the gain inside a counter, a common E/L distribution was used as the template for all "units". The small logarithmic effect of L on the dE/dx distribution is reintroduced afterwards by a factor close to 1.0 (and equal to 1.0 when $L = 100\,\mathrm{cm}$), $1 + a \times \ln(\frac{L}{100\,\mathrm{cm}})$, associated with each measured E/L at any counter after the geometrical correction which moves the dE/dx peak in every "unit" to the same location[5] is made. The a is found to be 0.039 by the parameters in eq. 5.4.

5.3 The Inclusive dE/dx Distribution in LVD Scintillator

After the calibration of the scintillator counters and the geometrical gain correction inside a counter, the E/L distribution from muon tracks that pass all the data selection cuts described in the last chapter, in two regions of track length L, is shown in Fig. 5-4. The muon energy is unknown. All geometrically selected clean, straight, through[6] muons are included in these distributions. The required minimum energy for a muon to pass through 3 meters of scintillator and at least 7 cm of steel, entering the detector at an angle and going through only three levels in a corner of a tower, is less than 1 GeV. For a muon to go vertically through all 8 levels requires about 2 GeV. The criteria used to select straight, through muons raise the lower limit on muon energy by about $\sim$ 2 to 4 GeV. This can be

---

[5] The fitting procedure does not exactly move the peaks to the same point, but rather moves the whole distributions to the same location. But since the visible part of a low-statistics measured dE/dx distribution in a unit is more weighted near the peak, the statement is approximately valid. It all depends on the fact that the dE/dx distribution changes very little in the relevant range of L.

[6] "Through" here only means that when a track goes through any functioning scintillator counter, with $L \geq 50\,\mathrm{cm}$ and $D \geq 5\,\mathrm{cm}$, readout is required from that counter; otherwise the track is rejected. This is one of the track selection criteria mentioned in chapter 4. A similar and less stringent condition applied on the readout from streamer tubes during track reconstruction is inadequate because the functional status and efficiency of the tracking system are only known down to the level of a whole layer of readout strips in a module, for the low rate of cosmic muons at LVD.

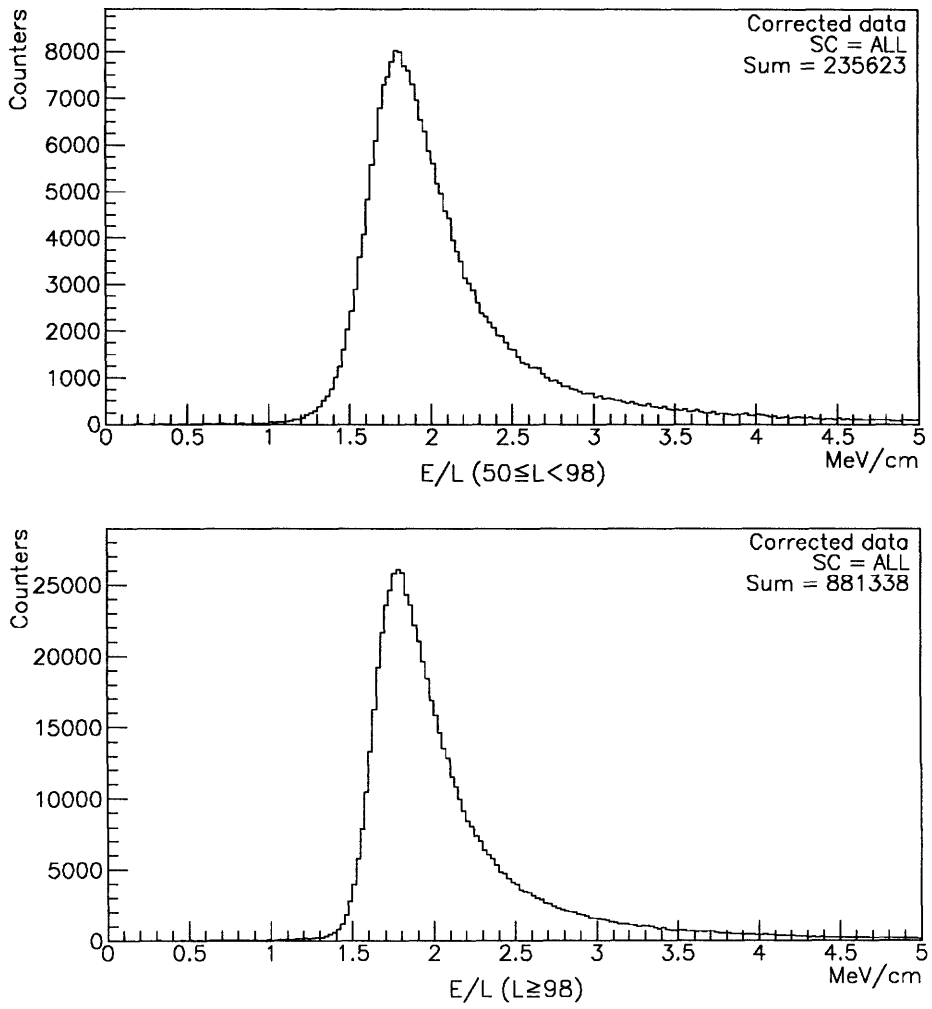

Figure 5-4: The measured E/L distribution after whole-counter gain calibration and geometrical corrections inside the counter. The data are in two separate regions of track length L.

estimated by the predicted amount of multiple scattering [ABCC+84]

$$\theta_0 = \frac{14.1\,\mathrm{MeV/c}}{p\beta} Z_{inc}\sqrt{L/L_R}[1 + \frac{1}{9}\log_{10}(L/L_R)]\,(\mathrm{radian}), \tag{5.5}$$

$$s^{rms}_{plane} = \frac{1}{4\sqrt{3}} L\theta^{rms}_{plane} = \frac{1}{4\sqrt{3}} L\theta_0. \tag{5.6}$$

where p, β, and Z_{inc} are the momentem (in MeV/c), velocity, and charge number of the incident particle, and L/L_R is the thickness, in radiation lengths, of the scattering medium;

θ^{rms}_{plane} is the rms of deflection angle in a plane, s^{rms}_{plane} the transverse deviation from a straight line in a plane.

For a vertical track the amount of iron and scintillator traversed is $L/L_R = 10.4$ and $L/L_R = 14.2$, respectively. Setting $s^{rms}_{plane} \sim 10\,\mathrm{cm}$ as the upper limit allowed by the track selection criteria, and using 8 m as the L in eq. 5.6, then the lower limit on p from eqs. 5.5 and 5.6 is approximately 5 GeV.

The dE/dx distribution of muons of energy below 3 GeV is considerably different from the Landau distribution, especially on the left side of the peak. Low energy ($E_\mu < 2\,\mathrm{GeV}$) muons may lose all their energy in the detector. They widen the inclusive dE/dx distribition on the left side. In this analysis they are few, and largely rejected by the applied cuts.

5.4 The Monte Carlo *dE/dx* Distribution

Using the formulas stated in section 5.1 for the angular and energy distribution of incident muons that reach LVD, a number of muons comparable to the amount of data from the detector are generated on the upper hemisphere surrounding the first tower. Each of these single muons is traced through the detector elements using the LVD simulation program based on the GEANT3 [BBM+87] package from CERN. The simulated readout data are processed by the same LVD track-finding program that processed the data from the detector, after which the found tracks in the geometrical parameters given by the track-finding undergo the same selection as was described in chapter 4 to pick clean, straight, through tracks from real data. The E/L distribution from this Monte Carlo calculation is shown in Fig. 5-5. The inclusive (over all muon energy) dE/dx distribution is wider than the pure Landau distribution by less than 20% [KR92]. This is because the energy of most muons is below 1 TeV, the discrete processes do not add too much onto the ionization loss. Above 1 TeV, bremsstrahlung and pair production start to dominate the energy loss of the muon in the LVD liquid scintillator. The average energy of muons reaching LVD is 280 GeV;

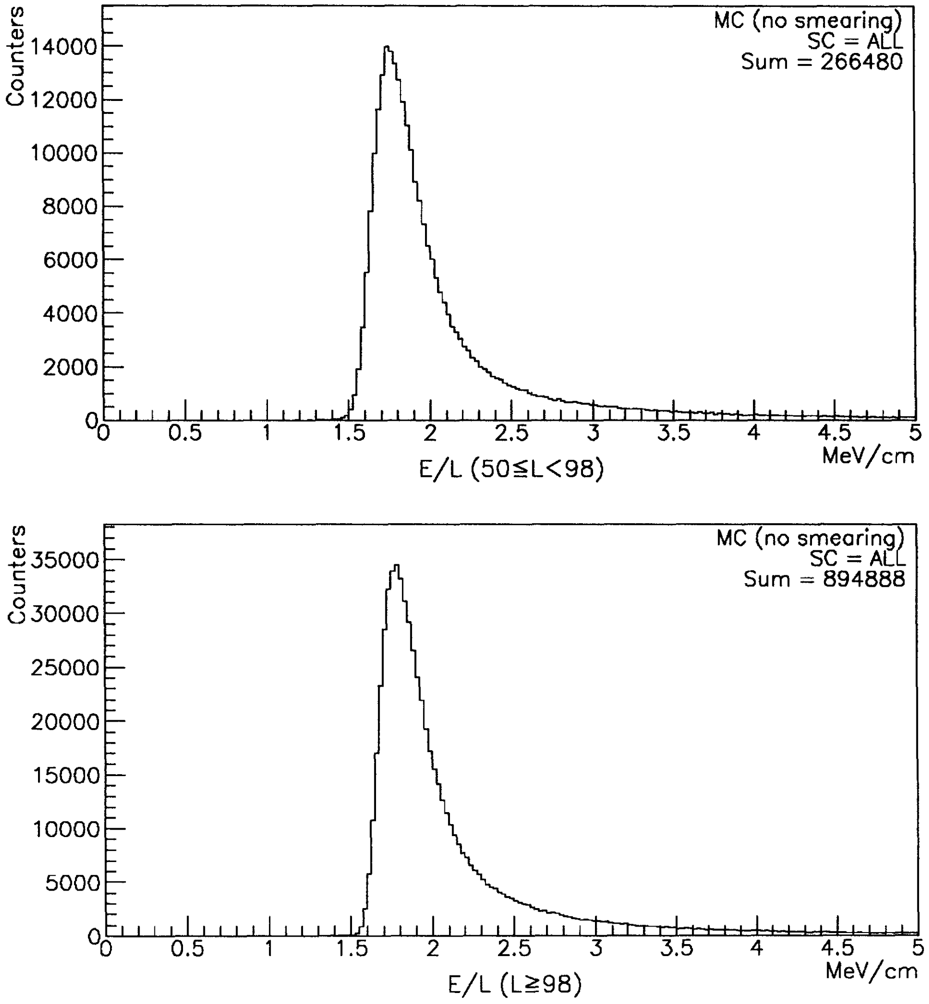

Figure 5-5: The Monte Carlo E/L distribution not taking into account instrumental errors.

only 3–4% are above 1 TeV. So the inclusive dE/dx distribution is close to the Landau distribution.

Apparently, compared to Fig. 5-4, the fluctuation of dE/dx from Monte Carlo is smaller than what has been measured in this experiment. This is because, even after the geometrical corrections, not all instrumental errors have been accounted for in the real data. The scintillation light generation, propagation, reflection, and collection are not simulated, only the energy loss by particles in the scintillator counter is given by the Monte Carlo simulation. To approximately account for all the errors, the E in E/L of Fig. 5-5 at each counter is smeared by a Gaussian fluctuation (with $\sigma = 7.6\%$) that makes the resultant E/L distribution best resemble the measured E/L distribution. The Monte Carlo E/L after this smearing is in Fig. 5-6. While 21% of measurement data from this experiment are in the shorter range of L, that fraction is 23% in Monte Carlo. This is because tracks can be more accurately reconstructed out of Monte Carlo data which are cleaner (and readout strip clusters leaner) than out of real data; and so the requirement $\frac{\delta L}{L} \leq 0.12$ rejects more data from the real data than from the Monte Carlo data when L is smaller.

A simple Gaussian fluctuation applied on Monte Carlo data does not simulate accurately all the instrumental errors, so although after this smearing the width of the Monte Carlo dE/dx distribution is about the same as that of the measured dE/dx , their overall shape is still somewhat different, especially when track length is short.

The smeared Monte Carlo dE/dx distribution (the sum of the two in the two regions of L) was used as the template only in the initial step of the iterative fitting procedure to calibrate the scintillator counter gain factors (using an even wider Gaussian fluctuation, with $\sigma = 12\%$, see chapter 4) and to find the geometrical correction factors inside the counter.

5.5 The Precision of the dE/dx Measurement

In conclusion, the difference between the measured dE/dx in the LVD scintillator counters (after the geometrical correction to the gain inside the counter) and the Monte Carlo dE/dx , caused by less well known instrument imprecisions, can be approximated by a Gaussain fluctuation[7] with $\sigma = 7.6\%$ (or equivalently $\frac{FWHM}{Peak\,(=1.)} = 0.18$).

The one σ precision of this measurement is 7.6%. In the following search for WIF particles by the dE/dx data on a track, this amount of fluctuation due to measurement

---

[7] This fluctuation is different from the intrinsic muon dE/dx fluctution in the LVD scintillator material dictated by physics, which is (integral over the muon energy spectrum) close to the Landau distribution because most of the cosmic muons at LVD are relativistic, but not ultrahigh-energy.

errors is taken into account because the dE/dx probability density functions are taken directly from the measurement results.

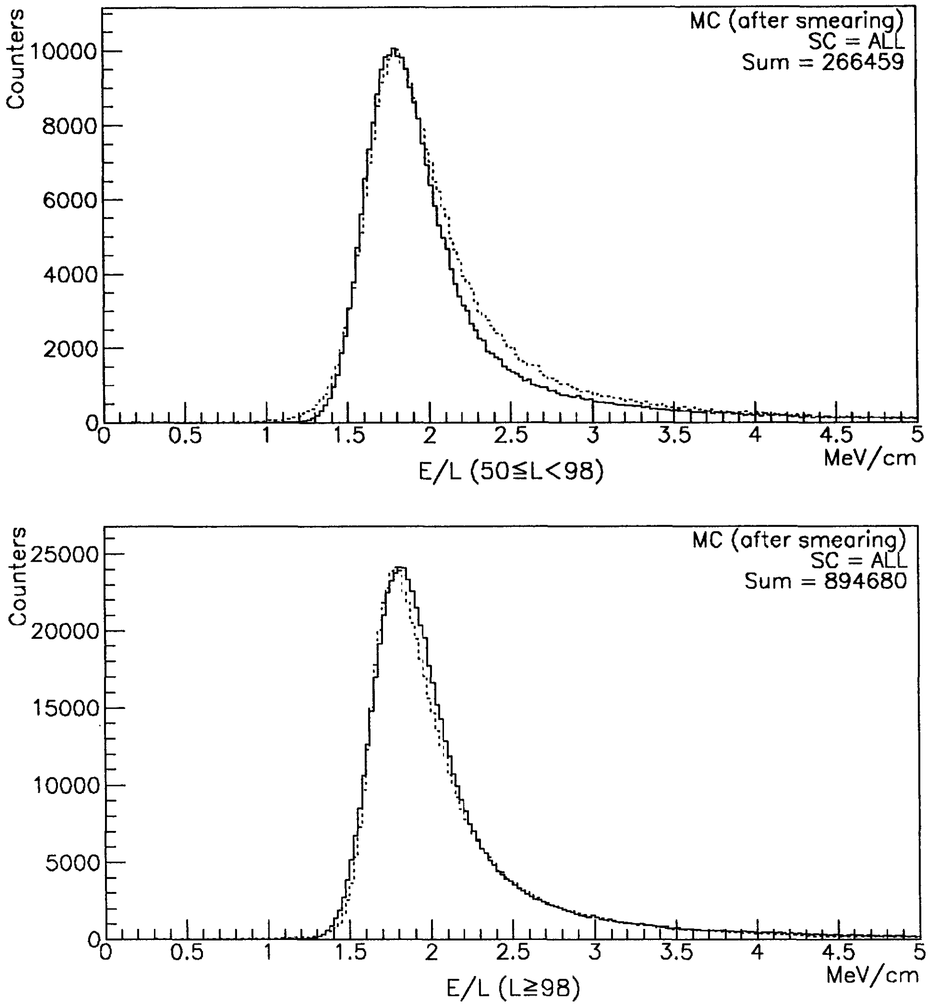

Figure 5-6: The Monte Carlo E/L distribution after E is smeared by a Gaussian random distribution. The width of the Gaussian is chosen to make the smeared E/L distribution approximately fit the measurement result in Fig. 5-4, which is copied to this figure in dashed lines. Note that when the E/L distributions in the two regions of L are combined, the MC and the measured distributions have the same width at half maximum.

Chapter 6

Searching for WIFs

dE/dx is proportional to the square of the charge carried by the incident particle. A fractionally charged particle, for example, one of $\frac{2}{3}\,e$, will demonstrate itself by its dE/dx distribution located to the left of the muon dE/dx distribution by a factor $\frac{4}{9}$. This feature is employed in the search for WIFs at LVD.

The search is conducted within the same data sample that was selected in chapters 4 and 5 to produce the measured dE/dx distributions. Two E/L distributions are chosen, in the two ranges of L respectively:

$50\,\mathrm{cm} \leq L < 98\,\mathrm{cm}$, and

$L \geq 98\,\mathrm{cm}$.

The E/L distribution is divided into two because the amount of measurement error is different in the two ranges of L, as was discussed in previous chapters.

In order to determine whether a given track which passes through several scintillator counters has energy loss consistent with a muon, it is necessary to define a metric for a collection of muon tracks. Assume that (1) all counters are statistically independent and after the corrections they have the same features in dE/dx and its readout, (2) there is no correlation between the energy deposited by a muon in several counters as it passes through these counters. Under these two assumptions a metric α can be defined for the sample of data in the following manner.

The product F_N is formed

$$F_N = \prod_{i=1}^{N} f_{L_i}(E_i/L_i).$$

Where $f_{L_i}(E_i/L_i)$ is the value of the probability density function at the point E_i/L_i, corresponding to a muon that deposits energy E_i in counter i with track length L_i. N is the number of counters along the track. There are only two different functions $f_L(E/L)$ depending on in which of the two ranges L is.

It can be calculated what fraction of the sample of data should have had this value of F_N or less. This fraction is here called α. It is assigned to that particular track. The value of α has two important properties:

1. $N_{total} \times \alpha = N(\alpha)$,
2. α has a flat distribution in the sample of data.

N_{total} = total number of events in the sample. $N(\alpha)$ = number of events in the sample that have the value α or less. These two properties (either one can be derived from the other) are because of the construction of α, which represents the integral of a probability density function from zero to the value of α. The details of the metric and its implementation are discussed in ref. [PP93] and in section 6.3.

As just discussed, the metric[1] calculated in the way described in this chapter will be in a flat distribution in the region 0.0–1.0 if the tracks are all relativistic muons and the counters they traverse are not correlated in dE/dx along a track. It will concentrate near 0.0 if the tracks are $\frac{2}{3}e$ charged particles. The search for such particles is thus conducted in a systematic way by a high-resolution distribution of this metric, which combines the information about a track from several scintillator counters.

---

[1] This integral of a probability density function is a flat distribution in the range 0.0–1.0.

6.1 dE/dx Distribution of WIFs

Fig. 6-1 shows the location of dE/dx of $\frac{1}{3}e$, $\frac{2}{3}e$ WIFs, relative to the muon dE/dx distribution. They are not submerged by the muon distribution, the more so when a coincidence requirement of more than one counter with accepted readout on the track is applied to the data. About half of all 3-point (tracking points) tracks go through more than 2 counters[2]. In the scintillator counters even a $\frac{1}{3}e$ particle will lose enough energy

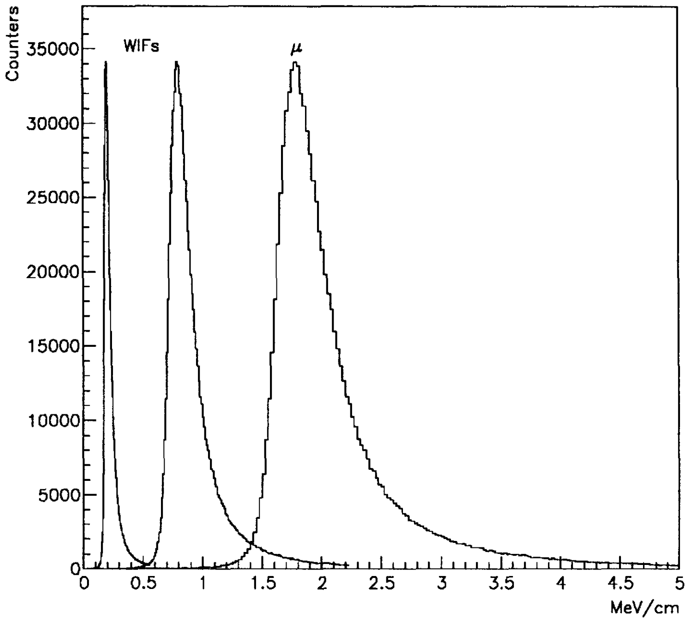

Figure 6-1: The measured E/L distribution of cosmic muons in the LVD scintillator counters, where E is energy loss in a counter, $L(\geq 50\,\text{cm})$ is length of reconstructed track in the counter, no distortion caused by overflow at different points allowed. Also shown are the muon distribution scaled by $\frac{1}{9}$, $\frac{4}{9}$, as the distribution of $\frac{1}{3}e$, $\frac{2}{3}e$ WIFs respectively.

over 100 cm to be above the high threshold in the trigger and readout system. But its track can be determined only when it also causes a sufficient amount of ionization in the 1 cm thick limited streamer tubes filled with a gas mixture at 1 atm.

From data tables (e.g., one in ref. [Fer86]) about gas properties, the number of primary

---

[2] Not merely through any counter, but through a normal, calibrated counter, within a corrected "unit" in it, and with $L \geq 50\,\text{cm}$, $D \geq 5\,\text{cm}$.

ionizations by a minimum ionization particle at 1 atm of gas pressure along 1 cm of track length can be calculated. For the two different gas mixtures employed in the LVD streamer tubes these numbers are

	e	$\frac{2}{3}e$	$\frac{1}{3}e$
Ar(25%):C_4H_{10}(75%) (until Nov, 19, 1992)	41.8	18.6	4.6
Ar(2%):C_4H_{10}(10%):CO_2(88%) (after)	35.1	15.6	3.9

For a charged particle to be detected, it has to generate enough ionization so that at least one primary electron will survive the quenching processes and reach the anode wire causing a limited avalanche. It can be estimated that the *recombination* will not reduce the number of elections in a short time interval less than 1 μs, but *attachment* to an unknown amount of water vapor might be important because the LVD experimental area is moist and there is a certain transparency to water vapor in the 1 mm thick plastic material PVC constituting the cover of the streamer tubes. At 20°C and 1 atm, saturated water vapor diminishes the number of electrons by a factor of 10^3 in 1 μs [RE74]. Consequently, if the water concentration is even 1% of saturation there could be detection difficulties.

The LVD tracking system can certainly detect a $\frac{2}{3}e$ particle, because the efficiency of a streamer tube in its active volume for a muon is nearly 100% and a $\frac{2}{3}e$ particle generates about half as many election-ion pairs in the streamer tubes as those generated by a muon. Assuming the muon detection efficiency in the streamer tube is 97%[3], the efficiency for $\frac{2}{3}e$ particles is about 80% in a single layer of streamer tubes. In a double-layer the detection efficiency is above 95%. For $\frac{1}{3}e$ particles, the detection efficiency is not certain, so this analysis is limited to the search for $\frac{2}{3}e$ WIFs.

---

[3] This is a conservative estimation. The overall single-layer efficiency measured in the detector is between 90% and 100% ([Sil94]) and varies in different layers. When gaps in the streamer tubes and between the tubes, dead electronic channels, and signal pickup inefficiency of readout strips are taken into account, the detection efficiency inside the active volume of a gas cell approaches 100%.

6.2 The Probability of a Muon Track by its dE/dx

When a track goes through several scintillator counters, it creates in each of these counters a different dE/dx. Assuming uniformity among the counters after the calibrations, the measured dE/dx distribution summed over all counters can be used as the sample probability density function for the dE/dx in any single counter.

Because the energy loss of the track is not large compared to its total energy, the dE/dx distribution is nearly constant in the different counters the track goes through. When the total energy is of the order of 100 GeV, the main component of the dE/dx comes from ionization, which does not change because the particle is relativistic. Hence even after the typical loss of 1–2 GeV in the detector, the dE/dx distribution remains the same. So when there are several active counters along the track, the probability distribution of the dE/dx in these counters can be assumed the same and independent of each other, and the product of the several single-counter probability density functions can be used as the joint probability density function.

There are two main sources of inaccuracy. (1) For any individual counter the real dE/dx distribution is narrower than the summed distribution used as the probability density function for all. This will cause the α distribution to tilt systematically upwards when it goes from 0.0 to 1.0, starting from a point near 0.0. (2) A small number of tracks with relatively large measurement errors, and dE/dx values off the peak of the distribution, will make the α distribution rise up near 0.0.

6.3 The Calculation of a Muon Track dE/dx Probability

The two basic dE/dx distributions, in the two respective regions of track length L in a counter, are each fitted to eleven pieces of third-order polynomial functions, as shown in Fig. 6-2. In the fitting, the start and stop points of each piece of polynomial (overlapping

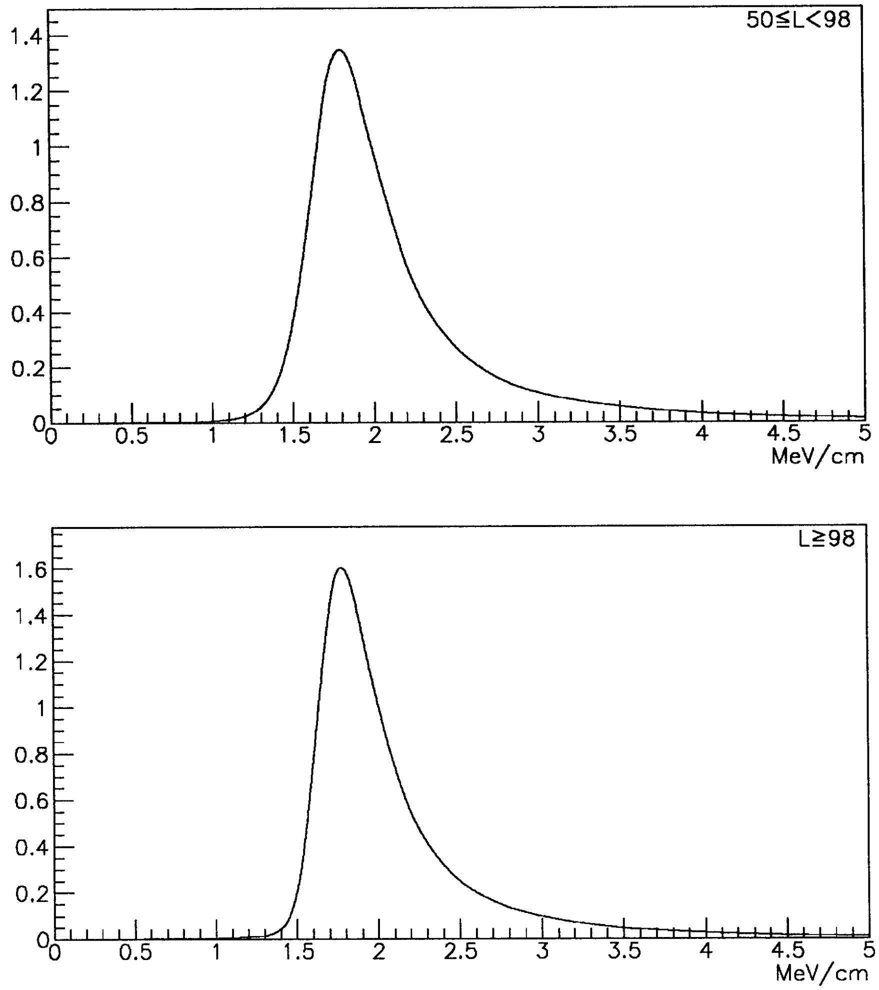

Figure 6-2: The distributions of Fig. 5-4 each fitted by eleven pieces of 3rd-order polynomials, each normalized to become the probability density function of E/L in the respective range of L. Due to the effect of readout threshold at about 7 MeV, the function on top starts at 0.175 MeV/cm, the lower one starts at 0.075 MeV/cm.

the adjacent pieces by at least two bins as those in Fig. 5-4) are deliberately chosen to make the curves in Fig. 6-2 have the following properties: (1) continuous at connection points; (2) the first derivative has the correct sign everywhere and is almost continuous or at least jumps in the right direction at connection points; (3) the second derivative has the correct sign everywhere, and jumps in the right direction at connection points.

The result of this fitting, normalized, is used as the E/L probability density function in the respective range of L for any single counter. When more than one counter are hit along the track, the product of the several density functions, each at its own E/L, is assumed to be the multi-variable density function.

When there is only one variable in a probability density function, usually by integration one may easily use the term *confidence level* to describe how well a result conforms to a hypothesis. In the search for WIFs in this thesis, however, the first test is on how well a track going through several counters, each of which gives some value of E/L, conforms to the hypothesis that in each counter the track loses some energy according to the probability density functions found in Fig. 6-2. In this case the density function has more than one variable.

A particular integral of the multi-variable density function is found by a Monte Carlo method [PP93], by generating large numbers of events according to the density functions in Fig. 6-2. For any specific number, n, of counters a track may go through, there are $n+1$ combinations (counters in which $L < 98\,\mathrm{cm}$ are called *short*, $L \geq 98\,\mathrm{cm}$ are called *long*):

short	*long*
0	n
1	n-1
⋮	
n-1	1
n	0

for n = 3–8 there are in total 39 combinations[4]. For each combination a large number of events are generated, with random E/L in each counter according to the functions in Fig. 6-2, to fill a table of the integral function α that will be used later for real tracks and measured E/L values in the detector.

The table contains the distribution of a particular integral of the multi-variable density function. It is created by repeating the following calculation many times till an accurate and smooth function appears:

1. calculate the product H of the several single-counter density functions at the E/L values randomly generated according to the density functions[5],
2. increment by 1 all the bins in the table above the one that corresponds to this specific value of H.

This is a numerical way to calculate an integral of F_m using a single variable H (the height of F_m itself at any point) as the horizontal coordinate. What is stored in any bin of the table is the integration of F_m from zero height at the edges to a height H at that bin. Because several of the functions in Fig. 6-2 are multiplied by each other, F_m has numerically a very sharp peak around one point. To achieve precision for the table two methods are applied in the calculation: (1) throw many more events in a small area around the peak and weight each of the events (all random) in this area by the factor of relative increase in frequency; (2) use a nonlinear (but monotonically increasing) function of H as the horizontal coordinate of the integral.

This integral is here called α. Small H close to zero is accompanied by small α close to zero, and corresponds to points at the edges of the multi-variable density function F_m.

---

[4] Very few tracks traverse more than 8 counters with valid E/L, and very high statistics is needed in the Monte Carlo calculation to carry out the integration for $n = 9, 10$. The $n = 1, 2$ cases are skipped because they are less reliable. The α distribution of a WIF overlaps the α distribution of the muons by a larger fraction in these cases, which is not favorable to the search for WIFs based on α, as will be explained later.

[5] This product is the height H of the multi-variable density function F_m at that point, F_m still has only one peak, when H is small it means that the point is at the edges of F_m.

When H is maximum, at the single peak of F_m, $\alpha = 1$. The distribution of α for any number of counters produced by random events distributed according to the two basic functions in Fig. 6-2 is flat in the range 0.0–1.0. This is by the nature of any integral of a probability density function.

Fig. 6-3 shows the distribution of α by all the measured tracks that traverse 3–8 counters each with E/L corrected by the procedures of chapter 4. This distribution has a slow, gradual rise when α goes from 0.0 to 1.0 and a sharper rise when α nears 0.0. The reasons of these two features were explained at the end of section 6.2. The slow rise means in real data α approaches 1 more quickly, or in other words the real multi-variable E/L distribution of the tracks is slightly narrower. When the two basic density functions in Fig. 6-2 are made slightly narrower, this slow rise disappears. The quicker rise when α nears 0 is caused by relatively large errors in E/L on certain tracks, more likely due to the incomplete geometrical gain corrections inside the scintillator counters assuming all counters are identical; this rise is more marked when the criteria used to select clean, straight, through tracks (uniformly applied on all found tracks, based solely on geometrical features, without introducing bias against low α tracks), stated in chapter 4, are relaxed.

The same α distribution of muons is displayed in logarithmic scales in Fig. 6-4. The more intersting region of very small α is thereby magnified. The rise near $\alpha = 0$ in Fig. 6-3

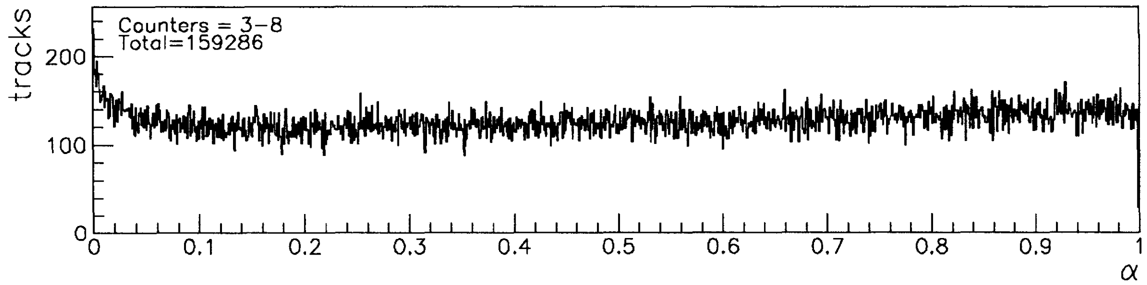

Figure 6-3: The α distribution of muons traversing 3–8 counters each with valid E/L. Some of the jitters are caused by small errors in the tables which contain the integral α as a function of H. Such small errors show up as jitters because the bins are very thin in this figure.

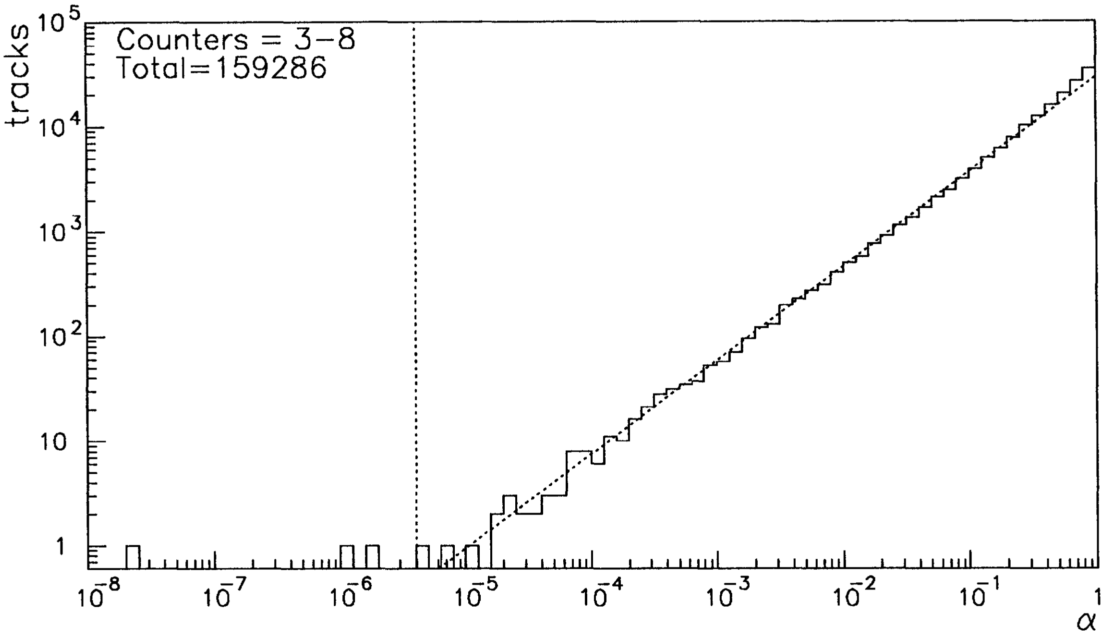

Figure 6-4: The α distribution of muons traversing 3–8 counters each with valid E/L, in logarithmic scales. Almost all the data are on a straight line. There are 3 tracks to the left side of the vertical dashed line, one track exactly on the line.

is suppressed in Fig. 6-4. However, Fig. 6-4 clearly indicates 4 events that are not consistent with being muons.

To know whether these 4 events might be WIFs, it is necessary to see the α distribution generated by a comparable amount of simulated $\frac{2}{3}e$ WIF tracks, yet using the same tables based on the two functions in Fig. 6-2 for muons. This is in Fig. 6-5. The dE/dx distributions of the $\frac{2}{3}e$ WIFs are obtained by scaling the two functions in Fig. 6-2 horizontally by $\frac{4}{9}$ and extending them to 5 MeV/cm linearly where they become zero[6]. The same sample of muon tracks, except that the E/L in each counter along the track is artificially generated from the dE/dx distribution of a $\frac{2}{3}e$ WIF, are used to produce Fig. 6-5.

Note that the logarithmic scales in Fig. 6-5 stretch out the distribution near $\alpha = 0$. If it

---

[6] Another way to simulate the dE/dx distribution of a $\frac{2}{3}e$ WIF is to use the muon Monte Carlo data, scale the muon energy loss by $\frac{4}{9}$, and smear it by a Gaussian fluctuation. However, it is found that directly scaling the measured muon dE/dx horizontally by $\frac{4}{9}$ gives a more realistic WIF dE/dx distribution, which overlaps with the muon dE/dx more, making this experiment more realistic.

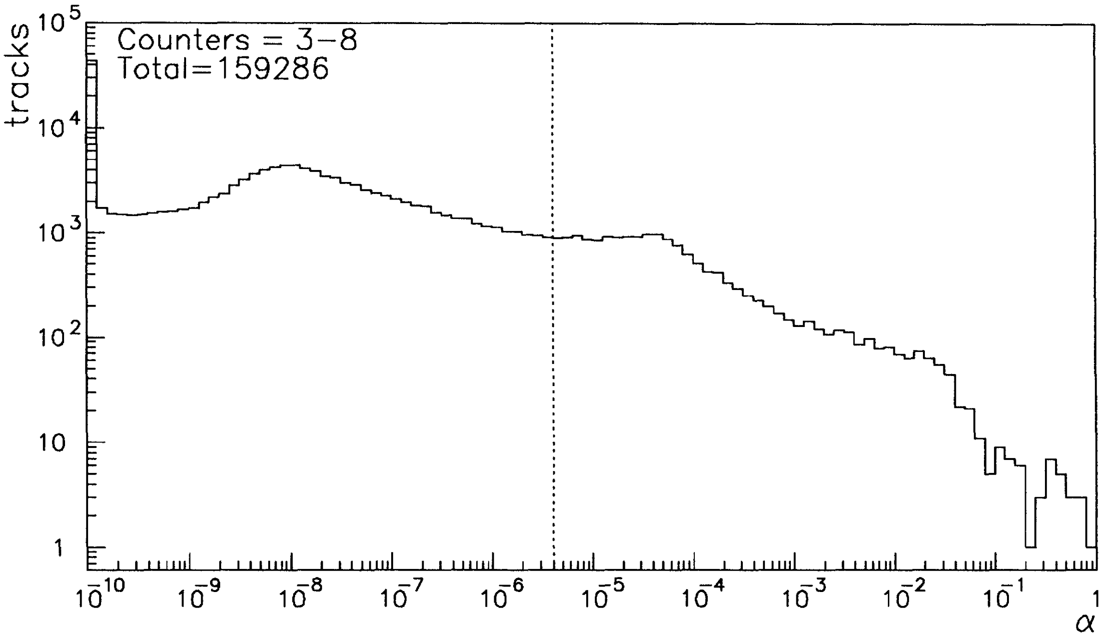

Figure 6-5: The α distribution of hypothetical $\frac{2}{3}e$ WIFs. The dE/dx is by the WIFs, but the α is calculated using the same tables based on Fig. 6-2 which produced Fig. 6-4; this is to learn where a WIF would be in Fig. 6-4. The first bin on the left also contains all the data below 10^{-10}. Notice the difference in horizontal scale between this figure and Fig. 6-4. 90% of the total amount of data is located to the left side of the vertical dashed line.

was rendered in linear scales as in Fig. 6-3, only the first bin at the left end would be visible. In fact, 90% of the total in Fig. 6-5 is to the left side of the point where $\alpha = 4.011 \times 10^{-6}$. This is also the point in Fig. 6-4 from where to the left there are only 4 events which stray from the straight line formed by the rest of the total. If the hypothesis that in each counter a track loses some energy according to the probability density functions in Fig. 6-2 is correct, then Fig. 6-3 should be a flat distribution and Fig. 6-4 should be a straight line.

The 4 events in Fig. 6-4 at the left end of the distribution, which are away from the line formed by muon tracks going through any number of counters and losing energy in each of them according to the dE/dx distributions found from this experiment, and which are located in the region where a WIF would most likely fall[7], are the ones to be examined in

---

[7] By a probability of 90% as found in the previous paragraph and in Fig. 6-5, not 100%; this much ambiguity is intrinsic—it is because the dE/dx distribution of a $\frac{2}{3}e$ WIF overlaps the muon dE/dx distribution. By the method used here to simulate the WIF dE/dx distribution, see the previous footnote and Fig. 6-1.

detail. Below that point where $\alpha = 4.011 \times 10^{-6}$ in Fig. 6-4, by the integral definition of α and the total number of tracks, there are only $4.011 \times 10^{-6} \times 159286 = 0.63$ expected tracks. Hence the 4 tracks there cannot be explained as statistical fluctuation. These events may have correlation among the scintillator counters along the tracks, in particular the correlation could be that the charge of the particles passing through the counters are $\frac{2}{3}e$.

These 4 events are presented in Fig. 6-6 to Fig. 6-9. The causes of their appearance in the region of very low α, characteristic of WIFs, are explained in the captions. In these figures there are two numerals in each counter with "high threshold" readout, the one on top is the time in nanoseconds after the earliest hit, the one below is the calibrated energy loss in that counter in MeV, before the "unit" by "unit" (see section 4.6) geometrical corrections. The α is calculated according to the corrected energy loss. When in a certain counter a track does not go through a correctable "unit" that counter is ignored.

In addition to the α based on the muon dE/dx found in Fig. 6-2 and calculated for a set of E/L data along either a muon or a WIF, another quantity was defined in the same manner but based on the dE/dx distributions of a hypothetical $\frac{2}{3}e$ WIF. This new quantity is called α_W. When it is close to 1.0 it means all E/L data are close to the dE/dx peak of a WIF.

The events in Figs. 6-6, 6-7, and 6-8 have correlation among counters along the tracks; they pass close to the walls of the counters where energy errors are larger than the average. The event in Fig. 6-9 cannot be explained in the same way. It is believed that this is a normal event but the data selection criteria in this event reject those scintillator counters that had large E/L and leave three counters with low E/L.

The amount of overlapping is more than 10% in both the *short* and *long* regions of track length L. In this experiment there is a probability of 10% for a $\frac{2}{3}e$ WIF to be buried as a muon, unless their dE/dx distributions overlap each other less, or not at all. In the α distributions in Figs. 6-4 and 6-5, on which this systematic search is based, if single- or double-counter tracks are included the ambiguity will be more than 10%. That's why only 3-counter-and-above tracks are used.

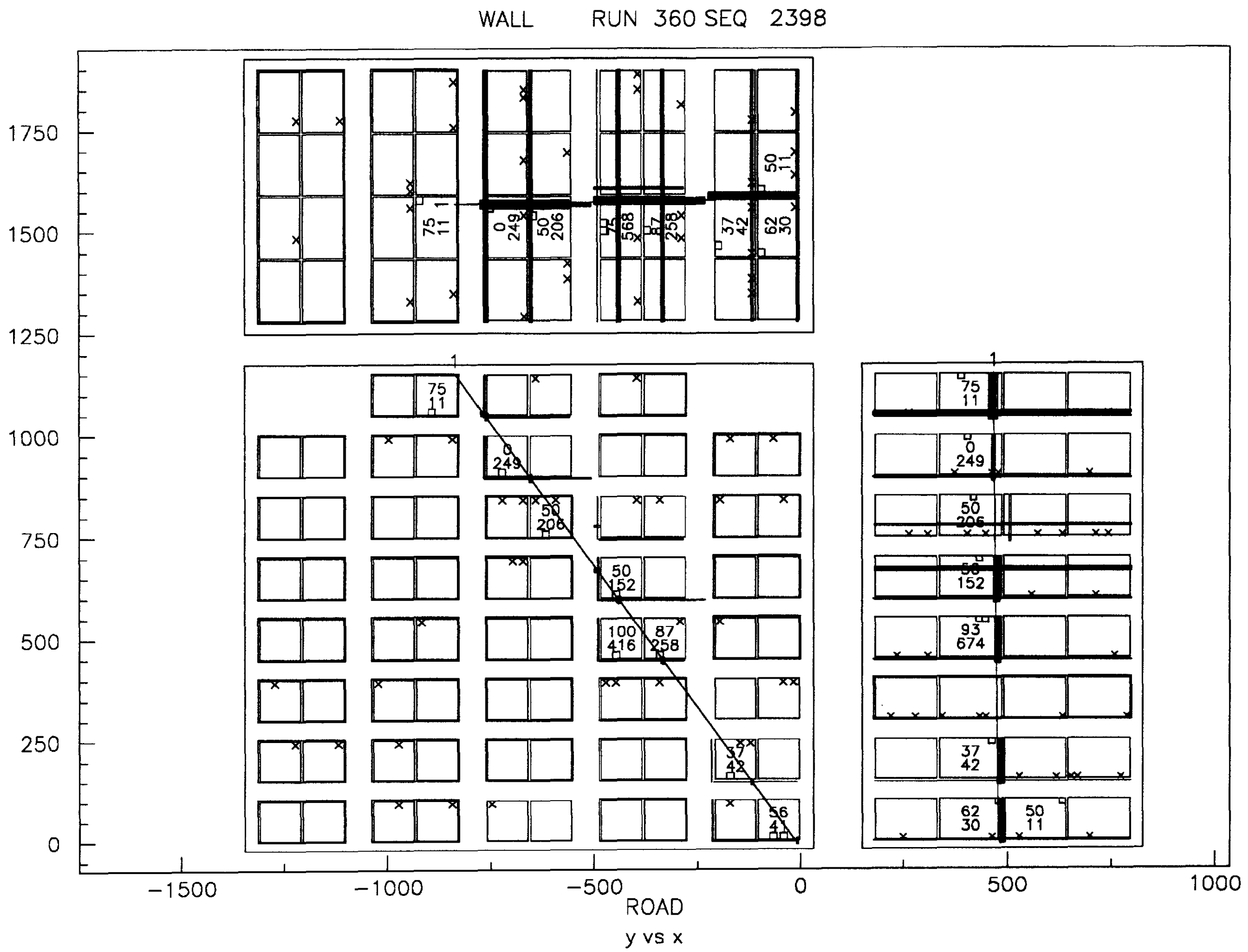

Figure 6-6: This is a track too close to the walls of the counters it traverses, for all the counters, although the $D \geq 5\,\mathrm{cm}$ condition is satisfied. Six of the counters (2 *short*, 4 *long* in L), on the track and with readout, entered the calculation of α. $\alpha = 4.011 \times 10^{-6}$. The α by the tables based on the dE/dx of a $\frac{2}{3}e$ WIF is $\alpha_W = 9.978 \times 10^{-11}$.

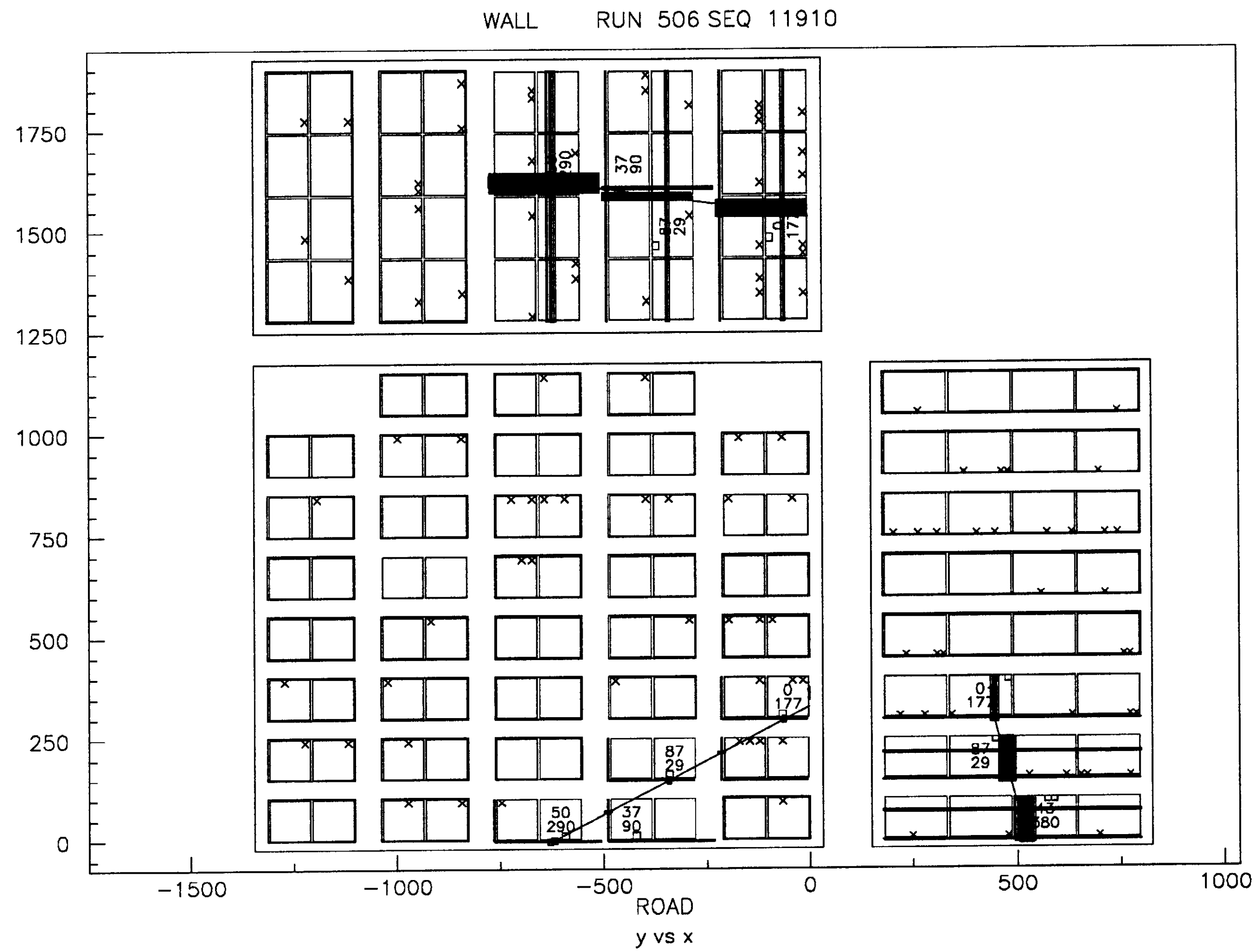

Figure 6-7: The Y-strip clusters on this track are wide, although because the X-strip clusters are narrow, precise, and sufficiently wide-spaced the track was considered accurate on average. The 3 counters included in the calculation of α are all *short* in L (close to 50 cm). Moving the track by a small amount within the boundaries of the Y-strip clusters would make the track very close to walls of the counters. $\alpha = 1.019 \times 10^{-6}$, $\alpha_W = 1.428 \times 10^{-2}$.

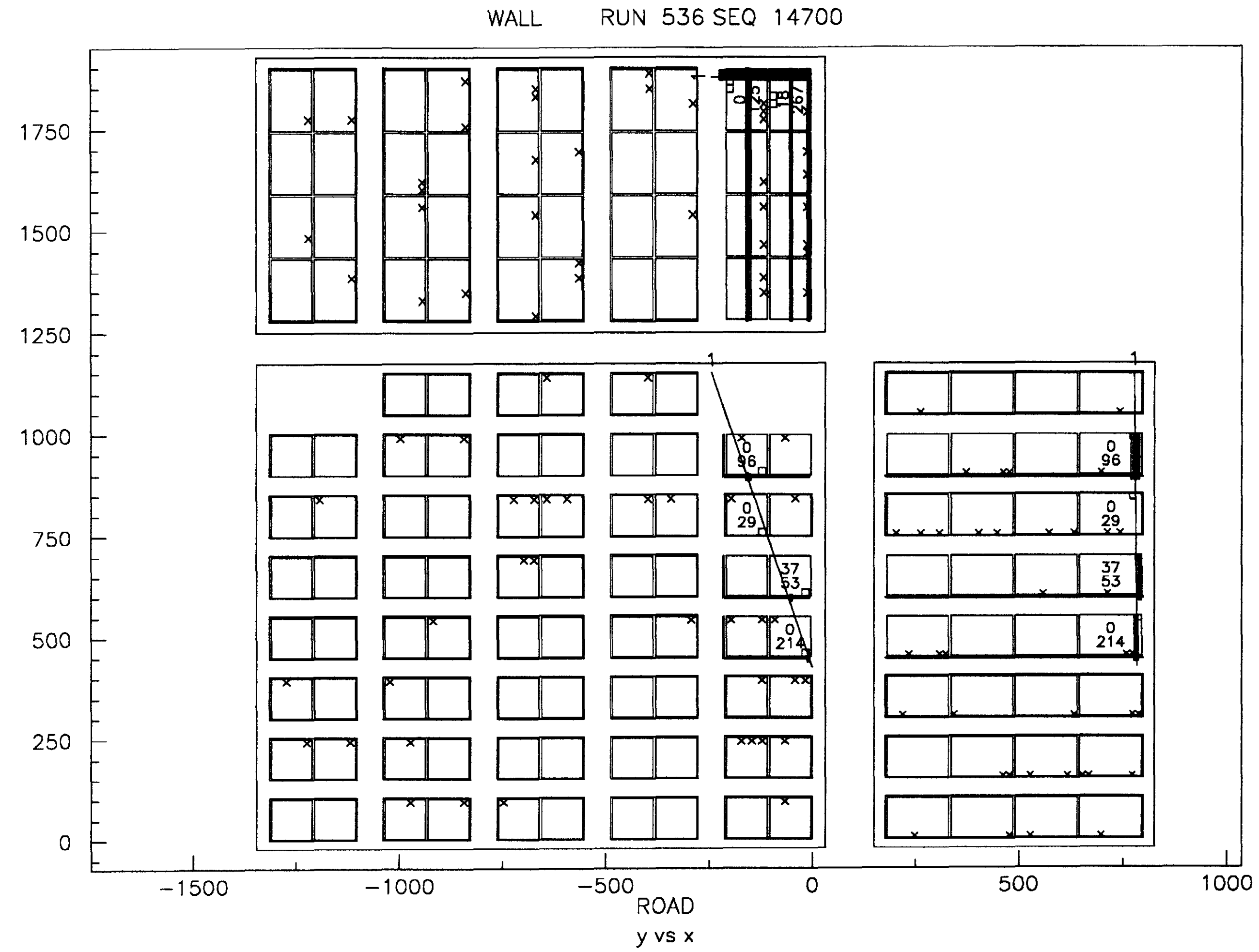

Figure 6-8: All 4 counters, *long* in L, are used in the calculation of α, but the track is at one end of all counters, which is less reliable in geometrical corrections on the gain. $\alpha = 2.215 \times 10^{-8}$, $\alpha_W = 8.607 \times 10^{-5}$.

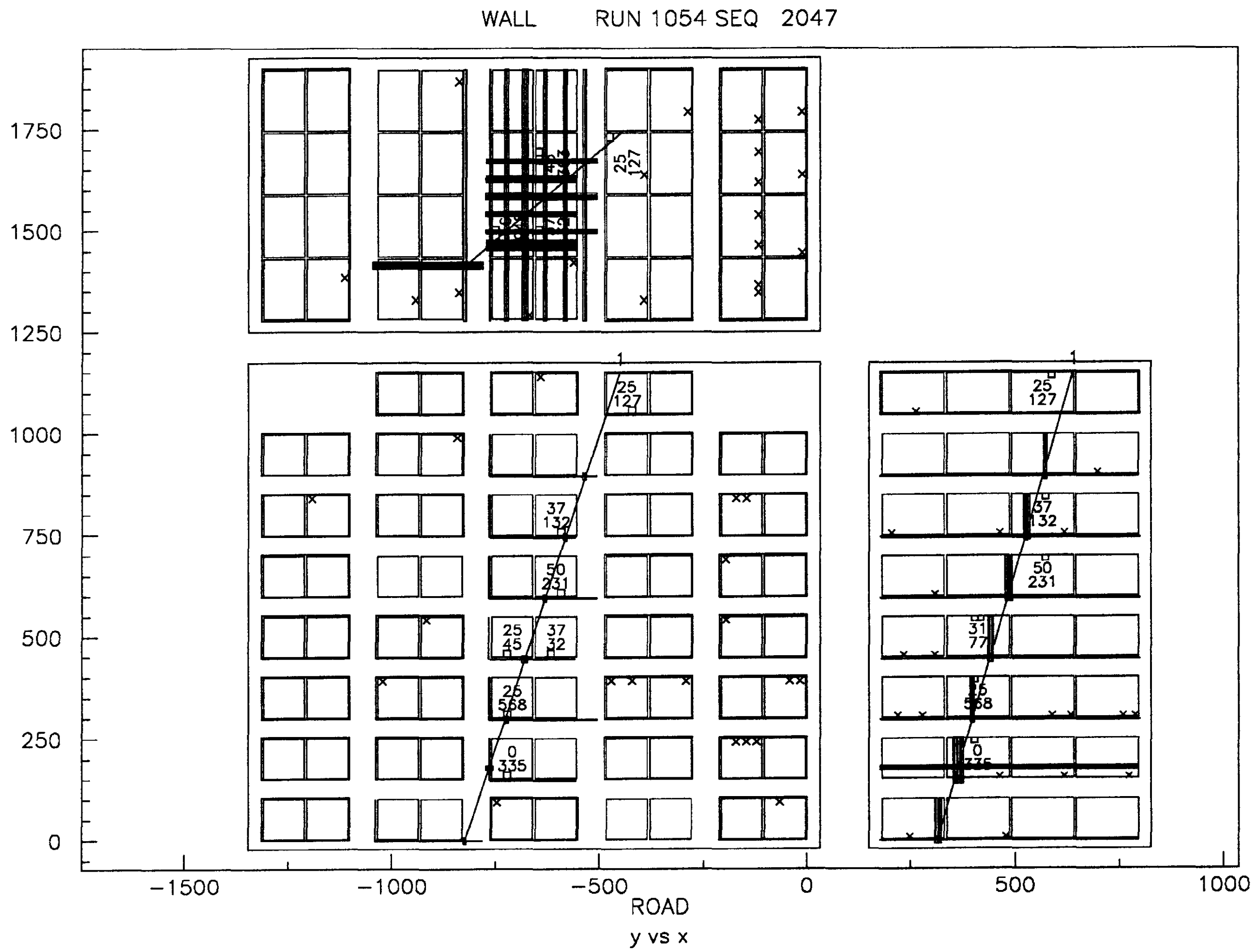

Figure 6-9: Only three counters (2 *long*, 1 *short*) are used in the calculation of α ($= 1.837 \times 10^{-6}$). Using only the 3 counters, $\alpha_W = 1.539 \times 10^{-1}$, a rather high value indicating on average the E/L's of the 3 counters are not too far from the dE/dx peak of a $\frac{2}{3}e$ WIF. The other counters were rejected because of their larger $\frac{\delta L}{L}$. If they (2 more *short* counters, with high E/L; another has an E/L value even higher, but was not used because the track does not go through a correctable "unit") are included in the calculation, α becomes 3.939×10^{-2}, and α_W becomes 9.631×10^{-2}. It moves to the area where most muons are located.

The main sources of background to this search for WIFs, which introduce abnormal dE/dx along a track, were eliminated by the track selection requirements described in chapter 4. These sources are

1. geometrical errors of a track—a small rotation or shift of the reconstructed track can change the track length L in a counter by a considerable amount when the track passes the counter at a corner—leading to miscalculated L;
2. shower events, within which wrong or partially wrong tracks are reconstructed, or energy deposit in a counter is not from one muon track;
3. non-straight or stopped tracks of low energy muons are reconstructed as straight lines, which do not yield the true track lengths in some of the scintillator counters.

The track quality criteria were found after testing various sets of them and examining hundreds of events in pictures such as Fig. 6-6. These criteria were uniformly applied geometrical requirements, so no bias was introduced against events that are low in α.

Even though they are consistent with WIFs by the value of α, none of the 4 events in Figs. 6-6 to 6-9 contains a WIF candidate; they all involve relatively large measurement errors not rejected by the data selection rules. The result of this search for WIF particles is negative.

6.4 The LVD Acceptance

The acceptance for an isotropic angular distribution of WIFs is calculated in the following way.

1. Pick a sphere that encloses the detector (only the first tower in this analysis). The acceptance of the sphere is $A_{sph} = 4\pi \times \pi r^2$ in the unit m^2·steradian.

2. Uniformly pick a random direction, generate particle tracks in that direction and randomly and uniformly spread over the sphere cross section normal to the direction.
3. Trace a track by Monte Carlo from the entrance into the detector to the exit or disappearence of the track or its secondaries, record the "hits" in both tracking (aluminum pickup strips) and scintillator counters.
4. Reconstruct tracks out of the simulated data.
5. Select reconstructed Monte Carlo tracks by the same standards used on real data in this analysis (The difference between a perfect detector in the Monte Carlo and the real detector with noise and background is suppressed by the stringent criteria on clean tracks. The unsimulated inefficiencies in the real detector will be taken into account by using a factor from real data. See the next step. It has been found that the acceptance of the detector for such tracks is nearly uniform, which makes it valid to calulate the acceptance for a uniform flux this way.).
6. suppose in total N_0 tracks were generated initially on the sphere, and in the last step N_L tracks were found and accepted, the acceptance of the detector is $Acc = A_{sph} \times \frac{N_L}{N_0} = 4\pi \times \pi r^2 \times \frac{N_L}{N_0}$ in m^2·steradian (or more accurately, $Acc = A_{sph} \times \frac{N_3}{N_0} \times \frac{N_L(real)}{N_3(real)}$, where N_3 is the number of found Monte Carlo tracks that are only required to pass at least tracking points, $N_3(real)$ is the number of such tracks in real data, $N_L(real)$ is the number of tracks in real data that satisfy all requiments).

The GEANT3 Monte Carlo simulation could be used in the above calculation. However, since the energy spectrum and interaction mechanisms of the hypothesized WIFs are unknown, the result of a simpler simulation done in ref. [A$^+$94b] assuming all initial tracks are straight lines through the detector (with inefficienies in the tracking system) is adopted. This gives $A_{sph} \times \frac{N_3}{N_0} = 20,160 \times \frac{539,187}{15\times10^6} = 725\,\mathrm{m}^2$·sterad. To correct for harder cuts here imposed on data from both tracking and scintillator counters, it is multiplied by the ratio found in real data $\frac{N_L(real)}{N_3(real)} = \frac{159286}{471033} = 0.34$. Notice that the 3-counter ($L \geq 50\,\text{cm}$, $D \geq 5\,\text{cm}$, past calibration and geometrical correction) requirement on the track and an average of 10% inoperative counters make this fraction considerably less than 1. So the acceptance for WIFs is

$$Acc = A_{sph} \times \frac{N_3}{N_0} \times \frac{N_L(real)}{N_3(real)} = 725 \times 0.34 = 246\,\text{m}^2 \cdot \text{sterad}. \tag{6.1}$$

6.5 The Upper Limit of the Flux of WIFs

Assuming an isotropic distribution of WIFs, by the negative search result of section 6.3 and the LVD first tower acceptance found in the last section, an upper limit on the flux of WIFs can be established. At 90% confidence level, it is $\frac{2.3}{Acc \cdot T}$. The total operating time of the data analysed is $T = 245\,\text{days} = 2.12 \times 10^7\,\text{sec}$. Therefore the upper limit on the flux of WIFs is $4.4 \times 10^{-14}\,\text{cm}^{-2}\text{sterad}^{-1}\text{sec}^{-1}$.

Chapter 7

Conclusion and Comments

The measurement of the dE/dx distribution of muon energy loss in LVD scintillator is facilitated by the fine tracking ability of the detector. The response of the scintillator system to the energy loss is calibrated by the muon dE/dx distribution, counter by counter in 20-day periods, to correct the variation in gain among counters and their instability. It is afterwards geometrically corrected inside a counter, bundle by bundle, using muon dE/dx data from all counters in the entire 245 days of running time analyzed.

The dE/dx distribution obtained after the calibration of the scintillator counters and the geometrical corrections is predominantly a Landau distribution which is simulated in the Monte Carlo program for LVD based on the GEANT3 package from CERN. Instrumental errors unaccounted for in the simulation can be approximately represented by a Gaussian smearing ($\sigma = 7.6\%$) on the simulated energy loss in a counter. The data are divided into two regions of track length in a counter: $50\,\mathrm{cm} \leq L < 98\,\mathrm{cm}$, and $L \geq 98\,\mathrm{cm}$. The region $L < 50\,\mathrm{cm}$ is not used, because the errors in both energy loss and track length are large when L is small, so the measured dE/dx fluctuates more. Within the knowledge of the response and precision ($\frac{\sigma}{mean} = 7.6\%$) of the scintillator counter, the dE/dx data are consistent with the Landau distribution. This is the first time such a dE/dx measurement on well-determined cosmic muon tracks has been made with large-volume scintillator counters.

When the two measured dE/dx distributions in the two separate regions of track length are used as the sample probability density functions of dE/dx and the scintillator counters traversed by a track are assumed independent of each other, a combined multi-variable probability density function for a track going through a few counters is the product of several of the two basic functions.

Using the height H on the multi-variable density function F_m as a variable, one integral function of F_m is the integration from height equal to zero to any height below or equal to the maximum at the peak. This integral, called α in this thesis, ranges between 0.0 and 1.0. The α of measured data is distributed uniformly in this range; this is a property of any integral of a probability density function which describes the sample exactly.

The distribution of the logarithm of this integral α, when the vertical scale is also logarithmic, is a straight line. Its left end extends over the region of very few muon tracks (solely because of the logarithmic scales), but this is where a WIF track would be most likely located. See Figs. 6-4 and 6-5.

The measured data, in Fig. 6-4, are consistent with muons. Only 4 events are off the straight line. They are due to inaccuracies in track location and energy loss readout from scintillator counters. The assumption that the counters along a track are independent of each other so that the joint probability density function is the product of the individual ones is violated when a track is along the edges of all counters it traverses. When this happens, the α of the track is more likely to be small. Three of these 4 tracks are close to the walls of counters. The fourth track has only 3 of the 6 counters traversed accepted by the criteria on the precision in geometry and calibration. The data from those counters which were rejected indicate that the track is a muon.

WIFs are not detected at LVD in the 159,286 uniformly, unbiasedly selected tracks, each of which traverses 3–8 normal counters with calibrated dE/dx in the range 0.0–5.0 MeV/cm where there is no overflow to distort the total sample dE/dx distributions used as probability density functions in the calculation.

The operating time during this analyzed period is 245 days and the geometrical acceptance of one LVD tower for such tracks in uniform distribution is $246\,\mathrm{m}^2$·sterad, so an upper limit for the flux of $\frac{2}{3}e$ WIF particles at LVD is $4.4\times10^{-14}\,\mathrm{cm}^{-2}\mathrm{sterad}^{-1}\mathrm{sec}^{-1}$.

This result can be compared to those of other experiments, especially other underground experiments. The upper limits established by various earlier searches for fractionally charged particles were summarized in ref. [Lyo85]. Here some more recent experiments are quoted and compared with this search at LVD. The upper limits are all established at 90% confidence level.

Experiment	Events	Time (days)	Upper Limit on Flux ($\mathrm{cm}^{-2}\mathrm{sterad}^{-1}\mathrm{s}^{-1}$)
Kamiokande-II	4.9×10^6	1009	2.3×10^{-15} [B+91a]
LVD	1.6×10^5	245	4.4×10^{-14}
LSD	4947	2097	3.1×10^{-13} [A+94a]
Tokyo	2.7×10^6	217	9.8×10^{-13} [K+84]

Compared to Kamiokande II, LVD has the advantages of a tracking system of good spatial resolution, direct energy measurement with less statistical fluctuation by the scintillator counters, and multiple sampling of the dE/dx on a track. It should be noted that only 4 events at LVD had to be examined by physicists, while at Kamiokande II 4808 events remained to be scanned after analysis. LSD is based on the same scintillator counters (smaller in number) as the ones in LVD, but it does not have a tracking system. The Tokyo experiment is composed of thin slabs of plastic scintillator, with energy resolution a few times worse than that of LVD and smaller volume. With more running time, and more towers coming into operation, LVD will be able to establish a more stringent upper limit.

The crucial part of this search for WIFs at LVD is the energy resolution of the scintillator counters, after a track has been well defined geometrically by the tracking system. If the measured dE/dx distribution were closer to the theoretical Monte Carlo prediction without much further smearing to account for instrumental errors, the dE/dx of the WIFs would be more clearly separated from the muon dE/dx distribution.

One possible improvement to the present method based on the integral function α would be to separate the left side of the muon dE/dx distribution from the right side in the procedure of integrating the multi-variable probability density function. Any integral function would still be uniformly distributed, but the left side is more relevant in the search for WIFs of charge less than $1e$. The right side could also be examined for WIFs of charge more than $1e$. This will not be possible if based on the dE/dx data from single counters—the two lower ends on both sides of the dE/dx distribution, though sufficiently far from the peak, still contain enough data to bury a WIF candidate. However, when the dE/dx data from several counters traversed by a track are combined to calculate a quantity such as the α used in this analysis, muons and WIFs are more distinguishable from each other.

Appendix A

LVD Author List

M. Aglietta[19], B. Alpat[16], E. D. Alyea[8,10], P. Antonioli[19], G. Anzivino[7], G. Badino[19], Y. Ban[5], G. Bari[1], M. Basile[1], A. Benelli[1], V. S. Berezinsky[13], L. Bergamasco[19], R. Bertoni[19], S. Bianco[7], A. Bizzeti[6], A. Bosco[8], G. Brugnola[1], G. Bruni[1], Y. Cao[5], G. Cara Romeo[1], R. Casaccia[7], C. Castagnoli[19], A. Castellina[19], K. Chen[5], R. Chen[5], J. A. Chinellato[3], L. Cifarelli[1], F. Cindolo[1], G. Cini[19], S. Cong[5], A. Contin[1], V. L. Dadykin[13], M.Dardo[19], A. DeSilva[2], M. Deutsch[11], L. G. Dos Santos[3], R. I. Enikeev[13], F. L. Fabbri[7], W. Fulgione[19], P. Galeotti[19], P. L. Ghia[19], P. Giusti[1], F. Grianti[20], S. Gu[5], Y. Guo[11], E . S. Hafen[11], P. Haridas[11], G. Iacobucci[1], N. Inoue[17], F. F. Khalchukov[13], E. V. Korolkova[13], P. V. Kortchaguin[13], V. B. Kortchaguin[13], V. A. Kudryavtsev[13], G. Landi[6], K. Lau[9], X. Lin[5], L. Lu[5], M. Luvisetto[1], J. Ma[5], Z. Ma[5], G. Maccarrone[1], A. S. Malguin[13], Z. Mao[5], M. A. Markov[13], T. Massam[1], B. Mayes[9], N. Mengotti Silva[3], A. Misaki[17], G. H. Mo[9], B. Monteleoni[6], C. Morello[19], J. Moromisato[12], R. Nania[1], G. Navarra[19], L. Panaro[19], D. Parks[9], P. G. Pelfer[6], L. Periale[19], P. Picchi[19], P. Pinna[6], L. Pinsky[9], I. A. Pless[11], M. Pu[5], J. Pyrlik[9], J. Qiu[5], V. G. Ryasny[13], O. G. Ryazhskaya[13], O. Saavedra[19], K. Saitoh[18] D. Sanders[9], G. Sartorelli[1], S. Sarwar[7], D. Shen[5], N. Taborgna[8], V. P. Talochkin[13], H. Tang[6], J. Tang[11], W. Tian[5], G. C. Trinchero[19], A. Turtelli[3], I. Uman[16], P. Vallania[19], S. Vernetto[19],

E. von Goeler[12], L. Votano[7], T. Wada[14], F. Wang[5], H. Wang[5], S. Wang[5], R. Weinstein[9], M. Widgoff[2], L. Xu[11], Z. Xu[5], V. F. Yakushev[13], I. Yamamoto[15], A. Zallo[7], G. T. Zatsepin[13], X. Zhou[5], Q. Zhu[5], X. Zhu[5], B. Zhuang[5], A. Zichichi[4]

---

1. University of Bologna and INFN Bologna, Italy.
2. Brown University, Providence, RI 02912, USA.
3. University of Campinas, Campinas, Brazil.
4. CERN, 1211 Geneve 23, Switzerland.
5. Chinese Academy of Sciences, Beijing, China and I.C.S.C. World Laboratory.
6. University of Firenze and INFN Firenze, Italy.
7. INFN–LNF, Frascati, Italy.
8. INFN–LNGS, Assergi, Italy.
9. University of Houston, Houston, TX 77004, USA.
10. Indiana University, Bloomington, IN 47401, USA.
11. Massachusetts Institute of Technology, Cambridge, MA 02139, USA.
12. Northeastern University, Boston, MA 02115, USA.
13. INR, Russian Academy of Sciences, Moscow, Russia.
14. Okayama University, Okayama, Japan.
15. Okayama University of Science, Okayama, Japan.
16. University of Perugia and INFN Perugia, Italy.
17. Saitama University, Saitama, Japan.
18. Ashikaga Institute of Technology, Ashikaga, Japan.
19. Institute of Cosmo-Geophysics, CNR, Torino, Italy and University of Torino and INFN Torino, Italy.
20. University of Urbino and INFN Firenze, Italy.

Bibliography

[A+79] E. N. Alexeyev et al. In *Proc. 16th Intern. Cosmic Ray Conf., Vol. 10*, page 276, Kyoto, 1979.

[A+86] C. Alberini et al. *Nuovo Cimento C*, 9:237, 1986.

[A+92a] M. Aglietta et al. The most powerful scintillator supernovae detector: LVD. *Il Nuovo Cimento A*, 105(12):1793–1804, Dicembre 1992.

[A+92b] E. D. Alyea et al. A technique for analyzing the LVD scintillation counter data. LVD Note 109 (92–7), Indiana University, Massachusetts Institute of Technology, May 1992.

[A+93] G. Anzivino et al. *Nuclear Instruments and Methods in Physics Research*, A329:521, 1993.

[A+94a] M. Aglietta et al. Search for fractionally charged particles in the Mont Blanc LSD scintillation detector. *Astroparticle Physics*, 2, 1994.

[A+94b] M. Aglietta et al. Single muon angular distributions observed in the LVD particle astrophysics experiment. *Astroparticle Physics*, 2(2), 1994.

[ABCC+84] M. Aguilar-Benitez, R. N. Cahn, R. L. Crawford, R. Frosch, et al. Particle Properties Data Booklet. From "Review of Particle Properties" Reviews of Modern Physics Vol. 56 No. 2, Part II, April 1984.

[Ahl80] S. T. Ahlen. Theoretical and experimental aspects of the energy loss of relativistic heavily ionizing particles. *Reviews of Modern Physics*, 52(1):121–173, January 1980.

[B$^+$79] V. I. Beresnev et al. In *Proc. 16th Intern. Cosmic Ray Conf., Vol. 10*, page 293, Kyoto, 1979.

[B$^+$83] L. Bergamasco et al. Muon sea-level intensity and primary cosmic ray nucleon spectrum in the (1 to 100) TeV energy range from the Mt. Blanc underground experiment. *Nuovo Cimento C*, 6:569–594, 1983.

[B$^+$84] G. Badino et al. *Nuovo Cimento C*, 7:573, 1984.

[B$^+$89] G. Bari et al. The Large-Volume Detector (LVD) – a multipurpose underground detector at Gran Sasso. *Nuclear Instruments and Methods in Physics Research*, A277:11–16, 1989.

[B$^+$91a] E. W. Beier et al. Search for fractionally charged particles in Kamiokande II. *Physical Review D*, 43(9):2843–2846, May 1991.

[B$^+$91b] C. Boissat et al. *MODEL: A Software Suite for Data Acquisition.* DD Division, CERN, Geneva, January 1991.

[BB64] W. H. Barkas and M. J. Berger. Tables of energy losses and ranges of heavy charged particles. In *Stusies in the Penetration of Charged Particles in Matter.* National Academy of Sciences Publication 1133, 1964. Nuclear Science Series Report No. 39.

[BB81] L. B. Bezrukov and E. V. Bugaev. *Sov. J. Nucl. Phys.*, 33:625, 1981.

[BBM$^+$87] R. Brun, F. Bruyant, M. Maire, A. C. McPherson, and P. Zanarini. *GEANT3.* DD Division, CERN, Geneva, September 1987. Version 3.15, released April 7, 1992.

[Bet32] H. A. Bethe. *Z. Physik*, 76:293, 1932.

[BFP$^+$90] A. Bigongiari, W. Fulgione, D. Passuello, O. Saavedra, and G. C. Trinchero. High modularity fast charge-time digitizer in neutrino burst detection. *Nuclear Instruments and Methods in Physics Research*, A288:529–535, 1990.

[BH34] H. A. Bethe and W. Heitler. *Proc. R. Soc. London Ser. A*, 146:83, 1934.

[BL50] O. Blunck and S. Leisegang. *Z. Physik*, 128:500, 1950.

[Blo33] F. Bloch. *Ann. Phys. (Leipzig)*, 16:285, 1933.

[C$^+$92] A. Cavestro et al. *Nuclear Instruments and Methods in Physics Research*, A312:571, 1992.

[Dal83] R. H. Dalitz. *Prog. Nucl. Part. Phys.*, 8:7, 1983.

[DM83] J. Drees and H. E. Montgomery. *Annu. Rev. Nucl. Part. Sci.*, 33:383, 1983.

[EZK$^+$88] R. I. Enikeev, G. T. Zatsepin, E. V. Korol'kova, V. A. Kudryavtsev, A.S. Mal'gin, O. G. Ryazhskaya, and F. F. Khal'chukov. Study of the muon spectrum at a depth 570 m.w.e. underground by means of the 100-ton scintillator detector. *Sov. J. Nucl. Phys.*, 47(4):665–671, April 1988.

[F$^+$89] W. Fulgione et al. *IEEE Transactions on Nuclear Science*, 36:1635, 1989.

[Fan63] U. Fano. *Ann. Rev. Nucl. Sci.*, 13:1, 1963.

[Fer86] R. C. Fernow. *Introduction to experimental particle physics.* Cambridge University Press, Cambridge, New York, 1986.

[FK83] H. E. Fish and R. L. Kelly. *Annu. Rev. Nucl. Part. Sci.*, 32:499, 1983.

[Ful91] W. Fulgione, 1991. working place explanation.

[Gai90] T. K. Gaisser. *Cosmic Rays and Particle Physics.* Cambridge University Press, Cambridge, 1990.

[GM64] M. Gell-Mann. *Phys. Lett.*, 8:214, 1964.

[GM 2] H. Grote and I. McLaren. *EPIO Manual.* DD Division, CERN, Geneva, 1981-2. Revised September 1986.

[GZM76] V. I. Gurentsov, G. T. Zatsepin, and E. D. Mikhal'chi. Passage of a muon flux through thick layers of matter. *Sov. J. Nucl. Phys.*, 23(5):527–532, May 1976.

[Haf89a] Elizabeth S. Hafen. Muon reconstruction in large rectangular detectors. In G. B. Yodh and D. C. Wold, editors, *Proceedings of the Workshop on Physics and Experimental Techniques of High Energy Neutrinos and VHE and UHE Gamma-Ray Particle Astrophysics*, Little Rock, Arkansas, May 1989.

[Haf89b] Elizabeth S. Hafen. PIPR equations. APC Engineering Note 89-2, Massachusetts Institute of Technology, Cambrudge, Massachusetts, October 1989.

[Haf92] E. Hafen. NIMBLE Note 1 92-1, Massachusetts Institute of Technology, Cambrudge, Massachusetts, May 1992.

[HK83] A. G. Hey and R. L. Kelly. *Phys. Rep.*, 96:71, 1983.

[Iar83] E. Iarocci. *Nuclear Instruments and Methods in Physics Research*, A217:30, 1983.

[Jec88] B. Jeckelmann. Muon studies with the LVD tracking system. LVD Note 15 (87-10), January 1988. The mountain topographic data were improved by a new survey in 1992, and work by A. Bizzeti, A. Desilva, and E. Hafen generated new tables of the slant depth of the rock overburden.

[K$^+$83] K. Kawagoe et al. An underground search for anomalous penetrating particles such as massive magnetic monopoles. *Physics Letters*, 128B(5), September 1983.

[K$^+$84] K. Kawagoe et al. An underground search for fractionally charged penetrating particles. *Lettere al Nuovo Cimento*, 41(18), Dicembre 1984.

[KK68] S. R. Kelner and Yu. D. Kotov. *Sov. J. Nucl. Phys.*, 7:237, 1968.

[KP71] R. P. Kokoulin and A. A. Petrukhin. In *Proc. 12th Int. Conf. on Cosmic Rays, Vol. 6*, page A2436, Hobart, 1971.

[KR92] V. A. Kudryavtsev and O. G. Ryazhskaya. Energy calibration of LVD scintillator counters using cosmic ray muons. LVD Note 104 (92–02), Institute for Nuclear Research of the Russian Academy of Sciences, Moscow, Russia, 1992.

[Lan44] L. Landau. On the energy loss of fast particles by ionization. *Journal of Physics, USSR*, 8:201–205, 1944.

[Leo87] W. R. Leo. *Techniques for Nuclear and Particle Physics Experiments.* Springer-Verlag, Berlin, 1987.

[LKV85] W. Lohmann, R. Kopp, and R. Voss. Energy loss of muons in the energy range 1–1000 GeV. CERN, Experimental Physica Division 85-03, European Organization for Nuclear Research, Geneve, March 1985.

[Lyo85] L. Lyons. Quark search experiments at accelerators and in cosmic rays. *Physics Reports*, 129(4):225–284, 1985.

[MFO80] J. L. Matthews, D. J. S. Findlay, and R. O. Owens. *Nucl. Instr. and Meth.*, 180:573, 1980.

[MP69] H. D. Maccabee and D. G. Papworth. *Phys. Lett. A*, 30:241, 1969.

[PP93] I. Pless and D. Pless. LVD note, December 1993.

[PS68] A. A. Petrukhin and V. V. Shestakov. *Can. J. Phys.*, 46:S377, 1968.

[Pyr91] J. Pyrlik, 1991. Stating the finding at the streamer tube production factory at University of Houston, during a discussion on the LVD site.

[RE74] P. Rice-Evans. *Spark, Streamer, Proportional, and Drift Chambers*, chapter 10. 1974.

[Rya92] O. G. Ryazhskaya, 1992. Communication within the LVD collaboration.

[SB+78] W. R. Sheldon, J. R. Benbrook, et al. Measurement of the directional cosmic-ray muon range spectrum. *Physical Review D*, 17:114–125, 1978.

[SBS84] R. M. Sternheimer, M. J. Berger, and S. M. Seltzer. Density effect for the ionization loss of charged particles in various substances. *Atomic Data and Nuclear Data Tables*, 30(2):261–271, March 1984.

[SGK+67] P. Shulek, B. M. Golovin, L. A. Kulyukina, S. V. Medved, and P. Pavolich. *Sov. J. Nucl. Phys.*, 4:400, 1967.

[Sil94] A. De Silva, 1994. Data analysis done for PhD thesis at Brown University.

[SP71] R. M. Sternheimer and R. F. Peierls. General expression for the density effect for the ionization loss of charged particles. *Physical Review B*, 3(11):3681–3692, June 1971.

[Vav57] P. V. Vavilov. *Sov. Phys. JETP*, 5:749, 1957.

[VDR70] A. V. Voevodsky, V. L. Dadykin, and O. G. Ryazhskaya. *Pribory i Technica Experimenta (Instruments and Methods in the Experiment)*, 1:85, 1970. in Russian.

[VZK79] L. V. Volkova, G. T. Zatsepin, and L. A. Kuz'michev. The cosmic-ray muon spectrum at see level and the primary cosmic-ray nucleon spectrum. *Sov. J. Nucl. Phys.*, 29(5):645–651, May 1979.

[WW85] X.-G. Wen and E. Witten. *Nucl. Phys. B*, 261:651, 1985.

[Zic] A. Zichichi. CERN-EP.

[Zic81] A. Zichichi. In *Proceedings of GUD Workshop*, page 141, Rome (Frascati), 1981.

[Zwe64] G. Zweig. preprint 412, CERN-TH, 1964.